Dissertation

Studying the complexity of mitochondrial Ca^{2+} uptake: Structural reorganization of mitochondrial Ca^{2+} uptake 1 (MICU1) multimers for activation of mitochondrial Ca^{2+} uniporter (MCU) is exclusively controlled by cytosolic Ca^{2+}

submitted by

Warisara PARICHATIKANOND

for the Academic Degree of

Doctor of Medical Science

(Dr. scient. med)

at the

Medical University of Graz

Institute of Molecular Biology and Biochemistry

under the Supervision of

Univ.-Prof. Dr. Wolfgang F. GRAIER

2015

DECLARATION

I hereby declare that this dissertation is my own original work and that I have fully acknowledged by name all of those individuals and organizations that have contributed to the research for this dissertation. Due acknowledgement has been made in the text to all other material used. Throughout this dissertation and in all related publications I followed the guidelines of "Standards of Good Scientific Practice and Ombuds Committee at the Medical University of Graz".

Graz, 10th of December 2015

ACKNOWLEDGEMENTS

I would like to thank all those people who supported me during my doctoral study, in particular my parents, my family, my friends and all former and present colleagues of mine for their tremendous love, sacrifice, understanding and support.

First of all, I would like to express my most sincere gratitude and deepest appreciation to my principle investigator, Prof. Dr. Wolfgang F. Graier, Chair, Institute of Molecular Biology and Biochemistry, Medical University of Graz for his invaluable guidance, constructive support, continuous encouragement and critical evaluation throughout my study. The inspiration for performing high-quality research comes from him. He also provided me an enormous opportunity to join his great research team and successfully complete my doctoral study.

My appreciation is also expressed to Assoc.Prof. Dr. Roland Malli for his fruitful suggestion and comments. I would also like to sincerely acknowledge Dr. Markus Waldeck-Weiermair for providing his meaningful guidance, useful suggestions and constant support during my research work. My research could not have been completed without the generous assistance of them.

I would also like to thank the Institute of Molecular Biology and Biochemistry, Medical University of Graz for providing laboratory facilities, including all of people whom my thesis concerned with in many ways. I wish to thank my former and present colleagues at the institute, namely Alexander Bondarenko, Corina Madreiter-Sokolowski, Christiane Klec, Benjamin Gottschalk, Andras Deak, Neelanjan Vishnu, Muhammad Rizwan Alam, Muhammad Jadoon Khan, Lukas Groschner, Felix Karsten, Claire Jean-Quartier, Rene Rost, Sonja Barth, Sandra Blass, Nicole Hofmann, Therese Macher, Florian Enzinger, Emrah Eroglu and Anna Schreilechner for their cooperation, help, moral support and excellent technical assistance during my doctoral research. My study would not be feasible without them.

Finally, I gratefully acknowledge the Österreichischer Austauschdienst (OeAD) for granting me a scholarship to pursue my advanced study in Austria and providing me a chance to broaden my horizons and develop my profession as a researcher.

Warisara Parichatikanond

Graz, Austria

TABLE OF CONTENTS

DECLARATION II
ACKNOWLEDGEMENTS III
TABLE OF CONTENTS IV
LIST OF ABBREVIATIONS VII
ABSTRACT X
ZUSAMMENFASSUNG XII
INTRODUCTION **1**
1.1 Mitochondria: structure and function 1
1.2 Ca^{2+} signaling and physiological roles of Ca^{2+} in mitochondria 2
1.3 The mitochondrial Ca^{2+} function coupling with other organelles 3
1.3.1 The Ca^{2+} communication between mitochondria and the plasma membrane 4
1.3.2 The Ca^{2+} crosstalk between mitochondria and the ER/SR 5
1.4 Mitochondrial Ca^{2+} transport 6
1.4.1 Mitochondrial Ca^{2+} influx 6
1.4.2 Mitochondrial Ca^{2+} efflux 8
1.4.3 Mitochondrial Ca^{2+} buffering regulates the activity of Ca^{2+} channels 8
1.5 Key components of the mitochondrial Ca^{2+} uptake machinery: The uniporter complex in the IMM 9
1.5.1 Mitochondrial Ca^{2+} uptake 1 (MICU1) 11
1.5.2 Mitochondrial Ca^{2+} uptake 2 (MICU2) 15
1.5.3 Mitochondrial Ca^{2+} uniporter (MCU) 16
1.5.4 Mitochondrial Ca^{2+} uniporter b (MCUb) 17
1.5.5 Essential MCU regulator (EMRE) 18
1.5.6 Uncoupling protein 2 and 3 (UCP2/3) 19
1.5.7 Mitochondrial Ca^{2+} uniporter regulator 1 (MCUR1) 19
1.5.8 Others 20
1.6 Aims of the study 22
MATERIALS AND METHODS **23**
2.1 Chemicals 23
2.2 Cell culture 23
2.3 Plasmids and small interfering RNA (siRNA) 24

2.4 Transfection of cells 25
2.4.1 Transfection of plasmid DNA 25
2.4.2 Transfection of siRNA together with plasmid DNA 26
2.5 Ca^{2+} measurement 26
2.5.1 Buffer solutions for Ca^{2+} imaging experiments 26
2.5.2 Mitochondrial Ca^{2+} measurements 27
2.5.3 MICU1-FRET rearrangement 28
2.5.4 Cytosolic Ca^{2+} measurements 28
2.5.5 Simultaneous mitochondrial and cytosolic Ca^{2+} measurements 29
2.5.6 Imaging system, data acquisition, and analysis 29
2.6 Analysis of mitochondrial morphology 31
2.7 Molecular biology methods 32
2.7.1 Total RNA isolation 32
2.7.2 First strand cDNA synthesis (revere transcription, RT) 32
2.7.3 Quantitative real-time polymerase chain reaction (qPCR or RT-PCR) 32
2.8 Statistical analysis 33
RESULTS **34**
PART I
3.1: MICU1 is a negative regulator of MCU that is under the control of UCP2/3 in mitochondrial Ca^{2+} uptake 34
3.1.1 Knock-down efficiency of MCU and UCP2 in MCU^{kd} and $UCP2^{kd}$ cells 34
3.1.2 The mitochondrial Ca^{2+} handling of MCU^{kd} and $UCP2^{kd}$ cells 34
3.1.3 MICU1 functions as a negative regulator of MCU in shControl cells 35
3.1.4 MCU is negatively regulated by MICU1 and independent of UCP2/3 in $UCP2^{kd}$ cells 37
3.1.5 Knockdown of MICU1 boosts the influence of UCP2/3 on MCU activity in MCU^{kd} cells overexpressed with UCP2/3 37
3.1.6 A widely distributed and dominant rising of mitochondrial Ca^{2+} entry in MCU^{kd} cells depleted with MICU1 and overexpressing MCU or UCP2/3 highlights the exclusive contribution between these particular proteins 40
3.1.7 EMRE contributes to MCU and UCP2 in the regulation of mitochondrial Ca^{2+} entry 42

3.1.8 In MCU^{kd} cells overexpressed with UCP2 and depleted with MICU1, the boosted $[Ca^{2+}]_{mito}$ signals depend on MCU (rest of MCU) and EMRE, but not on MCUR1 42
3.1.9 Mitochondrial Ca^{2+} sequestration from contact sites of the ER works exclusively via MCU and EMRE but not MCUR1 44
3.1.10 UCP2/3 facilitates the function of MCU/EMRE in mitochondrial Ca^{2+} entry. 45
PART II
3.2: Expression of MICU1 causes pronounced structural alteration pointing to the additional engagement of this protein in the structure and function of mitochondria..... 47
PART III
3.3: Rearrangement of MICU1 multimers for activation of MCU is solely controlled by cytosolic Ca^{2+} 49
3.3.1 Elevations of Ca^{2+} yield a rearrangement of MICU1 multimers in intact cells . 49
3.3.2 Ca^{2+}-triggered MICU1 de-multimerization occurs prior to mitochondrial Ca^{2+} sequestration 58
3.3.3 Rearrangement of MICU1 multimers is independent on the mitochondrial membrane potential and matrix Ca^{2+} elevation 59
3.3.4 MICU1 multimers rearrange irrespective of the expression level of MCU and EMRE 61
DISCUSSION **63**
PART I
4.1: MICU1 is a negative regulator of the MCU that is under the control of UCP2/3 in mitochondrial Ca^{2+} uptake 63
PART II
4.2: Expression of MICU1 causes pronounced structural alteration pointing out to the additional engagement of this protein in the structure and function of mitochondria..... 68
PART III
4.3: Rearrangement of MICU1 multimers for activation of MCU is solely controlled by cytosolic Ca^{2+} 69
BIBLIOGRAPHY 74
PUBLICATIONS 90

LIST OF ABBREVIATIONS

aa	Amino acid
ADP/ATP	Adenosine di/triphosphate
AMPK	AMP-activated protein kinase
BHQ	2,5-di-tert-butylhydroquinone
$[Ca^{2+}]_{cyto}$	Cytosolic free Ca^{2+} concentration
$[Ca^{2+}]_{mito}$	Mitochondrial free Ca^{2+} concentration
CaM	Calmodulin
cDNA	Complementary DNA
cds	Coding sequence
CFP/YFP/OFP/RFP	Cyan/Yellow/Orange/Red fluorescent protein
co-IP	Co-immunoprecipitation
CRAC	Ca^{2+} release-activated Ca^{2+} channels
DMEM	Dulbecco's modified eagle medium
dNTPs	Deoxynucleotide triphosphates
DRP1	Dynamin related protein 1
EB-buffer	Experimental buffer
EGTA	Ethylene glycol tetraacetic acid
EMRE	Essential MCU regulator
ER/SR	Endoplasmic/Sarcoplasmic reticulum
ETC	Electron transport chain
FAD/ $FADH_2$	Flavin adenine dinucleotide: oxidized/reduced
FCCP	Carbonyl cyanide-4-(trifluoromethoxy) phenylhydrazone
FCS	Fetal calf serum
FP	Fluorescent protein
FRET	Förster resonance energy transfer
Fura-2/AM	Fura-2 acetoxymethyl ester
GAPDH	Glyceraldehyde-3-phosphate dehydrogenase
GECI	Genetically encoded Ca^{2+} indicator
HEPES	4-(2-Hydroxyethyl)piperazine-1-ethanesulfonic acid, N-(2-Hydroxyethyl)piperazine-N′-(2-ethanesulfonic acid)
His	Histamine
IMM/OMM	Inner/Outer mitochondrial membrane
IMS	Intermembrane space
INS-1	Insulinoma cell line
IP_3	Inositol 1,4,5-trisphosphate

IP_3R	Inositol 1,4,5-trisphosphate receptor
KD	Knockdown
K_d	Dissociation constant
kDa	Kilodalton
LETM1	Leucine zipper-EF-hand-containing transmembrane protein 1
M13	Myosin light chain kinase
MAMs	Mitochondria-associated membranes
mCa2	Mitochondrial Ca^{2+} current type 2
MCU	Mitochondrial Ca^{2+} uniporter
MCUb	Mitochondrial Ca^{2+} uniporter b
MCUR1	Mitochondrial Ca^{2+} uniporter regulator 1
MFN-2	Mitofusin 2
MICU1/2	Mitochondrial Ca^{2+} uptake 1/2
MIRO	Mitochondrial RHO GTPase
mPTP	Mitochondrial permeability transition pore
mRyR	Mitochondrial ryanodine receptor
mtDsRed	Mitochondrial *Discosoma sp.* red fluorescent protein
MTS	Mitochondrial targeting sequence
NAD/ NADH	Nicotinamide adenine dinucleotide: oxidized/reduced
NCLX	Mitochondrial Na^+-Ca^{2+}-Li^+ exchanger
NO	Nitric oxide
OPA1	Optic atrophy 1 protein
PBS	Phosphate-buffered saline
qPCR/ RT-PCR	Quantitative real-time polymerase chain reaction
RaM	Rapid mode of Ca^{2+} uptake
ROS	Reactive oxygen species
RT	Reverse transcription
RuR	Ruthenium red
SERCA	Sarcoplasmic/endoplasmic reticulum Ca^{2+} ATPase
shRNA	Short hairpin RNA
siRNA	Small interfering RNA
SOCE	Store-operated Ca^{2+} entry
STIM1	Stromal interacting molecule 1
TCA cycle	The citric acid cycle

TMD	Transmembrane domain
TRPC	Transient receptor potential channel
UCP2/3	Uncoupling protein 2/3
VDAC	Voltage-dependent anion channel
VDCC	Voltage-gated Ca^{2+} channel
Δ_{max}	Maximum mitochondrial Ca^{2+} uptake
Ψ_{mito}	Mitochondrial membrane potential

ABSTRACT

Mitochondrial Ca^{2+} uptake plays an important role in the regulation of cellular signaling, aerobic metabolism, and apoptosis. Mitochondria are able to buffer Ca^{2+} from locally high cytosolic Ca^{2+} levels that modulates various Ca^{2+} signaling events. Recently, several proteins located in the inner mitochondrial membrane (IMM) have been described to be essential for mitochondrial Ca^{2+} machineries, including mitochondrial Ca^{2+} uniporter (MCU), mitochondrial Ca^{2+} uptake 1 (MICU1), uncoupling proteins 2 and 3 (UCP2/3), essential MCU regulator (EMRE), and mitochondrial Ca^{2+} uniporter regulator 1 (MCUR1). Although the characteristics and physiological consequences of mitochondrial Ca^{2+} sequestration have been reported, the actual mechanisms of protein-protein interactions involved in this phenomenon are still unclear. In this study, overexpression and/or silencing of the distinct proteins were applied to reveal that mitochondrial Ca^{2+} uptake upon IP_3-mediated depletion of the endoplasmic reticulum (ER) Ca^{2+} stores works exclusively via MCU and EMRE but not MCUR1. MICU1 functions as negative regulator of the MCU/EMRE complex. In addition, UCP2/3 facilitates MCU/EMRE functions and counteracts MICU1, while diminution of MICU1 boosts the effect of UCP2/3 on MCU activity in MCU knockdown cells overexpressed with UCP2/3. Our results indicate that UCP2/3 facilitates mitochondrial Ca^{2+} uptake by MCU/EMRE and thereby controls the mitochondrial Ca^{2+} entry by function of MICU1.

The crystal structure of MICU1 has been recently revealed that in the absence of Ca^{2+} MICU1 exists as a hexamer, while Ca^{2+} binding to the two EF-hands results in a rearrangement to MICU1 dimers. Although, the Ca^{2+}-sensing gatekeeper function of MICU1 has been well investigated for MCU that together with the EMRE forms the mitochondrial Ca^{2+} channel, mechanisms by which MICU1 controls MCU/EMRE activity to tune mitochondrial Ca^{2+} signals remain ambiguous. Furthermore, overexpression of MICU1 causes pronounced structural alteration of mitochondria pointing to an additional engagement of this protein in the ultrastructure of mitochondria. In this study, we established a Förster-Resonance-Energy-Transfer (FRET)-based live-cell imaging approach to dynamically monitor the kinetics of the structural reorganization of MICU1 oligomers and demonstrate that elevations of cytosolic Ca^{2+} rearranges MICU1 multimers with an EC_{50} of approximately 4.4 μM, resulting in activation of mitochondrial Ca^{2+} uptake via MCU. Moreover, MICU1 rearrangement essentially requires the EF-hand motifs and

strictly correlates with the shape of cytosolic Ca^{2+} rises. Hence, these data show that rearrangements of MICU1 multimers were independent of matrix Ca^{2+} concentration, mitochondrial membrane potential (Ψ_{mito}), and expression levels of MCU and EMRE. These data provide novel insights in the dynamics, regulation, and molecular effect of the structural reorganization of MICU1 that adds to the current understanding of the complex molecular mechanisms of MCU/EMRE activation in intact cells.

ZUSAMMENFASSUNG

Die mitochondrielle Ca^{2+} Aufnahme spielt eine wichtige Rolle in der Regulierung von zellulären Signalprozessen, aerobem Metabolismus und Apoptose. Mitochondrien können hohe lokale Ca^{2+} Konzentrationen puffern und dadurch verschiedene Ca^{2+} gesteuerte Prozesse modulieren. Erst kürzlich wurden Proteine der inneren Mitochondrienmembran (IMM) beschrieben, welche essentiell an der mitochondriellen Ca^{2+} Aufnahme beteiligt sind. Diese Proteine sind der mitochondrial Ca^{2+} uniporter (MCU), mitochondrial Ca^{2+} uptake 1 (MICU1), uncoupling proteins 2 und 3 (UCP2/3), essential MCU regulator (EMRE) und mitochondrial Ca^{2+} uniporter regulator 1 (MCUR1). Zwar konnten Charakteristika und die physiologischen Auswirkungen dieser Proteine auf die mitochondrielle Ca^{2+} Aufnahme beschrieben werden, aber die verschiedenen Interaktionsmechanismen zwischen den Proteinen, welche in dieses Phänomen involviert sind, werfen nach wie vor Fragen auf. In dieser Studie haben wir bestimmte Proteine überexprimiert und/oder herunterreguliert und konnten letztlich zeigen, dass die mitochondrielle Ca^{2+} Aufnahme nach IP3-mediierter Ca^{2+} Freisetzung aus dem Endoplasmatischen Retikulum (ER) ausschließlich via MCU und EMRE, allerdings nicht unter Beteiligung von MCUR1, abläuft. MICU1 fungiert als negativer Regulator des MCU/EMRE Komplexes. Darüber hinaus unterstützt UCP2/3 die Funktion des MCU/EMRE Komplexes und ist ein Gegenspieler von MICU1. Die Wegnahme von MICU1 erhöht den Effekt von UCP2/3 auf die MCU Aktivität in MCUkd Zellen mit Überexpression von UCP2/3. Unsere Resultate deuten darauf hin, dass UCP2/3 die mitochondrielle Ca^{2+} Aufnahme via MCU/EMRE fördert und dadurch diese über die Funktion von MICU1 kontrolliert.

Die Analyse der MICU1 Kristallstruktur hat vor kurzem gezeigt, dass in Abwesenheit von Ca^{2+} MICU1 als Hexamer vorliegt, während die Bindung von Ca^{2+} an die zwei EF-hands zu einer Umorientierung in MICU1 Dimere führt. Obwohl die Ca^{2+}-sensitive Regulatorwirkung von MICU1 auf MCU, welcher zusammen mit EMRE den Kanal für die mitochondrielle Ca^{2+} Aufnahme darstellt, gut erforscht ist, sind die Mechanismen, über welche MICU1 die Aktivität des MCU/EMRE Komplexes steuert, immer noch ungewiss. Darüber hinaus führt die Überexpression von MICU1 zu nennenswerten Veränderungen der Mitochondrienstruktur. Dies deutet darauf hin, dass sich dieses Protein auch auf die Ultrastruktur der Mitochondrien auswirkt. In der

vorliegenden Studie haben wir die Förster-Resonance-Energy-Transfer (FRET)-basierte Bildgebung in der lebenden Zellen etabliert, um die dynamischen Veränderungen der strukturellen Umorientierung von MICU1 Oligomeren zu beobachten und konnten zeigen, dass die Erhöhung von cytosolischem Ca^{2+} zu einer Umstrukturierung in MICU1 Multimere mit einer EC_{50} von ca. 4,4 µM führt, welche eine Aktivierung von MCU zur Folge hat. Die Umstrukturierung von MICU1 benötigt das EF-hand Motif und korreliert mit der Form des cytolischen Ca^{2+} Anstiegs. Diese Daten zeigen weiters, dass die Umorientierung von MICU1 Multimeren unabhängig von der Matrix Ca^{2+} Konzentration, dem mitochondriellen Membranpotential (Ψ_{mito}) und dem Expressionslevel von MCU und EMRE ist. Unsere Resultate gewähren neue Einblicke in die Dynamik, die Regulation und den molekularen Effekt der strukturellen Umorientierung von MICU1, welcher maßgeblich zum derzeitigen Verständnis des komplexen molekularen Mechanismus' der MCU/EMRE Aktivierung in lebenden Zellen beiträgt.

CHAPTER I
INTRODUCTION

1.1 Mitochondria: structure and function

Mitochondria serve as the main energy providers for diverse activities of eukaryotic cells and act as crucial signaling nodes to generate and transduce intracellular signals (Rizzuto et al., 2012, Chandel, 2014) that are important for various cellular processes, including ion homeostasis, apoptosis, and autophagy (Pagliarini and Rutter, 2013). Mitochondria are bilayer membranes-bound organelles consisting of inner and outer mitochondrial membranes (IMM and OMM) separated by an intermembrane space; IMS. The IMM forms extensively folded into numerous cristae extending the surface area of the IMM and thereby raising the production of adenosine triphosphate; ATP (**Figure 1.1**) (Cooper and Hausman, 2007). The contents of small molecules and ions found in the IMS are identical with the cytosol as they freely diffuse between the cytosol and mitochondria through the OMM whereas the IMM is impermeable to most of them. As a consequence, the transportation of these molecules between the cytosol and the mitochondrial matrix primarily depends on the IMM as the vital barrier that maintains the proton gradient and precedes oxidative phosphorylation. In addition, the characteristic of mitochondria which is different from other cytoplasmic organelles is that their matrix contains their individual DNA, which encodes rRNAs, tRNAs, and some mitochondrial proteins. However, almost all mitochondrial proteins are translated on free ribosomes in the cytosol, then, imported into the mitochondria by distinct targeting signals (Cooper and Hausman, 2007).

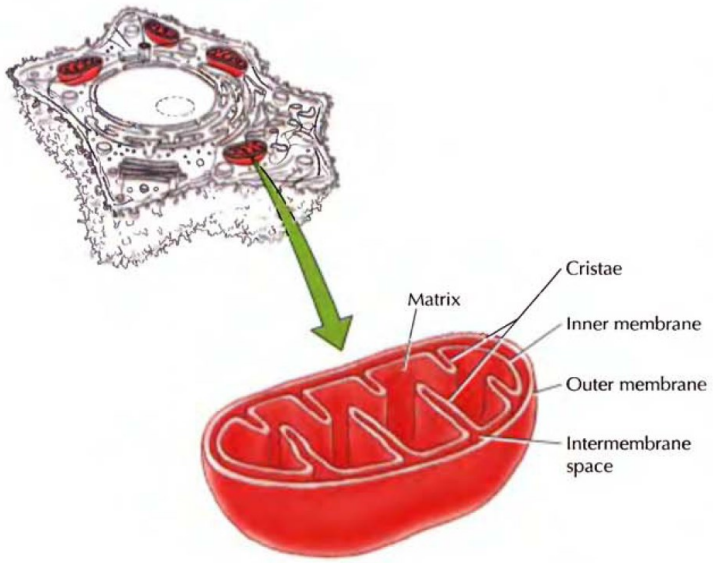

Figure 1.1: Structure of mitochondria. Each of the compartments of the double-membraned mitochondrion has specific functional roles. Particularly, the matrix and the IMM are the main working parts of mitochondria [Modified and adopted from (Cooper and Hausman, 2007)].

In eukaryotic cells, mitochondria have three essential functions in the maintenance of homeostasis, mainly biosynthesis, bioenergetics, and signaling. They are responsible for most of the energy derived from the breakdown of carbohydrates and fatty acids which further undergo oxidative phosphorylation and generate ATP in the IMM (**Figure 1.2**) (Cooper and Hausman, 2007). The citric acid cycle (TCA cycle) is the central pathway of oxidative metabolism that generates metabolites produced from the biosynthesis of various macromolecules such as lipids, carbohydrates, proteins and nucleotides and reduces equivalents including NADH and $FADH_2$. Then, the high-energy electrons from NADH and $FADH_2$ are imported into the mitochondrial electron transport chain; ETC, which pumps protons across the IMM to produce an electrochemical gradient which is highly demand for many cellular events, particularly ATP production and effective interchanging of proteins between mitochondria and cytosol. The mitochondrial ATP production is useful to maintain a high ATP/ADP ratio, which is indispensable for thermodynamically processes of various biochemical reactions (Chandel, 2014).

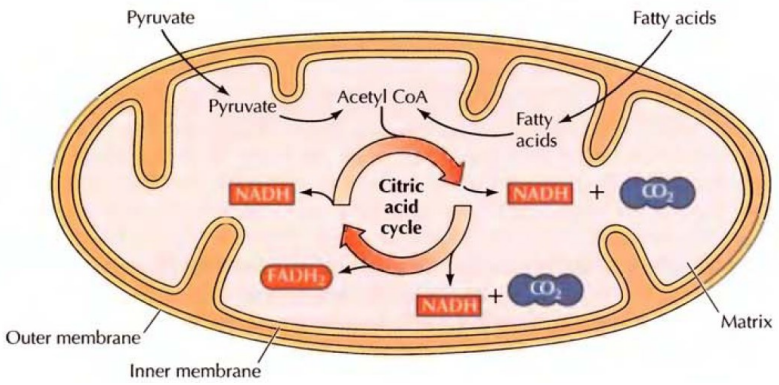

Figure 1.2: The oxidative metabolism of glucose and fatty acids is the principal source of metabolic energy in eukaryotic cells. Pyruvate and fatty acids are transferred from the cytosol into the mitochondrial matrix and converted to acetyl CoA. Then, acetyl CoA is oxidized to CO_2 by the TCA cycle and the oxidation of acetyl CoA to CO_2 is coupled to the reduction of NAD^+ and FAD to NADH and $FADH_2$, respectively. The enzymes of the TCA cycle are main players in these processes [Modified and adopted from (Cooper and Hausman, 2007)].

1.2 Ca^{2+} signaling and physiological roles of Ca^{2+} in mitochondria

Calcium ion (Ca^{2+}) is a second messenger that influences almost all aspects of life and death in eukaryotic cells (Clapham, 2007). Ca^{2+}-mediated signal transductions are sophisticatedly controlled by various ion channels, pumps and exchangers, which transport Ca^{2+} through the plasma membrane and many organelles inside the cells (Feske et al.,

2012). Cellular Ca^{2+} homeostasis regulates mitochondrial movement, function, and viability (Graier et al., 2007). All these processes are under the finely tuned of the ER and mitochondria (Rowland and Voeltz, 2012). Mitochondrial Ca^{2+} transport is involved with diverse physiological processes, especially controlling the metabolic rate for cellular energy production (Williams et al., 2015) and shaping the cytosolic Ca^{2+} transients (Herrington et al., 1996, Babcock et al., 1997). The overload of Ca^{2+} in the mitochondrial matrix results in an activation of the cell death pathway (Orrenius et al., 2003, Takeuchi et al., 2015). Furthermore, an elevation of $[Ca^{2+}]_{mito}$ in the matrix leads to an activation of dehydrogenase enzymes, that are pyruvate dehydrogenase, isocitrate dehydrogenases, and oxoglutarate dehydrogenase, resulting in a rise of the mitochondrial NADH-to-NAD ratio which eventually causes an enhancement of the electron flow in the respiratory chain and an adjusting of ATP biosynthesis according to the increase of ATP demands of a cell (McCormack et al., 1990, Satrustegui et al., 2007). In addition, an activation of NADH oxidase increased by Ca^{2+} in mitochondria also triggers an accumulation of mitochondrial reactive oxygen species (ROS) in many cell types, such as cardiomyocytes and neurons, leading to an impaired respiration and cell cytotoxicity (Chacon and Acosta, 1991, Gandhi et al., 2009). A large influx of Ca^{2+} into the mitochondrial matrix induces an opening of the mitochondrial permeability transition pore (mPTP) causing several sequential mitochondrial events, including depolarization of the IMM, uncoupling of oxidative phosphorylation, swelling of mitochondria, and followed by necrosis (Bernardi, 1999, Crompton, 1999, Bernardi et al., 2006, Rizzuto et al., 2012). In addition, a release of various pro-apoptotic factors through mPTP to the cytosol after its opening, for instance, pro-caspases, cytochrome c, and Ca^{2+}, triggers an apoptotic process (Wang, 2001, Hajnoczky et al., 2003, Lemasters et al., 2009). Nevertheless, mitochondrial Ca^{2+} may induce nitric oxide (NO) synthase, leading to a cardiac prevention against mPTP opening induced by NO in cardiomyocytes (Dedkova and Blatter, 2009).

1.3 The mitochondrial Ca^{2+} function coupling with other organelles

Presently, accumulating evidence represents the engagement of mitochondrial Ca^{2+} buffering and the Ca^{2+} crosstalk between mitochondria and main compartments, particularly the plasma membrane and the endoplasmic/sarcoplasmic reticulum (ER/SR) (**Figure 1.3**) (Takeuchi et al., 2015). Mitochondria create an extensively interconnected and dynamic network and form numerous close appositions with the ER. Since a high concentration of Ca^{2+} is found in close contacts between these organelles upon activation

of the inositol 1,4,5-trisphosphate receptor (IP_3R) of the ER, the Ca^{2+} signal at these close contacts is the main determinant of the mitochondrial responses to the Ca^{2+} (Rizzuto et al., 1998). Consequently, the Ca^{2+} released from the ER can be transported into mitochondria via a uniporter complex on the IMM and a voltage-dependent anion channel (VDAC) on the OMM (Rizzuto et al., 2012). Although the contribution of mitochondrial proteins to the plasma membrane remains elusive, many associated protein complexes involved with interactions between mitochondria and the ER/SR and their molecular mechanisms have been extensively clarified, pointing to the close relationship between these interactions and regulation of various cellular functions (Rowland and Voeltz, 2012, van Vliet et al., 2014).

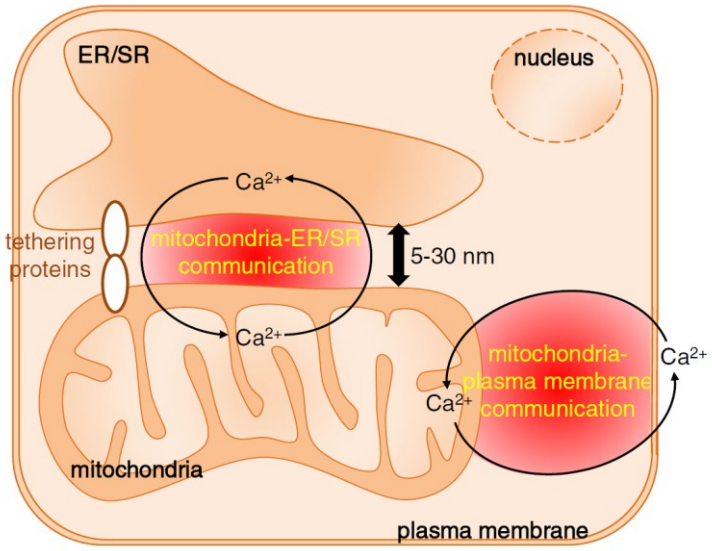

Figure 1.3: The Ca^{2+} crosstalk between mitochondria and principal compartments. The close contacts are observed between the plasma membrane or the ER/SR and adjacent mitochondria [Modified and adopted from (Takeuchi et al., 2015)].

1.3.1 The Ca^{2+} communication between mitochondria and the plasma membrane

The entering Ca^{2+} via the voltage-gated Ca^{2+} channel (VDCC) and store-operated Ca^{2+} entry (SOCE) is mobilized into mitochondria adjacent to the plasma membrane (Lawrie et al., 1996, Babcock et al., 1997, Park et al., 2001, Giacomello et al., 2010). After depletion of ER Ca^{2+} stores, a re-addition of extracellular Ca^{2+} causes largely enhancement of $[Ca^{2+}]_{mito}$, whereas has no effect on $[Ca^{2+}]_{cyto}$ in human umbilical vein endothelial cell line, in which 14% of mitochondria were found within 700 nm of the inner surface of the plasma membrane (Lawrie et al., 1996). Ca^{2+} levels were found to specifically increase in the junction of microdomains, leading to predominant Ca^{2+} uptake by mitochondria facing to those sites. However, the cell type is one of the factor that determine the involvement of

the Ca^{2+} microdomains since this phenomenon was not observed in HeLa cell, in which <6% of mitochondria are located in the proximity of the plasma membrane (Lawrie et al., 1996). In addition, Ca^{2+} influx via Ca^{2+} release-activated Ca^{2+} channels (or CRAC) through the basolateral membrane of pancreatic acinar cells has been found to influence predominantly Ca^{2+} uptake by sub-plasmalemmal mitochondria (Park et al., 2001). Therefore, Ca^{2+} crosstalk could occur between Ca^{2+} channels at the plasma membrane and the mitochondria located in close contact to plasma membrane in bidirectional manner, which is crucial for the regulation of cellular functions. Moreover, the Ca^{2+}-dependent presence of this junction might be involved with a contribution of various canonical transient receptor potential channel (or TRPC) family members, stromal interaction molecule 1; STIM1, and Ca^{2+} release-activated Ca^{2+} channel protein 1; Orai1 (Liao et al., 2007, Ong et al., 2007) or an unknown linkage protein between the OMM and the TRPC/STIM1/Orai complex, or a protein of the OMM that interacts with the SOCE complex and modulates the entering Ca^{2+} (Csordas et al., 2006, Graier et al., 2007).

1.3.2 The Ca^{2+} crosstalk between mitochondria and the ER/SR

The regulation of diverse cellular functions, including lipid biosynthesis, mitochondrial division, and Ca^{2+} signaling is finely controlled by the communication between mitochondria and ER/SR (Rowland and Voeltz, 2012, Friedman et al., 2011). The ER/SR, which is the main internal Ca^{2+} store, is located close to mitochondria (~5-30 nm) and the narrow contacts between these organelles presences in some cell types, such as cardiomyocytes and B lymphocytes (Csordas et al., 2006). Various tethering proteins have been described to have a role in these close appositions, for example mitofusin 2 (MFN2), dynamin related protein 1 (DRP1), mitochondrial RHO GTPase (MIRO), and Mmm1/Mdm10/Mdm12/Mdm34 complex (Rowland and Voeltz, 2012, van Vliet et al., 2014). In addition, Ca^{2+} levels detected in these narrow spaces are higher than in the cytosol (up to 9-50 μM), enabling the mitochondrial Ca^{2+} uniporter (MCU) which has low Ca^{2+} affinity to transport enough Ca^{2+} into mitochondria (Sharma et al., 2000, Csordas et al., 2010). Several studies suggested that a direct Ca^{2+} pathway generated by an IP_3R of the ER and a VDAC of the OMM located in the mitochondria-ER space has an influence on the regulation of energy metabolism and apoptosis in many cell types, such as fibroblasts, HeLa cells, CHO cells, and yeast (Rizzuto et al., 1998, Szabadkai et al., 2006). Furthermore, a reverse Ca^{2+} movement from mitochondria back to the ER/SR has also been reported to be involved with Ca^{2+} refilling process of ER/SR after stimulation by the

agonist to reduce cytosolic Ca^{2+} elevation and prevent depletion of ER/SR Ca^{2+} in endothelial cells, HeLa cells, and vascular smooth muscle cells (Arnaudeau et al., 2001, Malli et al., 2005, Poburko et al., 2009).

1.4 Mitochondrial Ca^{2+} transport

The Ca^{2+} homeostasis of cells is sophisticatedly orchestrated by various types of channels, pumps, and exchange proteins principally compartmentalized in the mitochondria, the ER/SR, and the cytosol (**Figure 1.4**) (Marchi and Pinton, 2014, Finkel et al., 2015). In steady state, the mitochondrial Ca^{2+} transportation is under the balance between Ca^{2+} influx and efflux in order to maintain Ca^{2+} homeostasis that is required for normal intracellular physiological function.

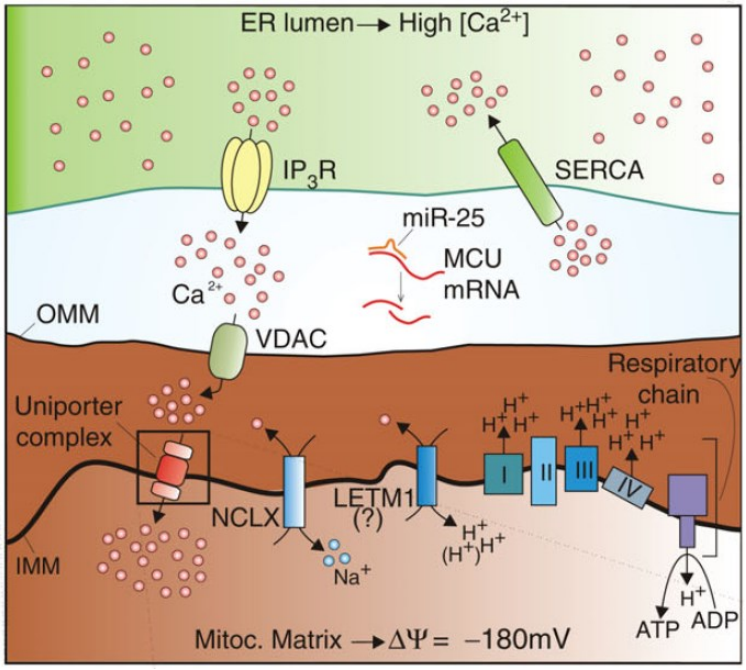

Figure 1.4: The mitochondrial Ca^{2+} homeostasis machinery. Numerous compartments located in the mitochondria, the ER/SR, and the cytosol is working together in order to balance mitochondrial Ca^{2+} influx and efflux [Modified and adopted from (Marchi and Pinton, 2014)].

1.4.1 Mitochondrial Ca^{2+} influx

In the 1960s, researchers described for the first time that rat kidney mitochondria could uptake large amounts of Ca^{2+} by an ATP demanding process (Deluca and Engstrom, 1961, Vasington and Murphy, 1962, Carafoli, 2012) and the Ca^{2+} carrier was later defined as the MCU (Brand et al., 1976). It was shown that the uniporter at the IMM is a highly selective Ca^{2+} channel by patch-clamping technique (Kirichok et al., 2004). The uniporter

rapidly transports Ca^{2+} across the high electrochemical gradient and this process is suppressed by ruthenium red (RuR) (Reed and Bygrave, 1974, Moore, 1971) and its more specific form; Ru360 (Matlib et al., 1998). Mitochondrial Ca^{2+} uptake was described to have a low affinity (high K_m) of ~5-10 μmol/L (Carafoli, 2012). Since the basal level of $[Ca^{2+}]_{cyto}$ was ~100 nmol/L and the peak of cytosolic Ca^{2+} transients were only <1 μmol/L (Allen and Blinks, 1978) which is much lower than the affinity of mitochondrial Ca^{2+} uptake (5-10 μmol/L), it was questioned at that time how $[Ca^{2+}]_{cyto}$ could increase to the level that is high enough to activate MCU under a normal physiological conditions. However, this phenomenon was later described by the existence of microdomains of high Ca^{2+} (Ca^{2+} hotspots) between the mitochondria and the ER/SR that yield Ca^{2+} uptake into the mitochondria via the MCU (Rizzuto and Pozzan, 2006). In addition, a large mitochondrial membrane potential (Ψ_{mito}) produced by the proton pump of the mitochondrial respiratory chain across the IMM is the major driving force for Ca^{2+} mobilization in the mitochondrial matrix through the uniporter (Drago et al., 2011).

Nowadays, several molecules contributing to mitochondrial Ca^{2+} entry have been revealed. The leucine zipper-EF-hand-containing transmembrane protein 1 (LETM1) is one of the targets found to function as a mitochondrial Ca^{2+}/H^+ antiporter located in the IMM, therefore regulating the Ca^{2+} sequestration of mitochondria (Tsai et al., 2014, Doonan et al., 2014). Nevertheless, some publications have described that LETM1 acts as a mitochondrial K^+/H^+ exchanger (Nowikovsky and Bernardi, 2014, Froschauer et al., 2005). The mitochondrial Na^+-Ca^{2+}-Li^+ exchanger (NCLX), which mainly has a role in the mitochondrial Ca^{2+} efflux pathway, has also been reported to transport Ca^{2+} in a reverse manner by mobilizing Ca^{2+} into the mitochondrial matrix under the condition that the Ψ_{mito} is dissipated and the Na^+ gradient is favorable (Griffiths, 1999). Another channel that has been under investigation is a skeletal ryanodine receptor (RyR) which is the main Ca^{2+} release channel in skeletal SR and located in the mitochondria and it was found that a compound ryanodine, an inhibitor of RyR, could effectively inhibit mitochondrial Ca^{2+} entry (Deluca and Engstrom, 1961, Beutner et al., 2005). Although it remains unclear whether and how this process is mediated by the same transporter with different regulatory factors or different transporters, accumulating studies still continue to represent other forms or modes of Ca^{2+} uptake into the mitochondria, for instance, rapid mode of Ca^{2+} uptake (RaM) (Sparagna et al., 1995, Buntinas et al., 2001), Coenzymes Q_{10} (Bogeski et al., 2011), and mCa1/2 (Michels et al., 2009).

1.4.2 Mitochondrial Ca^{2+} efflux

Mitochondrial Ca^{2+} extrusion in most cells is mainly mediated by the function of the NCLX (Palty et al., 2010), which is pharmacologically inhibited by the benzothiazepine compound, CGP-37157 (Cox et al., 1993). NCLX was originally identified as a member of the Na^+/Ca^{2+} exchanger family and expected to localize to the ER or the plasma membrane (Lytton, 2007). However, NCLX was found to catalyze Na^+- or Li^+-dependent Ca^{2+} transport at similar rates which is a unique feature of the mitochondrial exchange and the subcellular localization of NCLX was later proven and found that the endogenous protein distributed to the IMM in several tissues (Palty et al., 2010).

Despite of some reports identifying the stoichiometry of the NCLX as an electrogenic that exchanges 3 Na^+ ions for 1 Ca^{2+} ion, their molecular identity remains unclear (Boyman et al., 2013). The large negative Ψ_{mito} (-150 to -180 mV), coupled with the inwardly directed Na^+ gradients and the mitochondrial Na^+ is lower than cytosolic Na^+, the Na^+ gradient thereby creates a driving force and pump Ca^{2+} from the matrix to the cytosol via the NCLX. In addition, extramitochondrial Na^+ could stimulate Ca^{2+} extrusion from mitochondria and RuR could not block this process, but stimulated it which could be the explanation for an efflux pathway (Carafoli et al., 1974, Nicholls and Crompton, 1980). Moreover, mitochondrial Na^+-dependent Ca^{2+} efflux was found to increase upon overexpression of NCLX and reduced by silencing of NCLX, which could be rescued by the expression of heterologous NCLX (Palty et al., 2010, Boyman et al., 2013). Another pathway which has been proposed as an additional mitochondrial Ca^{2+} efflux is the mPTP (Gunter et al., 2000). Even though the transient opening of mPTP is involved with the Ca^{2+} extrusion process under physiological conditions, it can also trigger cell death signaling under the presence of Ca^{2+} overload in the mitochondrial matrix (Kroemer et al., 2007).

1.4.3 Mitochondrial Ca^{2+} buffering regulates the activity of Ca^{2+} channels

Mitochondria function as high capacity Ca^{2+} buffers that tune cytosolic Ca^{2+} transients by either modulating the kinetic properties of Ca^{2+} channels or retaining Ca^{2+} in the area of the open channels (Rizzuto et al., 2012). Upon agonist exposure, the mitochondria rapidly accumulate Ca^{2+} generating a cytosolic Ca^{2+} rise. The orchestrating of cytosolic Ca^{2+} sophisticatedly regulated by the two different sources of Ca^{2+}, including intracellular Ca^{2+} stores (>100 μM) and the extracellular Ca^{2+} entering (~1 mM) (Rizzuto and Pozzan, 2006, Pozzan et al., 1994, Streb et al., 1983). The main intracellular Ca^{2+}

stores are the ER/SR, whereas other compartments, such as the Golgi apparatus (Pinton et al., 1998), endosomes and lysosomes (Calcraft et al., 2009), also participate in this function by undergoing a rapid Ca^{2+} release through the channels which distinctly function depending on each organelle. In addition, other molecules (channels, pumps, and regulatory proteins) localized in these compartments are important determinants that characterize the spatiotemporal pattern of the cytosolic Ca^{2+} rises (Berridge, 2001). The changing of $[Ca^{2+}]_{cyto}$ levels is directly controlled by a specific Ca^{2+}-binding site or indirectly modulated via the function of Ca^{2+}-dependent enzymes (such as kinases and phosphatases) and scaffolding proteins (Rizzuto et al., 2012).

The mitochondrial Ca^{2+} entry influences the spatiotemporal properties of the $[Ca^{2+}]_{cyto}$ and regulates the activity of Ca^{2+} channels (Rizzuto et al., 2012). At the microdomains, the local $[Ca^{2+}]_{cyto}$ is modulated by a rapid removal of Ca^{2+} from the opened Ca^{2+} channels on the ER/SR or the plasma membrane by energized mitochondria. After Ca^{2+} release from the ER, the free $[Ca^{2+}]_{cyto}$ allows a regulatory feedback to Ca^{2+} channels in many types of responses, including activation, inhibition or biphasic, depending on the concentration of cytosolic Ca^{2+} (Bezprozvanny et al., 1991). The mitochondrial Ca^{2+} buffering depends on the bell-shaped effect of $[Ca^{2+}]_{cyto}$ on IP_3R activity since high and low $[Ca^{2+}]_{cyto}$ inhibit IP_3Rs activity, whereas intermediate $[Ca^{2+}]_{cyto}$ activates the opening of IP_3R. Therefore, a movement of Ca^{2+} from the area around IP_3Rs inhibits the opening of channels but also diminishes inhibition of channels mediated by Ca^{2+} that are already open, followed by, an increase of Ca^{2+} release (Jouaville et al., 1995).

1.5 Key components of the mitochondrial Ca^{2+} uptake machinery: The uniporter complex in the IMM

Since mitochondrial Ca^{2+} uptake widely varies among cells and tissues, and its channel opening strongly relies on the $[Ca^{2+}]_{cyto}$ that represents low capacity at resting level of Ca^{2+} and high activity as soon as Ca^{2+} signaling is activated, these features allow mitochondria to distinct from other organelles (De Stefani and Rizzuto, 2014). Such complexity requires specialized molecular machinery, where several primary components can be variably gathered together in order to match energy demands and protect from toxic stimuli (De Stefani et al., 2015). Importantly, a series of discoveries during the past decade highlight that the uniporter is not a single protein but rather a macromolecular complex and its molecular identities have been recently revealed by many researchers (Wang et al., 2015, Takeuchi et al., 2015, Foskett and Philipson, 2015, Finkel et al., 2015, De Stefani et

al., 2015). The uniporter complex includes pore-forming and various regulatory subunits, that are the channel subunit (MCU), the endogenous MCU dominant-negative protein (MCUb), the two Ca^{2+}-sensing regulatory proteins (MICU1 and MICU2), the essential MCU regulator (EMRE), and the MCU regulator 1 (MCUR1) (**Figure 1.5**, **Table 1**) (Wang et al., 2015).

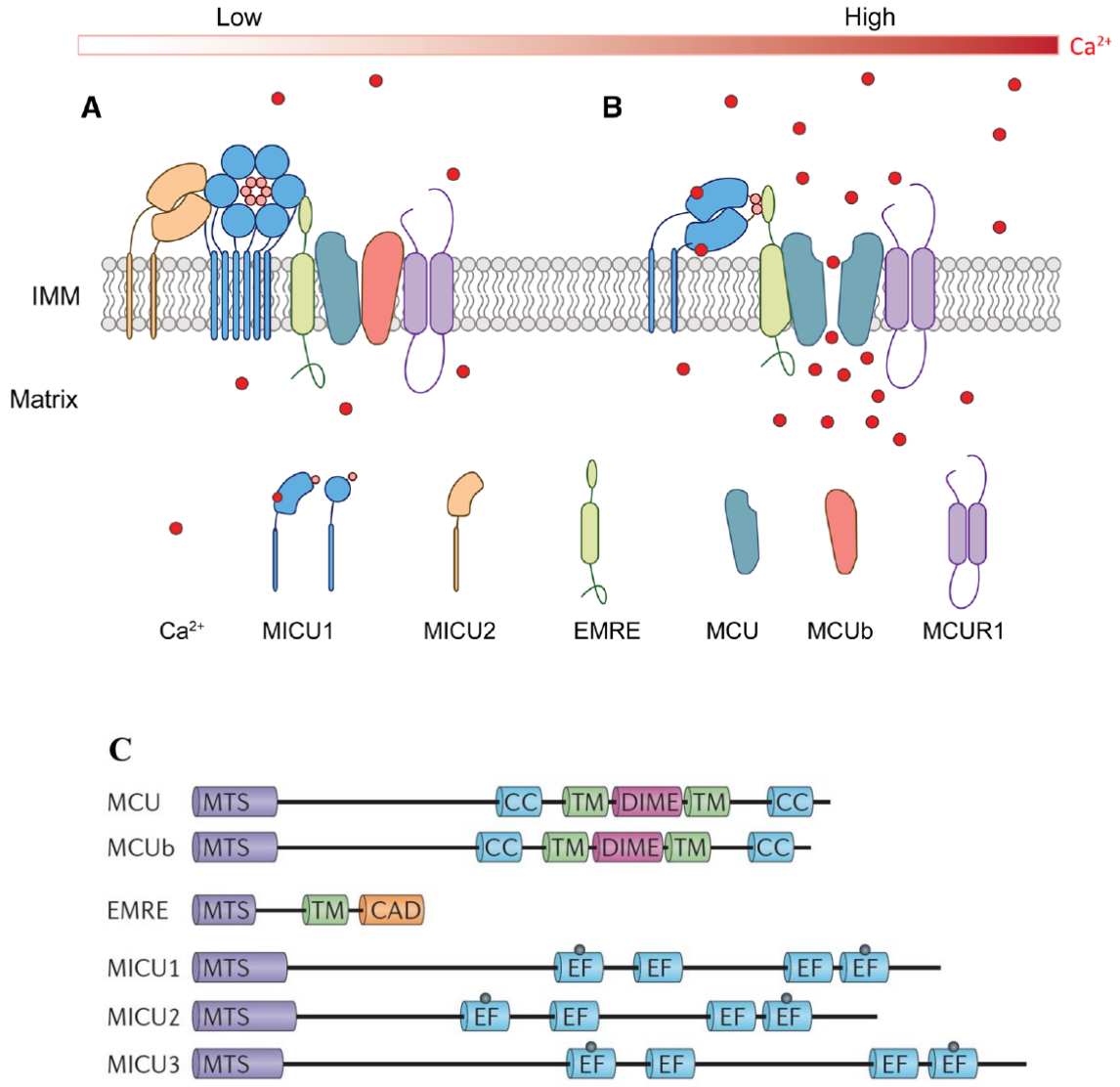

Figure 1.5: The principal components of the uniporter complex based on the current published data. Schematic representation of the MCU complex in the low Ca^{2+} state **(A)** and high Ca^{2+} state **(B)** [modified and adopted from (Wang et al., 2015)]. **(C)** The predicted domain architecture of the six *Homo sapiens* uniporter components. Black circles represent Ca^{2+}-binding sites. MTS; mitochondrial targeting signal, TM; transmembrane domain, EF; EF hand domain, CC; coiled-coil domain, CAD; carboxy-terminal acidic domain [Modified and adopted from (Kamer and Mootha, 2015)]

Table 1: The summarized table of the components found in the MCU complex based on current understanding of published data [Modified and adopted from (Marchi and Pinton, 2014)]

Name (Known as)	MW (kDa)	Topology	Functions	Ref
MCU (C10orf42, CCDC109A)	40→35	2-TMD N- and C-terminal span into the mitochondrial matrix	Channel-forming subunit of the uniporter complex Silencing of MCU diminishes Ca^{2+} uptake; overexpression of MCU potently increases Ca^{2+} entry	(Baughman et al., 2011, De Stefani et al., 2011)
MICU1 (CALC, CBARA1, EFHA3)	54→50	1-TMD Two EF-hands span into the IMS	MICU1 interacts with MCU Set a Ca^{2+} threshold of MCU Silencing of MICU1 increases the $[Ca^{2+}]_{mito}$ under resting conditions or during small cytosolic Ca^{2+} rises	(Perocchi et al., 2010, Mallilankaraman et al., 2012b, Csordas et al., 2013)
MICU2 (EFHA1)	50→45	1-TMD Two conserved EF-hands, probably faced on the IMS	MICU2 associates with the MCU/MICU1 complex Depletion of MICU2 reduces the mitochondrial Ca^{2+}uptake	(Plovanich et al., 2013)
MCUb (CCDC109B)	40→37	2-TMD N- and C-terminal span into the mitochondrial matrix	Paralog of MCU The expression is lower than MCU No Ca^{2+} channel activity Overexpression of MCUb decreases the mitochondrial Ca^{2+}entry	(Raffaello et al., 2013)
MCUR1 (C6ORF79, CCDC90A)	40→37	2-TMD N- and C-terminal span into the IMS Large portion of the protein faced on the mitochondrial matrix	MCUR1 interacts with MCU, but not with MICU1 Silencing of MCUR1 abolishes Ca^{2+} entry Overexpression of MCUR1 enhances the mitochondrial Ca^{2+} uptake	(Mallilankaraman et al., 2012a)
EMRE (C22ORF32, SMDT1)	12→10	1-TMD, highly conserved aspartate-rich tail	Diminution of EMRE diminishes mitochondrial Ca^{2+} entry EMRE is required for the interaction of MCU with MICU1/MICU2	(Sancak et al., 2013)

TMD; Transmembrane domain, MCU; Mitochondrial Ca^{2+} uniporter, MICU1; Mitochondrial Ca^{2+} uptake 1, MICU2; Mitochondrial Ca^{2+} uptake 2, MCUb; Mitochondrial Ca^{2+} uniporter b, MCUR1; Mitochondrial Ca^{2+} uniporter regulator 1, EMRE; Essential MCU regulator

1.5.1 Mitochondrial Ca^{2+} uptake 1 (MICU1)

MICU1 is the first protein in the uniporter complex characterized based on data from comparative physiology, evolutionary genomics, organelle proteomics and genome-wide RNAi screening and was found to be located in the IMM and expressed in most mammalian tissues (Perocchi et al., 2010, Collins and Meyer, 2010). MICU1 is a ~54-kDa protein with a N-terminal mitochondrial targeting sequence (MTS), a single

transmembrane domain (TMD), and a cytosolic C-terminal (aa 53-476) containing two conserve EF-hand domains, which are the binding sites of Ca^{2+} and regulate the activity of the MCU channel (Hajnoczky and Csordas, 2010). MICU1 and MCU are homologous in many organisms, such as metazoan, plants, and protozoa but not fungi (Bick et al., 2012). Their genes are adjacent and share a similar bidirectional promoter, which could be the mechanism for their coordinated expression (Baughman et al., 2011). In addition, MICU1 and MCU were represented to physically interact with each other from co-immunoprecipitation (co-IP) experiments (Baughman et al., 2011, Mallilankaraman et al., 2012b, Hoffman et al., 2013, Wang et al., 2014).

MICU1 is a fundamental component of the uniporter complex participating in the orchestrating of mitochondrial Ca^{2+} sequestration and its EF-hands take an important part in this process. Perocchi et al. (Perocchi et al., 2010) demonstrated the upon IP_3-mediated depletion of ER Ca^{2+} stores, the potent abrogation of mitochondrial Ca^{2+} entry was observed by shRNA knockdown of MICU1 in HeLa cells and could be fully rescued by overexpression of the MICU1 cDNA. On the other hand, the mitochondrial Ca^{2+} entry is ineffective to be restored by the expression of the EF-hands mutant MICU1. Moreover, diminution of MICU1 disrupted metabolic coupling between cytosolic Ca^{2+} transients and activation of matrix dehydrogenases, whereas Ψ_{mito} and respiration were unaltered.

However, Mallilankaraman et al. (Mallilankaraman et al., 2012b) later reported that MICU1 acts as a MCU gatekeeper. MICU1 keeps the MCU channel closed to preserve normal $[Ca^{2+}]_{mito}$ under resting conditions at low $[Ca^{2+}]_{cyto}$ (< 3 μM), whereas it has no function on Ca^{2+} uptake at higher $[Ca^{2+}]_{cyto}$. In the absence of MICU1, mitochondria become Ca^{2+} overload which leads to the accumulation of basal $[Ca^{2+}]_{mito}$ via MCU-induced Ca^{2+} mobilization, which thereby overstimulating ROS generation and increasing the sensitivity of apoptotic stress. Therefore, the main function of MICU1 is to set a Ca^{2+} threshold for mitochondrial Ca^{2+} entry mediated by MCU without changing its kinetic properties that are essential to prevent mitochondrial Ca^{2+} overload and associated stress. In addition, this gatekeeper function was not observed in the expression of the EF-hands mutant of MICU1, pointing that EF-hands serve a high-affinity $[Ca^{2+}]_{mito}$-sensing mechanism that allows MICU1 to exert its regulation when $[Ca^{2+}]_{cyto}$ is at resting states (<100 nM) to minimize uniporter activity (Kevin Foskett and Madesh, 2014, Mallilankaraman et al., 2012b).

The study of Csordas et al. (Csordas et al., 2013) confirmed the role of MICU1 as MCU gatekeeper, but on the other hand they showed that in the absence of MICU1,

mitochondrial Ca^{2+} uptake is less efficient. The MICU1 regulation of MCU-induced Ca^{2+} entry was dose-dependent depending on $[Ca^{2+}]_{cyto}$. MICU1 not only controls the threshold of MCU opening but also contributes to cooperative activation of the channel at high $[Ca^{2+}]_{cyto}$. These data thus indicated MICU1 is the main determinant of the sigmoidal response of organelle Ca^{2+} uptake to the $[Ca^{2+}]_{cyto}$. Loss of MICU1 in mouse liver and cultured cells resulted in Ca^{2+} accumulation in mitochondrial matrix during small $[Ca^{2+}]_{cyto}$ rises but attenuated response to agonist-induced $[Ca^{2+}]_{cyto}$ pulses. In contrast to the previous study (Mallilankaraman et al., 2012b), Csordas et al. reported that the mutation of EF-hands in MICU1 inhibits the uniporter at low $[Ca^{2+}]_{cyto}$, which shows the same response as in the wild-type MICU1 and could not handle a cooperative activation as the $[Ca^{2+}]_{cyto}$ increased. Therefore, MICU1 is a molecular switch that binds Ca^{2+} and strongly enhances MCU-mediated mitochondrial Ca^{2+} uptake. Since MICU1 does not bind Ca^{2+} under low $[Ca^{2+}]_{cyto}$, hence, Ca^{2+}-free MICU1 inhibits Ca^{2+} mobilization into mitochondria and sets a threshold for MCU. In contrast, rising of $[Ca^{2+}]_{cyto}$ enables MICU1 to bind Ca^{2+} and then activate mitochondrial Ca^{2+} entry. Nevertheless, the group of Wang et al. (Wang et al., 2014) later suggested that experimental condition is one of the factor that leads to varied results from different research groups, particularly the fluorescent dyes used for Ca^{2+} measurements. In order to avoid different interpretations, the fluorescent dye used for Ca^{2+} measurement should be well-selected based on the range of Ca^{2+} concentration imposed in the experiment. The Ca^{2+} affinity of MICU1 is ~15-20 μM, consequently, MICU1 shows fewer tendencies to bind Ca^{2+} in resting cells, which is in concordance with the model proposed by Csordas et al. (Csordas et al., 2013).

Recently, the crystal structures of Ca^{2+}-free and Ca^{2+}-bound human MICU1 was revealed in the study of Wang et al. (Wang et al., 2014) (**Figure 1.7**). The structure revealed that each MICU1 monomer contains an N-domain (residues 103-177), N-lobe (183-318), C-lobe (324-445) and a C-helix (445-465) in a structure encompassing residues 103 to the C-terminal at position 476. Each MICU1 molecule can bind two Ca^{2+} ions in canonical EF-hands. Ca^{2+}-free MICU1 forms a hexamer that interacts and blocks MCU activity. Upon Ca^{2+} binding, MICU1 changes its conformational structures, leading to the formation of multiple oligomers and activate MCU. In the Ca^{2+}-free conditions, the C-helix region of MICU1 hexamer packed in the center of the six molecules and forms a helix bundle, thus, inhibit the MCU activity. In contrast, deletion of the C-helix potently disrupts the MICU1-MCU interaction under both Ca^{2+}-free and Ca^{2+}-bound conditions;

consequently, mitochondrial Ca^{2+} uptake is deficit, indicating that the C-helix plays a main functional role that need to be present in the MICU1 crystal structure.

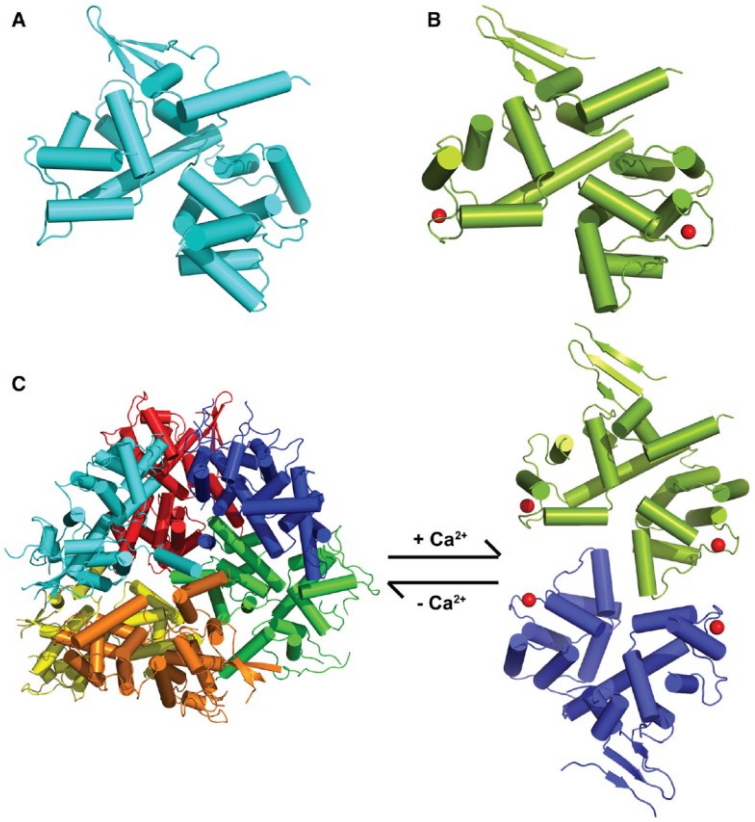

Figure 1.7: Conformational changes of MICU1 in the Ca^{2+}-free and Ca^{2+}-bound states. Ca^{2+} is shown in red. **(A)** Ca^{2+}-free MICU1 **(B)** Ca^{2+}-bound MICU1 **(C)** The rearrangement of MICU1 oligomer upon Ca^{2+} binding. The Ca^{2+}-free MICU1 hexamer is shown in red, blue, green, cyan, yellow and orange, respectively. The Ca^{2+}-bound MICU1 dimer is shown in green and blue, respectively [Modified and adopted from (Wang et al., 2015)].

Considering its topology, there is a controversy about the exact localization of MICU1 and the roles of its EF-hands. Nevertheless, accumulating data predicted that MICU1 includes a single TMD at its N-terminal and the large, soluble C-terminal of MICU1 is located in the IMS. This assumption is supported by the findings of several studies and is consistent with the function of MICU1 since it senses $[Ca^{2+}]_{cyto}$ change and regulates mitochondrial Ca^{2+} uptake induced by MCU (Wang et al., 2014, Csordas et al., 2013, Patron et al., 2014). On the contrary with other articles, Hoffman et al. (Hoffman et al., 2013) indicated that MICU1 was mainly localized in the matrix side of the IMM by using imaging tagged mitochondrial proteins in plasma membrane-permeabilized cells in response to OMM and IMM permeabilization and human MICU1 requires the polybasic

motif (aa 99-110) for MCU binding, whereas its EF-hands do not involve in this process. Nevertheless, Hung et al. (Hung et al., 2014) has recently performed APEX technology combined with stable isotope labeling amino acids in a cell culture (SILAC)-based ratiometric tagging techniques and reported MICU1 was detected in the IMS. In addition, Kamer et al. (Kamer and Mootha, 2014) and Wang et al. (Wang et al., 2014) found that the C-terminal helix (aa 445-476) of MICU1 has an impact to interact with MCU. Nevertheless, the actual localization of MICU1 has been under conflict and need more investigations since both recent proteomic data (Hung et al., 2014, Lam et al., 2015) and the resolution of its function (Patron et al., 2014) strongly represent that the MICU1, as well as the other members of the family, are soluble proteins of the IMS.

1.5.2 Mitochondrial Ca^{2+} uptake 2 (MICU2)

MICU2 shares ~25% sequence identity with MICU1 and contains two conserved EF-hands (Plovanich et al., 2013). MICU2 is widely expressed in diverse mouse tissues, especially visceral organs. The topology of MICU2 is similar to MICU1 as both of them located on the IMM with its N-terminal MTS. The stability of MICU2 highly depends on the presence of MICU1 at protein level since silencing of MICU1 largely decreased protein expression of MICU2, whereas it had no effect on mRNA expression (Patron et al., 2014, Kamer and Mootha, 2014, Plovanich et al., 2013). Therefore, loss of MCU gatekeeping function in the absence of MICU1 described in the previously reported (Mallilankaraman et al., 2012b, Csordas et al., 2013), is likely to be due to the concomitant loss of MICU2 (De Stefani et al., 2015). However, diminution of MICU2 reduced MICU1 expression only in HeLa cells but not in HEK293T cells.

Recently, Kamer et al. (Kamer and Mootha, 2014) has been reported that the threshold for mitochondrial Ca^{2+} entry is changed by silencing of MICU1 or MICU2. Moreover, the mutation of MICU1 or MICU2 EF-hands diminishes the coordinated function of mitochondrial Ca^{2+} entry, leading to a non-redundant role of MICU1 and MICU2 in modulating MCU-mediated Ca^{2+} uptake. Although MICU2 did not involve with the MCU complex in the absence of MICU1, MICU1 still participates in MCU complex with the lacking of MICU2. In the same way, EF-hands-deficit MICU1 inhibited mitochondrial Ca^{2+} entry in the absence of MICU2, whereas no effect was detected from EF-hands-deficit MICU2 in the depletion of MICU1 (Kamer and Mootha, 2014, Ahuja and Muallem, 2014).

Patron et al. (Patron et al., 2014) reported that MICU1 and MICU2 physically interact with each other by forming the heterodimer via a disulfide bond in intact cells. In addition, the MICU1-MICU2 dimer interaction is highly engaged with the short loop between the 2-TMD of MCU, and hence, is interfered by the mutation of the acidic residues in this loop. In the presence of a large driving force, MICU2 exhibits the inhibitory effect to keep minimal Ca^{2+} accumulation under low $[Ca^{2+}]_{cyto}$, thus, prevents the detrimental effects of Ca^{2+} overload. When $[Ca^{2+}]_{cyto}$ increases, Ca^{2+} rapidly mobilized into mitochondrial matrix by an activation of MICU1 and inhibition of MICU2, consequently, induced aerobic metabolism and increasing ATP production. In addition, Patron et al. verified that MICU2 is an MCU inhibitor. In conclusion, MICU1 and MICU2 form a regulatory dimer and modulate MCU with opposing effects.

1.5.3 Mitochondrial Ca^{2+} uniporter (MCU)

MCU, a 40-kDa protein located at the IMM, was identified in 2011 and ubiquitously expressed in all eukaryotes except for yeast (Bick et al., 2012). The MCU is predicted to compose of two coiled-coil domains and 2-TMD connected with a short loop containing several acidic-residues known as the DIME motif, which are highly conserved among MCU orthologs (Baughman et al., 2011, De Stefani et al., 2011). For its topology, the N- and C-terminal of MCU are located in the mitochondrial matrix and the linker between 2-TMD faces into the IMS (Baughman et al., 2011, Csordas et al., 2013, Martell et al., 2012). Recently, MCU has been reported to contribute to the uniporter pore and arranges as a tetramer by a co-IP experiment (Raffaello et al., 2013).

Several lines of evidence support that MCU is the pore forming domain of the uniporter. In the model of intact cells, permeabilized cells and purified mouse liver mitochondria, Baughman et al. (Baughman et al., 2011) demonstrated that diminution of MCU substantially reduced $[Ca^{2+}]_{mito}$ upon an extra-mitochondrial Ca^{2+} readdition or histamine stimulation, whereas $[Ca^{2+}]_{cyto}$ was unchanged. Moreover, other mitochondrial properties, including O_2 consumption, ATP synthesis, Ψ_{mito}, and mitochondrial morphology had no effect by deletion of MCU. In addition, Baughman et al. (Baughman et al., 2011) reported that reconstitution of recombinant human MCU into planar lipid membranes generated single channel Ca^{2+} currents and the channel activity was inhibited by RuR and activated by strongly hyperpolarized voltages. In addition, no channel activity and substantially abolished mitochondrial Ca^{2+} uptake was observed by the site-specific mutation of two acidic residues (D261A and E264A) in the DIME motif, which is in line

with the study reported by Kirichok et al (Kirichok et al., 2004). Furthermore, a mutant MCU with replacement of a serine residue in the DIME motif with alanine (S259A) was recorded by patch clamping of mitoplasts to confirm that MCU is the pore forming subunit and they found that the RuR sensitivity of uniporter currents was abrogated (Baughman et al., 2011). Recently, Kovacs-Bogdan et al. (Kovacs-Bogdan et al., 2014) reported that expression of *Dictyostelium* MCU could reconstitute RuR-sensitive mitochondrial Ca^{2+} entry in yeast that lacks all uniporter components. In contrast, *Dictyostelium* MCU with the mutated acidic residues of the DIME motif was inactive. Taken together, these results confirm that MCU is the Ca^{2+} pore.

Recently, the role of MCU as a necessary component for the mitochondrial Ca^{2+} entry was confirmed in different cell tissues, for instance liver (Baughman et al., 2011), heart (Joiner et al., 2012), neonatal rat cardiac myocytes (Drago et al., 2012), pancreatic β-cells (Alam et al., 2012, Tarasov et al., 2012), and neurons (Qiu et al., 2013). Analysis of isolated organelles from many tissues of MCU knockout mice also showed the deficit of the ability to transport Ca^{2+} into mitochondrial matrix, highlighting the importance of MCU (Pan et al., 2013). However, it was clearly represented that MCU alone could not finely tune the mitochondrial Ca^{2+} signals within the cell, also other components within the MCU complex bring significantly importance, particularly after the identification of two components of the channel, especially MCUb (Raffaello et al., 2013) and EMRE (Sancak et al., 2013).

1.5.4 Mitochondrial Ca^{2+} uniporter b (MCUb)

MCUb (originally reported as CCDC109B) is a paralog of MCU with 50% sequence identity and similar predicted topological features, possesses two coiled-coil domains and 2-TMD separated by a short loop that slightly differs from MCU. The MCUb gene is present in most of the vertebrates but does not exist in some organisms, such as *Kinetoplastids*, *Nematoda* and *Arthropoda*. MCUb is located on the IMM and contains ~330 aa (Pendin et al., 2014). The study of Raffaello et al. (Raffaello et al., 2013) showed that MCU forms a multimer (tetramer) in which MCU oligomerizes as homo- or hetero-oligomer with MCUb. In addition, silencing of MCUb significantly increased mitochondrial Ca^{2+} entry in HeLa cells upon histamine challenging, whereas MCUb overexpression greatly reduced the uptake of Ca^{2+} into mitochondria. Moreover, the insertion of a recombinant MCUb within the oligomer could efficiently inhibit the activity of Ca^{2+} channel since no current was observed when Ca^{2+} used as permeating ion in the

medium and co-expression of MCU and MCUb markedly decreased the open probability in planar lipid bilayer, even when MCUb is present in low amount. Notably, MCU and MCUb have distinct expression profiles; hence, the relative expression of these both proteins may explain the magnitude of the Ca^{2+} permeability (Raffaello et al., 2013). Therefore, MCUb is an endogenous dominant-negative subunit of the MCU complex, which changes Ca^{2+} permeation across the heteromeric channel. Sancak et al. (Sancak et al., 2013) also found that MCUb is a component of the MCU complex.

1.5.5 Essential MCU regulator (EMRE)

EMRE, an additional component of the MCU complex discovered by Sancak et al., is a 10-kDa, metazoan-specific IMM protein with a 1-TMD and possesses a highly conserve C-terminal rich in aspartate residues, with its topology remains unclear (Sancak et al., 2013). Like MCU and MICU1, EMRE was identified by proteomic analysis of mitochondria and ubiquitously expressed among mammalian tissues and its protein stability depends upon the presence of MCU (Pagliarini et al., 2008). EMRE homologs are absent in plants, fungi, or protozoa, where MCU and MICU1 are highly conserved. In HeLa cells and permeabilized HEK-293T, silencing of EMRE abrogated mitochondrial Ca^{2+} sequestration after histamine stimulation. EMRE is required for Ca^{2+} channel activity and keeps the MICU1-MICU2 dimer interacted to the MCU complex since deletion of EMRE abolished the interaction between MICU1-MICU2 and MCU. Reduction of the uniporter complex size to ~300-kDa on a native gel, which is identical to MICU1-lacking cells, was observed by deletion of EMRE. Therefore, Sancak et al. (Sancak et al., 2013) suggested that EMRE interacts with MICU1-MICU2 in the IMS and with MCU oligomers in the IMM, therefore bridging the calcium-sensing role of MICU1 and MICU2 with the channel-conducting activity of MCU. Nevertheless, the molecular details of its interactions with MCU and MICU1 are needed to be further investigated.

Remarkably, Kovacs-Bogdan et al. (Kovacs-Bogdan et al., 2014) noted that although EMRE is absent in some organisms that express MCU, including *Dictyostelium discoideum*, *Dictyostelium* uniporter activity is still present. In addition, mitochondrial Ca^{2+} entry could be restored by adding a recombinant *Dictyostelium* MCU in MCU knockout mammalian cells. However, expression of *Dictyostelium* MCU did not rescue expression of EMRE, but *Dictyostelium* MCU was functional in EMRE knockout cells, indicating that *Dictyostelium* MCU can function in the absence of EMRE in mammalian cells, in contrast to mammalian MCU.

1.5.6 Uncoupling protein 2 and 3 (UCP2/3)

UCP2/3 is located in the IMM and creates proton leaks which uncoupling oxidative phosphorylation from ATP synthesis (Stuart et al., 2001). For its structure, UCP2/3 consists of 6-TMD form a channel-like structure which can be divided into three pseudo repeats with similar folds and each of the 2-TMD, along with the loop and amphipathic helix between them, forms a repeat (Berardi et al., 2011). Trenker et al. (Trenker et al., 2007) discovered that UCP2/3 is crucial for the MCU activity by using overexpression, siRNA and mutagenesis experiments. In addition, the RuR-sensitive Ca^{2+} uptake was abolished in mitochondria isolated from liver of UCP2-/- knockout mice. UCPs belong to a family of H^+ channels/transporters, which their prototype is UCP1, the protein responsible for the physiological uncoupling of brown adipose tissue in mitochondria (Nicholls and Rial, 1999, Ricquier and Bouillaud, 2000). Neither UCP2 nor UCP3 is expressed in budding yeasts (Trenker et al., 2007). Trenker et al. found that silencing of UCP2/3 dramatically reduced mitochondrial Ca^{2+} entry, whereas overexpression of UCP2/3 enhanced the sequestration of Ca^{2+} into mitochondrial matrix (Trenker et al., 2007). In addition, both of them had no influence on mitochondrial Ca^{2+} handling when expressed in budding yeast, indicating it is unlikely that UCP2/3 transports Ca^{2+} directly into mitochondria, but UCP2/3 is modulator of MCU and not MCU itself (Trenker et al., 2007). Nevertheless, the involvement of these proteins in mitochondrial Ca^{2+} uptake remains unclear and need more investigation.

1.5.7 Mitochondrial Ca^{2+} uniporter regulator 1 (MCUR1)

In order to identify other components of the Ca^{2+} uptake machinery, Mallilankaraman et al. (Mallilankaraman et al., 2012a) performed a direct human RNAi screen of 45 mitochondrial membrane proteins in HEK293T cells predicted to be part of the IMM and reported that MCUR1 plays an important role in mitochondrial Ca^{2+} uptake. MCUR1 (also known as CCDC90A) is a ~40-kDa protein located in the IMM containing 2-TMD with N- and C-terminal facing to the IMS and a connecting loop present in the matrix. MCUR1 has a wide distribution, including the heart. MCUR1 interacts with MCU and regulates MCU-mediated Ca^{2+} uptake. Diminution of MCUR1 is not only extensively inhibiting agonist-induced mitochondrial Ca^{2+} entry, but also leads to decreased basal $[Ca^{2+}]_{mito}$. From Co-IP experiment, MCUR1 did not interact with MICU1, while both MCUR1 and MICU1 could bind with MCU, demonstrating that it is feasible MCU has different components in the complexes. Furthermore, knockdown of MCUR1 causes

oxidative phosphorylation disruption, AMP-activated protein kinase (AMPK) activation, and autophagy induction. However, the recent report of Paupe et al. (Paupe et al., 2015) is contradictory with the previous study since they demonstrated that diminution of MCUR1 results in a reduction of Ψ_{mito} that correlates with a decrease of complex IV assembly and activity, leading to the declination of $[Ca^{2+}]_{mito}$. In contrast, this alteration of Ψ_{mito} was not detected in the study of Mallilankaraman et al. Therefore, the involvement of MCUR1 in uniporter activity might be indirect, probably through effects on the respiratory chain, which produce the driving force to transport Ca^{2+} into mitochondria. Even though, it is believed that MCUR1 is one of the critical components of the MCU complex, further investigation is still in demand.

1.5.8 Others

In addition to the uniporter complex, several types of mitochondrial Ca^{2+} uptake related transporters or modulators have been studied (Dedkova and Blatter, 2013), for instance leucine zipper-EF-hand-containing transmembrane protein 1 (LETM1), mitochondrial ryanodine receptor (mRyR1), rapid mode of Ca^{2+} uptake (RaM), mitochondrial Ca^{2+} current type 2 (mCa2), and canonical transient receptor potential channel 3 ($TRPC_3$) (Feng et al., 2013).

Leucine zipper EF hand-containing transmembrane protein 1 (LETM1)

LETM1 is a highly conserved eukaryotic protein located in the IMM (Hashimi et al., 2013, Nowikovsky and Bernardi, 2014). Even though, LETM1 was firstly identified as a mitochondrial K^+/H^+ exchanger which was supported by several studies in yeast, mammals, and Drosophila (Hashimi et al., 2013, Nowikovsky et al., 2004, Dimmer et al., 2008), its actual function is still ambiguous. However, genome-wide siRNA screening in Drosophila suggested that LETM1 is a Ca^{2+}/H^+ exchanger and is inhibited by RuR (Jiang et al., 2009). Nevertheless, the recent study performed in liposomes containing purified LETM1 protein indicated that LETM1 is a Ca^{2+}/H^+ antiporter but it is insensitive to RuR (Tsai et al., 2014). In addition, LETM1 has been reported to mainly involve with mitochondrial Ca^{2+} uptake from the SOCE in endothelial cells (Waldeck-Weiermair et al., 2011). Although LETM1 has been shown to contribute with the processes of mitochondrial Ca^{2+} influx and efflux, its effect has a tendency to be mediated through other mechanisms which are independent of the uniporter complex (Kamer and Mootha, 2015).

Mitochondrial ryanodine receptor (mRyR1)

mRyR1 is a ryanodine receptor located in the IMM (Ryu et al., 2010) and has been reported to be involved with Ca^{2+} movement into mitochondrial matrix of cardiomyocytes and neurons (Beutner et al., 2001, Jakob et al., 2014). In response to cytosolic Ca^{2+} rise, mRyR accumulate Ca^{2+} into mitochondrial matrix and is inhibited by high concentrations of ryanodine and RuR (Beutner et al., 2001, Beutner et al., 2005, Altschafl et al., 2007, Ryu et al., 2011). More importantly, it was found that mRyR1 generated a large Ca^{2+}-sensitive conductance (500-800 pS) in a lipid bilayer experiments (Altschafl et al., 2007). Therefore, mRyR may be another mitochondrial Ca^{2+} uptake pathway.

Rapid mode of Ca^{2+} uptake (RaM)

RaM was first described in isolated mitochondria by Sparagna et al. (Sparagna et al., 1995). RaM is another pathway of MCU-independent mitochondrial Ca^{2+} uptake that can be activated by low $[Ca^{2+}]_{cyto}$ and inhibited by RuR. RaM has a role in the beginning of each cytosolic Ca^{2+} pulses and enables mitochondria to rapidly uptake Ca^{2+} from short pulses. In addition, this entry quickly resumes between pulses, which facilitate a mitochondrial response to repetitive Ca^{2+} transients (Sparagna et al., 1995, Buntinas et al., 2001).

Mitochondrial Ca^{2+} current type 1 and 2 (mCa1 and mCa2)

mCa1 and mCa2, identified in the study of Michels et al. (Michels et al., 2009) by direct electrophysiological recordings in isolated mitoplasts, are a voltage-gated mitochondrial Ca^{2+} selective channel similar to MCU and RaM (for mCa1 and mCa2, respectively). mCa2 is RuR-insensitive and has low sensitivity (Michels et al., 2009).

Canonical transient receptor potential channel 3 (TRPC3)

TRPC3 is a member of the superfamily of transient receptor potential channels (TRPC) and permeable to all cations (Ca^{2+}, Na^{+} and K^{+}) (Beech et al., 2009). For its structure, a domain of TRPC3 is localized to the IMM. It has been found that TRPC3 overexpression together with MCU silencing in HeLa cells presented mitochondrial Ca^{2+} uptake under high $[Ca^{2+}]_{cyto}$ condition, indicating that it is likely that TRPC3 channel is one of the targets that have a role in mitochondrial Ca^{2+} uptake (Feng et al., 2013).

In summary, the mechanisms of the mitochondrial Ca^{2+} uptake machinery have been extensively investigated by many research groups. Although it has been established for a long time that mitochondria take up Ca^{2+} by mitochondrial Ca^{2+} uniporter complex, the molecular components of this sophisticated complex as well as several regulators have been recently identified and revealed. Nevertheless, numerous questions about the regulation of uniporter complex in some certain conditions by its regulators and its topology are still raising and need a clear answer. In the future, more comprehensive studies will help us to broaden our understanding of mitochondrial Ca^{2+} uptake and pave the way for identification and development of promising pharmacological tools in this research area.

1.6 Aims of the study

Recently, several proteins located in the IMM have been described to be essential for mitochondrial Ca^{2+} uptake, including MCU, MICU1, UCP2/3, EMRE, and MCUR1. Although, the characteristics and physiological consequences of mitochondrial Ca^{2+} sequestration have been reported, the complete mechanistic of protein interactions involved in this phenomenon is still unclear. In addition, the Ca^{2+}-sensing gatekeeper function of MICU1 has been already extensively investigated for MCU that together with the EMRE forms the mitochondrial Ca^{2+} channel. However, mechanisms by which MICU1 controls MCU and EMRE activity to finely tune mitochondrial Ca^{2+} signals remain ambiguous and still need an appropriate approach for deeper investigations. This current work was performed to achieve the following objectives:

- To investigate the contribution of MCU, MICU1, UCP2/3, EMRE, and MCUR1 in mitochondrial Ca^{2+} uptake and their interaction involved with this phenomenon
- To establish a FRET-based live-cell imaging approach to dynamically monitor the kinetics of the structural reorganization of MICU1 oligomers and to explore its dependence from cytosolic and mitochondrial Ca^{2+} signals as well as Ψ_{mito}
- To identify whether the expression levels of MCU and EMRE have an influence on the Ca^{2+}-sensitive rearrangement of MICU1 multimers

CHAPTER II
MATERIALS AND METHODS

2.1 Chemicals

All reagents and chemicals for buffers and solutions were obtained from Carl Roth (Karlsruhe, Germany). Chemical reagents used in this study including their inherent activities were listed in the **Table 2**.

Table 2: Chemical reagents used for this study

Name	Company	Working conc.	Activities
Histamine	Sigma-Aldrich (Vienna, Austria)	100 µM	Endogenous H_1 and H_2 histamine receptor agonist; H_1 activation mobilizes Ca^{2+} from internal stores (Fu et al., 1997)
BHQ	Sigma-Aldrich (Vienna, Austria)	15 µM	SERCA inhibitor (selective and reversible) (Hassessian et al., 1994)
Ionomycin	Abcam Biochemicals (Cambridge, UK)	3-10 µM	Ca^{2+} ionophore, depolarizes mitochondrial membrane, promotes the equilibrium of Ca^{2+} gradients between cellular compartments (mitochondria, ER, and cytosol) (Abramov and Duchen, 2003)
Oligomycin	Abcam Biochemicals (Cambridge, UK)	2 µM	F_1F_0 ATP synthase inhibitor (Nagamune et al., 1993)
FCCP	Abcam Biochemicals (Cambridge, UK)	2 µM	Protonophore (H^+ ionophore), chemical uncoupler of oxidative phosphorylation in mitochondria; depolarizing plasma and IMM (Rey et al., 2010)
Fura-2/AM	TefLabs (Austin, Texas, US)	2 µM	Synthetic Ca^{2+} fluorescent indicator. Upon incubation, the compound selectively accumulates in the cytosol and allows ratiometric imaging of changes in $[Ca^{2+}]_{cyto}$ (Contreras et al., 2010)
EGTA	Sigma-Aldrich (Vienna, Austria)	1 mM	Chelating agent useful for Ca^{2+} ions determination in the presence of Mg^+ (Brauner and Fridlender, 1981)

2.2 Cell culture

Cell culture materials were obtained from PAA Laboratories (Pasching, Austria). Our experiments were performed in the HeLa cells, human umbilical vein endothelial cell line EA.hy926, and rat insulinoma cell line INS-1 832/13 (INS-1) grown on glass cover slips (Ø=30 mm) in 6-well plates at passage >50. For certain experiments, the HeLa SilenceX® knockdown cells (Tebu-bio, Le-Perray-en-Yvelines, France) stably expressing

scrambled siRNA (shControl), or siRNA against MCU (MCU^{kd}) or UCP2 ($UCP2^{kd}$) were employed. HeLa cells were grown in Dulbecco's Modified Eagle Medium (DMEM) supplemented with 10% fetal calf serum (FCS), 100 units/mL penicillin, 100 µg/mL streptomycin. For EA.hy926 cells, the culture medium was additionally supplemented with 1% HAT (5 mM hypoxanthin, 20 µM aminopterin and 0.8 mM thymidine). INS-1 cells were grown in RPMI-1640 (RMPI) medium containing 10 mM glucose supplemented with 10 % FCS, 10 mM HEPES, 100 units/mL penicillin, 100 µg/mL of streptomycin, 1 mM sodium pyruvate, and 50 µM β-mercaptoethanol. All cell lines were cultured in a humidified incubator at 37 °C and 5% CO_2 for 24-48 hours prior experiments.

2.3 Plasmids and small interfering RNA (siRNA)

The siRNAs and overexpression approaches were applied to investigate the function of target proteins throughout the present study. The siRNA was used to diminish the gene expression and cDNAs cloned in an expression plasmid was used for a gene overexpression. For engineering MICU1-CFP and MICU1-YFP the coding sequence (cds) of human MICU1 (hMICU1, NM_006077.3) without a stop codon was amplified from a HeLa cDNA by PCR using primers: forward: 5′-ACGGATCCACCATGTTTCGTCTGAA CTCAC-3′ and reverse: 5′-ACGAATTCCTGTTTGGGTAAAGCGAAGTCC-3′. The PCR fragment was cloned in a pcDNA3.1(+) vector via BamHI and EcoRI sites. The cds of either enhanced cyan fluorescent protein (CFP) or citrine (YFP) were amplified with the same primers; forward: 5′-AAGAATTCATGGTGAGCAAGGGCGAGGAG-3′ and reverse: 5′-CCTCTAGAACTTGTACAGCTCGTCCATGC-3′ and each C-terminally fused to hMICU1 using the EcoRI and XbaI sites. EF hand mutated MICU1 and O-GECO1 constructs were purchased from Addgene (Cambridge, MA, USA). The MICU1 with mutated EF hand (EFmut) was amplified using the same primers as described above and C-terminally fused with either ECFP or citrine like the wild-type MICU1. To generate a mitochondrial targeted mtO-GECO1, the O-GECO1 construct was amplified using forward primer 5′-AACTCGAGTATGGTCGACTCATCACGTCG-3′ and reverse primer 5′-GCAAGCTTTTACTTCGCTGTCATCAT-3′. The PCR fragment was N-terminally fused with the MTS (4mt) via XhoI and HindIII restriction sites in a pcDNA3.1(-) vector. Sensor 4mtD1GO-Cam was constructed as previously described (Waldeck-Weiermair et al., 2012) and 4mtD3cpV (Mt-cameleon-pcDNA3) was supported by Prof. Dr. Roger Tsien. All primers used in this study were obtained from Invitrogen (Vienna, Austria).

A siRNA is an effective approach to transiently knockdown the expression of a specific gene which its effect can be measured at functional level within 48-96 hours after transfection. All siRNAs used in this study were designed by a web-based tool provided on the website of Microsynth AG, Switzerland. The siRNAs against various proteins found in human IMM; hMICU1, hMCU, hEMRE, hUCP2, hUCP3, and hMCUR1 were obtained from Microsynth (Balgach, Switzerland) and their nucleotide sequences were represented as followed (5′-3′);

Negative control-si	5′-UUCUCCGAACGUGUCACGU-3′
hMICU1-si1	5′-GCAGCUCAAGAAGCACUUCAA-3′
hMICU1-si2	5′-GCAAUGGCGAACUGAGCAAUA-3′
3′UTR-MICU1-si*	5′-AGAAGUCUGUGAUGAUAAA-3′

(*; binds in the non-coding 3′ terminal untranslated region (UTR) of MICU1)

hMCU-si1	5′-GCCAGAGACAGACAAUACU-3′
hMCU-si2	5′-GGAAAGGGAGCUUAUUGAA-3′
hEMRE-si	5′-GAACUUUGCUGCUCUACUU-3′
hUCP2-si	5′-GCACCGUCAAUGCCUACAA-3′
hUCP3-si	5′-GGAACUUUGCCCAACAUCA-3′
hMCUR1-si1	5′-GAACAGAAAUAGUGGCAUU-3′
hMCUR1-si2	5′-UGAUAACACUGGUGAAUUU-3′

2.4 Transfection of cells

Fluorescent protein (FP)-tagged constructs alone or together with siRNAs was delivered into cells by using cationic liposomes designed for transient transfection, TransFast™ transfection reagent (Promega, Madison, WI). TransFast™ was prepared and used according to the manufacturer's instructions. Transient transfection protocols are briefly described in details below.

2.4.1 Transfection of plasmid DNA

Cells were seeded on glass cover slips (Ø=30 mm) in 6-well plates for 24-48 hours prior to transfection (at 60-80% confluence). The transfection mixture was prepared in DMEM medium (without serum and antibiotics/antifungals) using TransFast™. For each well, 1 mL of serum- and antibiotic-free DMEM medium, 1.5-2 μg of plasmid DNA encoding the respective FP-tagged construct and 4μL/well of TransFast™ were prepared. The transfection mixture was briefly vortexed and incubated at room temperature for 10-15

minutes to allow the formation of cationic liposomes. After removal of the growth medium, the cells were washed one time with phosphate-buffered saline (PBS) and incubated afterwards with 1 mL of the transfection mixture for 4 hours at 37 °C and 5% CO_2. Then, transfection mixture was removed and cells were incubated with complete DMEM medium. All experiments were performed 48-72 hours after transfection.

2.4.2 Transfection of siRNA together with plasmid DNA

When cells were transfected with plasmid DNA together with respective siRNA, a slightly modified protocol was applied. Cells on glass cover slips (at 60-80 % confluence) in 6 well plates were transfected with plasmid DNA in combination with either specific siRNA or scrambled control siRNA. For each well, 0.5 mL of serum- and antibiotic-free DMEM medium, 1.5-2 µg of plasmid DNA, 100-200 pmoles of siRNA and 4µL/well of TransFast™ were mixed well and incubated at room temperature for 10-15 minutes. After washing cells once with PBS, the transfection mixture was gently added onto the cells and kept in a humidified incubator (37 °C, 5% CO_2) for 1 hour. Subsequently, additional 0.5 mL DMEM was added in each well upon completion of 1 hour incubation period and further incubated for overnight. After overnight incubation, the transfection medium was replaced with complete DMEM medium and experiments were performed 48-72 hours after transfection.

2.5 Ca^{2+} measurement

2.5.1 Buffer solutions for Ca^{2+} imaging experiments

Prior to experiments cells were washed and stored for 15 minutes in a HEPES buffered solution (EH-buffer) containing: 138 mM NaCl, 2 mM $CaCl_2$, 5 mM KCl, 1 mM $MgCl_2$, 1 mM HEPES, 2.6 mM $NaHCO_3$, 0.44 mM KH_2PO_4, 0.34 mM Na_2HPO_4, 10 mM D-glucose, 0.1 % vitamins, 0.2 % essential amino acids and 1% penicillin/streptomycin; pH adjusted to 7.4 with NaOH or HCl. During the experiments cells were perfused with a Ca^{2+} containing experimental buffer (EB-buffer), which consisted of: 145 mM NaCl, 2 mM $CaCl_2$, 5 mM KCl, 1 mM $MgCl_2$, 10 mM HEPES, and 10 mM D-glucose; pH adjusted to 7.4 with NaOH or HCl. To achieve a nominal Ca^{2+} free environment, where a Ca^{2+} free buffer (Ca^{2+} free EB-buffer) was applied to the cells, the 1 mM EGTA was added instead of 2 mM $CaCl_2$. For dissociation constant (K_d) determination of MICU1 FRET, we used the same buffer containing 3 mM EGTA supplemented with 3-10 µM ionomycin and

$CaCl_2$ was added according to the CaBuff software (G. Droogmans, Fysiologie, Leuven) to obtain buffer solutions of 0.1, 1, 10, 100 and 1000 μ M free Ca^{2+} concentrations.

2.5.2 Mitochondrial Ca^{2+} measurements

Numerous types of Ca^{2+} indicators were developed in order to achieve the accurate quantification of intracellular Ca^{2+} concentration (usually determined as spectrophysical properties: fluorescence intensity and wavelength shift) in each organelle of living cells and further reduce concomitant pitfalls, for example unstable stoichiometry, low signal-to-noise ratio, and limited integration into the targeted organelles (Contreras et al., 2010). The Förster resonance energy transfers (FRET)-based Ca^{2+} sensors were the main molecular tool in this study to determine mitochondrial Ca^{2+} uptake.

FRET-based Ca^{2+} measurements

FRET-based Ca^{2+} sensors is a genetically encoded Ca^{2+} indicators (GECIs) that are commonly used as they have advantages among others, such as precise and long-term expression when trapped into the genome, less toxicity, and highly selective targeting to subcellular compartments (Contreras et al., 2010) by including specific target signal peptides into the sequence of GECIs (De Giorgi et al., 1999, Filippin et al., 2005, Palmer and Tsien, 2006). These ratiometric Ca^{2+} sensors consist of a Ca^{2+} binding peptide, the calmodulin (CaM) and its interacting peptide from the myosine light chain kinase (M13) which were fused in tandem between two different FPs possessing overlapping spectral properties (CFP and YFP) and occupying of Ca^{2+} to CaM resulted in a conformational change, thereby brings the two fluorophores in close vicinity enabling energy transfer from CFP (FRET-donor) to YFP (FRET-acceptor) and yielding an increase of the FRET signal between these two FPs (Nagai et al., 2001, Miyawaki et al., 1997). Then, the FRET ratio can be quantified by calculating the ratio of fluorescent emissions measured at 535 nm and 480 nm of excitation. In our study, the 4mtD3cpv cameleon and its red-shifted variant the 4mtD1GO-Cam were used to monitor the change of $[Ca^{2+}]_{mito}$ in the living cells. The 4mtD3cpv was developed in order to reduce interference from endogenous CaM by engineering both CaM and M13. This sensor encompasses a CFP and a circularly permuted Venus (D-cpv) as FRET-donor/acceptor fluorophore pair and contains a tandem duplicated targeting sequence of cytochrome C oxidase VIII, which selectively targets the sensor to mitochondrial matrix (Palmer et al., 2006). The excitation of 4mtD3cpv sensor is 430 nm and the emission ranges are 460-500 nm and 525-580 nm for CFP and YFP, respectively

(Palmer et al., 2006). HeLa cells were transfected with 4mtD3cpv and respective siRNA/plasmid DNA as described in *2.4 Transfection of cells*.

Single FP-based Ca^{2+} measurements

In some experiments, the mitochondrial targeted O-GECO1 sensor (mtO-GECO1) was used to observe an alteration of $[Ca^{2+}]_{mito}$ in order to avoid a spectral overlap of the FP-tagged MICU1 with 4mtD3cpv sensor which is based on the similar FPs (CFP and YFP). The mtO-GECO1 is a GECI that is classified as single FP-based Ca^{2+} sensors. Single FP-based Ca^{2+} sensors consist of a circularly permuted FP flanked by CaM and M13 (Contreras et al., 2010). The binding of Ca^{2+} ions to CaM domain leads to an alteration of the excitation spectrum of circularly permuted FP and accordingly the $[Ca^{2+}]$ is directly obtained from the ratio between two excitation wavelengths (Nagai et al., 2001). These class of probes include the pericams (Nagai et al., 2001), the GCamPs (Nakai et al., 2001) and the GECOs (Zhao et al., 2011). In this experiment, HeLa cells were transiently transfected with mtO-GECO1 as mentioned in *2.4 Transfection of cells*.

2.5.3 MICU1-FRET rearrangement

The rearrangement of MICU1 multimers was monitored by measuring intermolecular FRET between MICU1-CFP and MICU1-YFP (citrine). In the present study, HeLa cells were transiently transfected with the respective FP-tagged MICU1 constructs in the ratio of 1:1 with either control or specific siRNA as indicated in *2.4 Transfection of cells*.

2.5.4 Cytosolic Ca^{2+} measurements

Fura-2 measurements

An alteration of $[Ca^{2+}]_{cyto}$ was measured with fluorescent microscope using Fura-2 acetoxymethyl ester (Fura-2/AM). Fura-2/AM is the synthetic fluorescent indicator that could be easily delivered inside the cells through plasma membrane by incubation. Since the cellular esterases that hydrolyze the AM forms are primarily located in the cytoplasm, these indicators mainly accumulate in the cytosol and cannot be specifically targeted to other subcellular compartments (Contreras et al., 2010). Fura-2 is a dual excitation indicator (340 and 380 nm) and allows a ratiometric imaging of $[Ca^{2+}]_{cyto}$ with the K_d for Ca^{2+} of 0.224 μM. The peak excitation of Fura-2 shifts from 340 nm to 380 nm in states of Ca^{2+} bound and Ca^{2+} free, respectively and its peak emission is observed at 510 nm.

Therefore, an elevated $[Ca^{2+}]_{cyto}$ results in an amplification of signal at 340 nm while fluorescence decreases when the dye is excited at 380 nm (Grynkiewicz et al., 1985). Fura-2 loading was done by incubation of the cells in 2 μM Fura-2/AM containing EH-buffer for 30-45 minutes at room temperature and protected from light. After incubation period, cells were washed for two times with EH-buffer to remove extracellular Fura-2 and stored in EH-buffer for further experiment.

In addition, the cytosol targeted O-GECO1 sensor (O-GECO1) was also used to monitor an alteration of $[Ca^{2+}]_{cyto}$ in our study and its principal was mentioned above. In our experiment, O-GECO1 was applied to transfect HeLa cells as described in *2.4 Transfection of cells*.

2.5.5 Simultaneous mitochondrial and cytosolic Ca^{2+} measurements

Simultaneous measurement of $[Ca^{2+}]_{cyto}$ in the cytosol and $[Ca^{2+}]_{mito}$ in mitochondrial matrix within the same individual cell was performed by using Fura-2/AM in combination with a newly developed red-shifted mitochondrial cameleon FRET-based sensor 4mtD1GO-Cam (Waldeck-Weiermair et al., 2012). This sensor was designed in order to avoid the interference of spectral overlaps of the excitation and/or emission wavelengths between Fura-2/AM and CFP/YFP-based cameleon (Carlson and Campbell, 2009), enabling us to simultaneous monitor the kinetic change of $[Ca^{2+}]_{cyto}$ and $[Ca^{2+}]_{mito}$ within the same cells. In this study, HeLa cells were transfected with 4mtD1GO-Cam with either control or specific siRNA as mentioned in *2.4 Transfection of cells*. Cells were loaded with 2 μM Fura-2/AM in EH-buffer at room temperature for 30-45 minutes with light protection. Prior to experiments, cells were washed two times with EH-buffer and stored in the same buffer without Fura-2/AM and proceeded for co-imaging of Ca^{2+} in both the cellular compartments. Single cells containing both the Fura-2 and the 4mtD1GO-Cam were alternately excited at 340, 380 or 477 nm and emissions were recorded at 510 nm for Fura-2 and GFP or at 560 nm for FRET channel.

2.5.6 Imaging system, data acquisition, and analysis

Imaging setup for FRET-based and Fura-2 experiments

The $[Ca^{2+}]_{mito}$, $[Ca^{2+}]_{cyto}$ measurements as well as dynamic FRET rearrangement between MICU1-CFP and MICU1-YFP were performed on a Zeiss Axiovert inverted microscope (Zeiss, Vienna, Austria) equipped with a polychromator illumination system (VisiChrome High Speed, Xenon lamp, Visitron Systems, Puchheim, Germany) and a

thermoelectric-cooled charged coupled device (CCD) camera (Photometrics Coolsnap HQ, Visitron Systems, Puchheim, Germany). Cells were imaged using a 40x oil-immersion objective (Zeiss, Vienna, Austria) under continuous perfusion of EB-buffer with or without IP_3R agonists. For $[Ca^{2+}]_{mito}$ measurements, the excitation of the cameleon sensors was accomplished at 440 ± 10 nm and emission was recorded at 480 nm and 535 nm (480AF30 and 535AF26, Omega Optical, Brattleboro, USA). Regarding $[Ca^{2+}]_{cyto}$ measurements, Fura-2AM-loaded cells were alternately illuminated at 340 and 380 nm excitation and 510 nm emission filters (510WB40, Omega Optical). Software VisiView 2.0.3 (Universal Imaging, Visitron Systems) was employed for the acquisition of experimental data. Results of FRET measurements were shown as the ratio of $F_{535}/F_{480}/R_0$ or $F_{FRET}/F_{CFP}/R_0$ (where R_0 is the basal ratio) to correct for photobleaching and/or photochromism as previously described (Waldeck-Weiermair et al., 2012). Results of Fura-2AM measurements were represented as the ratio of F_{380}/F_{340}. GraphPad Prism version 5.00 for Windows (GraphPad Software, San Diego, CA, USA) was applied to analyze the acquired data.

Imaging setup for simultaneous Ca^{2+} measurements

Simultaneous co-imaging of Fura-2 and the red-shifted cameleons 4mtD1GO-Cam was employed on a digital wide field imaging system, the Till iMIC (Till Photonics Graefelfing, Germany) using a 40x objective (alpha Plan Fluar 40x, Zeiss, Gottingen, Germany) as described in (Waldeck-Weiermair et al., 2012). For illumination of the Fura-2 and the 4mtD1GO-Cam, an ultrafast switching monochromator, the Polychrome V (Till Photonics) was used. Fura-2 was excited alternatively at 340 nm and 380 nm and the 4mtD1GO-Cam were excited at 477 nm, respectively. To avoid contamination of the emission channels with excitation light an excitation filter (E500spuv, Chroma Technology Corp, Rockingham Vermont, USA) was installed. A dichroic filter (495dcxru) was installed to reflect the excitation light to the sample. Emission light was simultaneously collected at 510 nm (Fura-2 and GFP of GO-Cams) and at 600 nm (FRET-channel of GO-Cams) using a single beam splitter design (Dichrotome, Till Photonics) that was equipped with a dual band emission filter (59004m ET Fitc/Tritc Dual Emitter, Chroma Technology Corp) and a second dichroic filter (560dcxr, Chroma Technology Corp). Images were recorded with a CCD camera (AVT Stringray F145B, Allied Vision Technologies, Stadtroda, Germany). For the data acquisition and remote control of the fluorescence microscope, the live acquisition software version 2.0.0.12 (Till Photonics) was applied. Results of FRET measurements are shown as the ratio of $F_{560}/F_{510}/R_0$ (where R_0 is the

basal ratio) to correct for photobleaching and/or photochromism as described in (Waldeck-Weiermair et al., 2012). In addition, Dual recordings of MICU1 FRET and $[Ca^{2+}]_{cyto}$ were performed in HeLa cells co-transfected with MICU1-CFP, MICU1-YFP and O-GECO1 or mtO-GECO1, respectively. MICU1-CFP and (mt)O-GECO1 were alternately illuminated at 430 nm and 575 nm, respectively, in single individual cells. Emitted light was collected at approximately 535 nm for MICU1 FRET and 610 nm for (mt)O-GECO1 using the XF56 filter set of Omega Optical. Then, the acquired data were analyzed by GraphPad Prism version 5.00 for Windows (GraphPad Software, San Diego, CA, USA).

2.6 Analysis of mitochondrial morphology

Mitochondrial structure was analyzed in human umbilical vein endothelial cell lines (EA.hy926) and the rat pancreatic β-cell lines (INS-1 832/13) overexpressed with either human MICU1 (hMICU1)-citrine or mtDsRed (control). Cells were transiently transfected with 1.5-2.0 μg certain plasmid DNAs and visualized at 24 hours after transfection. For hMICU1-citrine construct, citrine fragment was cut from pcDNA3.1(-) citrin vector and cloned into EcoRI and XbaI restriction sites on the C-terminus of MICU1 in pcDNA3.1. High resolution images of cells were recorded by using a confocal spinning disk microscope (Axio Observer.Z1 from Zeiss, Gottingen, Germany) equipped with 100x objective lens (Plan-Fluor x100/1.45 Oil, Zeiss), a motorized filter wheel (CSUX1FW, Yokogawa Electric Corporation, Tokyo, Japan) on the emission side, AOTF-based laser merge module for laser line 405, 445, 473, 488, 551, and 561 nm (Visitron Systems) and a Nipkow-based confocal scanning unit (CSU-X1, Yokogawa Electric corporation). The constructs hMICU1-citrine and mtDsRed were excited with 488 and 551 laser lines respectively and emission was acquired with a charged CCD camera (CoolSNAP-HQ, Photometrics, Tucson, AZ, USA). The software VisiView acquisition software (Universal Imaging, Visitron Systems) was used to acquire the imaging data. To analyze mitochondrial morphology, cells were counted and categorized into three different classes based on the shape of mitochondria; normal tubular mitochondrial morphology (Network), network structure of shorter mitochondria or thick tubule (Intermediate), and fragmented mitochondrial structures (Fragments or Dots). In rare cases where mixed morphologies were observed or morphology was unclear, cells were ruled out.

2.7 Molecular biology methods

2.7.1 Total RNA isolation

HeLa cells were treated with the respective siRNAs and/or plasmid. Total RNA was isolated by using the PEQLAB total RNA isolation kit (PEQLAB Biotechnologie GmbH, Erlangen, Germany) following an instructions suggested by the manufacturer. Briefly, cells were cultured in 6-well plates without glass cover slip and treated based on certain experiments. Cells were washed with PBS and lysed with cell lysis buffer. The cell lysate was then transferred to a DNA removing column and centrifuged. The flow through was mixed well with an equal volume of 70% ethanol and transferred to a RNA binding column followed by another centrifugation step. Then the column was washed two steps by wash buffer and the RNA at the membrane was eluted with 50-80 µL of nuclease-free water and stored at -70 ˚C until further application.

2.7.2 First strand cDNA synthesis (reverse transcription, RT)

The concentration of RNA was determined by using a spectrophotometer (UviLine 9400, SCHOTT Instruments, Mainz, Germany) and 1-2 µg of each total RNA sample was reversed transcribed into complementary DNA (cDNA) with a High-capacity cDNA reverse transcription kit according to the manufacturer's protocol (Applied Biosystems, USA) using a thermal cycler (PEQLAB Biotechnologie GmbH). RNasin® Plus RNase inhibitor (Promega, Germany) was used to reduce RNA degradation. The reverse transcription mixture was composed of (20 µL total volume per reaction): 10.0 µL total RNA sample (1-2 µg), 2.0 µL 10x RT buffer, 0.8 µL dNTP mix (100 mM), 2.0 µL 10x RT random primers, 1.0 µL reverse transcriptase, 1.0 µL RNase Inhibitor, and 3.2 µL nuclease-free water. The thermal cycler protocol was set up as follows:

Step 1,	25 ºC,	10 minutes;
Step 2,	37 ºC,	120 minutes;
Step 3,	85 ºC,	5 minutes;
Step 4,	4 ºC,	forever

The transcribed cDNA can be stored at -70 ˚C until further used.

2.7.3 Quantitative real-time polymerase chain reaction (qPCR or RT-PCR)

To validate the knockdown efficiency of respective siRNAs and detect the expression level of target genes, the real-time PCR was performed with the QuantiFast SYBR Green RT-PCR kit according to the manufacturer's instructions (Qiagen, Hilden,

Germany) using 96-well plates on LightCycler 480 (Roche Diagnostics, Vienna, Austria). The qPCR reaction mix was consisted of (10 µL total volume per reaction): 1.0 µL cDNA (10-50x dilution), 2.0 µL SYBR Green PCR Master Mix, 1.0 µL forward primer (10 µM), 1.0 µL reverse primer (10 µM), and 5.0 µL nuclease free water. The thermal cycling protocol was specified as follows: initial heat activation, 95 ºC, 5 minutes; denaturation, 95 ºC, 10 seconds (40 cycles); annealing and extension, 60 ºC, 30 seconds (40 cycles). Relative expressions of the specific genes were normalized to the human glyceraldehyde 3-phosphate dehydrogenase (hGAPDH, no.QT01192646, QuantiTect® primer assay, Qiagen, Hilden, Germany) as a housekeeping gene. The obtained data were analyzed by the REST software (Qiagen, Hilden, Germany). All primers were designed by MS Dos Program primer designer version 2.0 and obtained from Invitrogen®, Austria and their sequences were listed as follows:

hMCU	forward: 5'-TTCCTGGCAGAATTTGGGAG-3'
hMCU	reverse: 5'-AGAGATAGGCTTGAGTGTGAAC-3'
hEMRE	forward: 5′-TCGCTGGCTAGTATTGGCAC-3′
hEMRE	reverse: 5′-GGAGAAGGCCGAAGGACATT-3′
hUCP2	forward: 5'-TCCTGAAAGCCAACCTCATG-3'
hUCP2	reverse: 5'-GGCAGAGTTCATGTATCTCGTC-3'
hUCP3	forward: 5'-AGAAAATACAGCGGGACTATGG-3'
hUCP3	reverse: 5'-CTTGAGGATGTCGTAGGTCAC-3'

2.8 Statistical analysis

The results were expressed as mean ± the standard error of mean (S.E.M.). All experiments were repeated at least three times independently. Statistical analyses were performed with unpaired Student's t-test or one-way ANOVA. A *p*-value of less than 0.05 ($p<0.05$) were considered as a statistically significant difference. Data were analyzed either with MS Excel 2011 or with Graphpad Prism version 5.0.

CHAPTER III
RESULTS

PART I

3.1: MICU1 is a negative regulator of MCU that is under the control of UCP2/3 in mitochondrial Ca^{2+} uptake

IP_3-mediated depletion of ER Ca^{2+} stores leads to mitochondrial Ca^{2+} uptake mainly from contact sites of the ER. Under this condition, Ca^{2+} is transferred into mitochondria, a process involving several proteins located in the IMM, mainly MCU and/or UCP2/3, which are essential for Ca^{2+} buffering. In this study, all experiments were performed in HeLa cell lines stably expressing a scrambled shRNA (shControl) or a shRNA against one of the two respective proteins that regulate mitochondrial Ca^{2+} entry, either UCP2 ($UCP2^{kd}$) or MCU (MCU^{kd}).

3.1.1 Knock-down efficiency of MCU and UCP2 in MCU^{kd} and $UCP2^{kd}$ cells

The silencing efficiency of MCU and UCP2 in HeLa cells stably expressing shRNA against particular proteins was verified using qPCR. The mRNA expression levels of MCU or UCP2 were effectively suppressed to 37.24 $\pm$ 1.18% and 15.59 $\pm$ 1.11% in MCU^{kd} or $UCP2^{kd}$ cells, respectively (**Figure 3.1**). Therefore, these cell lines are suitable for studying the involvement of MCU and UCP2 in the process of Ca^{2+} mobilization into mitochondria.

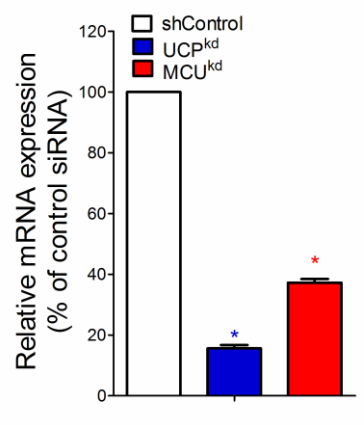

Figure 3.1: Expression analysis of MCU and UCP2 in MCU^{kd} and $UCP2^{kd}$ cells. Silencing efficiency of MCU and UCP2 in the HeLa SilenceX knock-down cell lines (n=3 for each samples) was validated by qPCR. Total RNA was isolated 48 hours after transfection with 4mtD3cpv. Relative mRNA expression of each gene was compared with respective controls and shown as the percentage of maximum expression. Human GAPDH was used as a housekeeping gene. Bar charts indicate mean ± S.E.M. *; $p < 0.05$ versus respective controls.

3.1.2 The mitochondrial Ca^{2+} handling of MCU^{kd} and $UCP2^{kd}$ cells

In addition, the mitochondrial Ca^{2+} sequestration of MCU^{kd} and $UCP2^{kd}$ cells was investigated by transient transfection together with the FRET-based mitochondrial targeted

Ca^{2+} sensor, 4mtD3cpv. The mitochondrial uptake of intracellular released Ca^{2+} was strongly diminished by a stable knockdown of either of the two proteins; MCU or UCP2 (**Figure 3.2A**). Furthermore, the inhibition of mitochondrial Ca^{2+} signals in MCU^{kd} cells was ~2 times stronger than in $UCP2^{kd}$ cells (**Figure 3.2A**). On the other hand, deletion of MCU suppressed mitochondrial sequestration of Ca^{2+} entering via SOCE, while depletion of UCP2 unaltered this process (**Figure 3.2B**). These results are consistent with our previous findings which revealed the engagement of MCU and UCP2/3 in the mobilization process of Ca^{2+} into the mitochondrial matrix upon IP_3-mediated intracellular Ca^{2+} release (Trenker et al., 2007, Waldeck-Weiermair et al., 2010b, Waldeck-Weiermair et al., 2011, Deak et al., 2014).

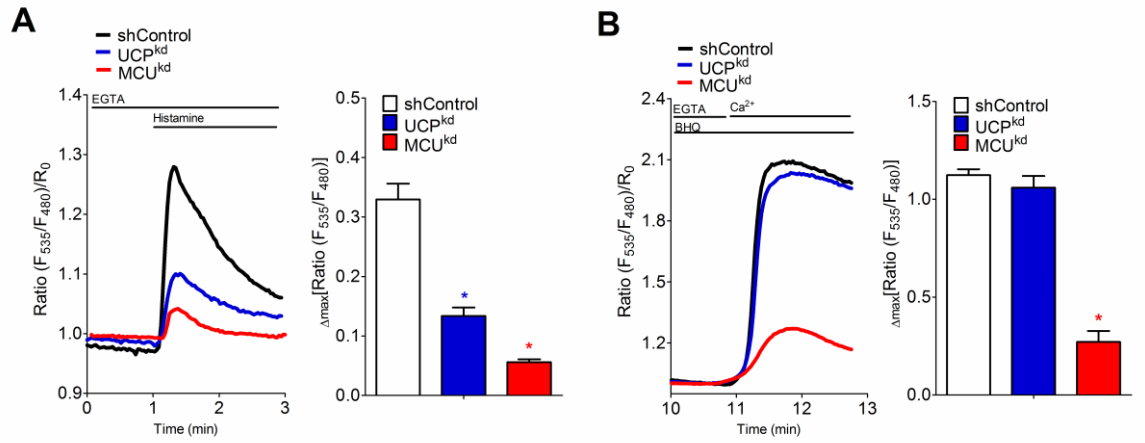

Figure 3.2: Characterization of mitochondrial Ca^{2+} handling in MCU^{kd} and $UCP2^{kd}$ cells. (A) Mitochondrial Ca^{2+} entry upon stimulation with 100 µM histamine in the absence of extracellular Ca^{2+} was determined in shControl (black, n=40/3), $UCP2^{kd}$ (blue, n=37/3), and MCU^{kd} (red, n=35/3) cells co-expressing 4mtD3cpv. Bar charts represent mean ± S.E.M. *; $p < 0.05$ versus control. **(B)** Mitochondrial Ca^{2+} signals upon Ca^{2+} re-addition following 15 µM BHQ treatments in the absence of extracellular Ca^{2+} were measured in the same cells shown in (B). Bar charts indicate mean ± S.E.M. *; $p < 0.05$ versus control.

3.1.3 MICU1 functions as a negative regulator of MCU in shControl cells

In shControl cells, MICU1 acts as a negative regulator of MCU. Silencing of MICU1 resulted in an increase of mitochondrial Ca^{2+} uptake released from ER and basal levels of mitochondrial Ca^{2+}. In this study, overexpression of one of the two main proteins (either MCU or UCP3) significantly augmented mitochondrial Ca^{2+} sequestration compared with control and MCU predominantly regulated this process. However, overexpression of UCP3 significantly enhanced $[Ca^{2+}]_{mito}$ (**Figure 3.3A, 3.3C**). Additionally, diminution of MICU1 led to dramatically increase of the amplitude and basal

levels of $[Ca^{2+}]_{mito}$ in response to histamine (~3-fold) and co-expressed with MCU or UCP3 rose the basal level of $[Ca^{2+}]_{mito}$ (**Figure 3.3B, 3.3C**). Our results confirm the finding of the previous study that indicated MICU1 is a gatekeeper of MCU-mediated mitochondrial Ca^{2+} entry that is essential to prevent $[Ca^{2+}]_{mito}$ overload and associated cellular stress response (Mallilankaraman et al., 2012b).

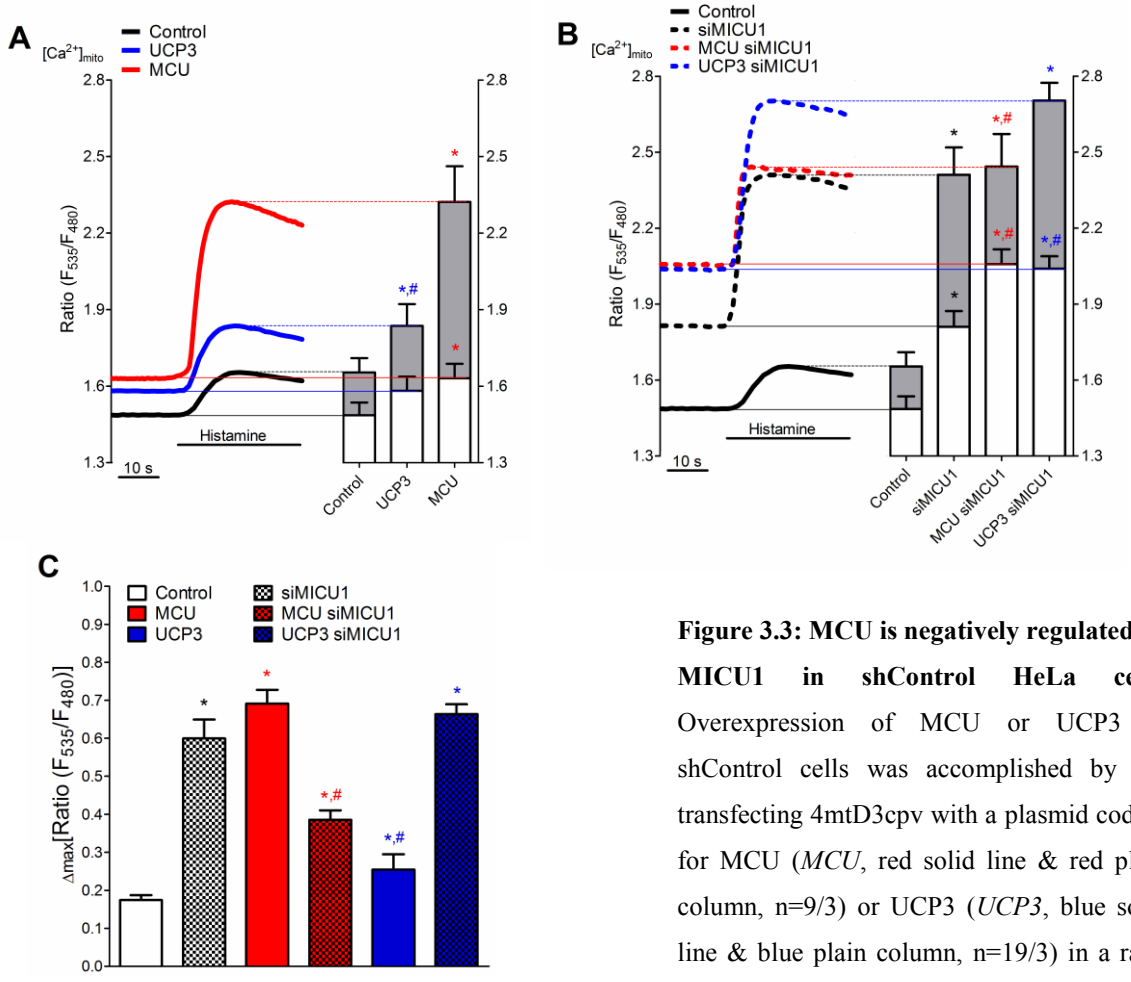

Figure 3.3: MCU is negatively regulated by MICU1 in shControl HeLa cells. Overexpression of MCU or UCP3 in shControl cells was accomplished by co-transfecting 4mtD3cpv with a plasmid coding for MCU (*MCU*, red solid line & red plain column, n=9/3) or UCP3 (*UCP3*, blue solid line & blue plain column, n=19/3) in a ratio 1:3 and either control siRNA (*Control*, black solid line & blank plain column, n=18/3) or siRNA against MICU1 (*siMICU1*, black dashed line & blank cross column, n=19/3) or the combination of respective plasmids and siRNAs (*MCU siMICU1*, red dashed line & red cross column, n=15/3; *UCP3 siMICU1*, blue dashed line & blue cross column, n=24/3). Cells were perfused with Ca^{2+}-free EB before stimulation. $[Ca^{2+}]_{mito}$ was analyzed upon cell treatment with histamine 100 µM in a Ca^{2+}-free buffer 48-72 hours after transfection. **(A-B)** Curves show an avarage of all cells represented as ratio of YFP/CFP over time after correction for photobleaching. **(C)** The peak $[Ca^{2+}]_{mito}$ amplitude of all conditions was calculated from individual curves and represented as Δ_{max} of ratio YFP/CFP. Bar charts indicate mean ± S.E.M. *; $p < 0.05$ versus *control*, #; $p < 0.05$ versus *siMICU1*.

3.1.4 MCU is negatively regulated by MICU1 and independent of UCP2/3 in UCP2^{kd} cells

The UCP2^{kd} cells were used in order to investigate the contribution of UCP2/3 to MCU and MICU1 in the buffering process of Ca^{2+} into mitochondria. In this cell model, a stable knockdown of UCP2 caused a deficiency of mitochondrial Ca^{2+} uptake that can be fully rescued by an overexpression of UCP3 (**Figure 3.4A, 3.4C**). Whereas, an overexpression of MCU in UCP2^{kd} cells increased $[Ca^{2+}]_{mito}$ to the same amplitude as in shControl cells (**Figure 3.3A, 3.3C**). This data demonstrate that mitochondrial Ca^{2+} entry via MCU do not directly depend on UCP2. Moreover, the sequestration of Ca^{2+} into mitochondria was reduced under the MCU overexpression and MICU1 silencing, while an overexpression of UCP3 together with MICU1 silencing unchanged $[Ca^{2+}]_{mito}$ when compared with depletion of MICU1 alone. These results represent MICU1 functions as a negative regulator of MCU which works independently from UCP2 (**Figure 3.4B, 3.4C**).

3.1.5 Knockdown of MICU1 boosts the influence of UCP2/3 on MCU activity in MCU^{kd} cells overexpressed with UCP2/3

To further explore the involvement of MCU with UCP2/3 and MICU1 in mitochondrial Ca^{2+} mobilization, MCU^{kd} HeLa cells were used in this study. In this cell model, mitochondrial Ca^{2+} entry was suppressed by stably silencing of MCU and recovered after an overexpression of indicated protein. On the other hand, the full function could not be restored upon an overexpression of UCP3. These data demonstrate that UCP2/3 is unable to replace MCU and fully functions in the process of mitochondrial Ca^{2+} uptake (**Figure 3.5A, 3.5C**). Additionally, MICU1 is ineffective to function as a negative regulator of mitochondrial Ca^{2+} entry since depletion of MICU1 in MCU^{kd} cells could not increase the level of $[Ca^{2+}]_{mito}$ in response to histamine. On the other side, a similar pattern of mitochondrial Ca^{2+} uptake was observed by MCU overexpression together with depletion of MICU1 in both MCU^{kd} and shControl cells, while, this pattern did not occur by an overexpression of UCP3 (**Figure 3.5B, 3.5C**). These results support our findings in UCP2^{kd} cells that MICU1 is negatively modulating MCU which is independent of UCP2/3. Remarkably, the full uptake of Ca^{2+} into the mitochondrial matrix was recovered by silencing of MICU1 and an overexpressing of UCP2/3 in MCU^{kd} cells (**Figure 3.5B, 3.5C**). This could be assumed that mitochondrial Ca^{2+} sequestration might be mainly mediated by UCP2 under the condition of UCP2/3 overexpression and silencing of MICU1 in MCU^{kd} cells.

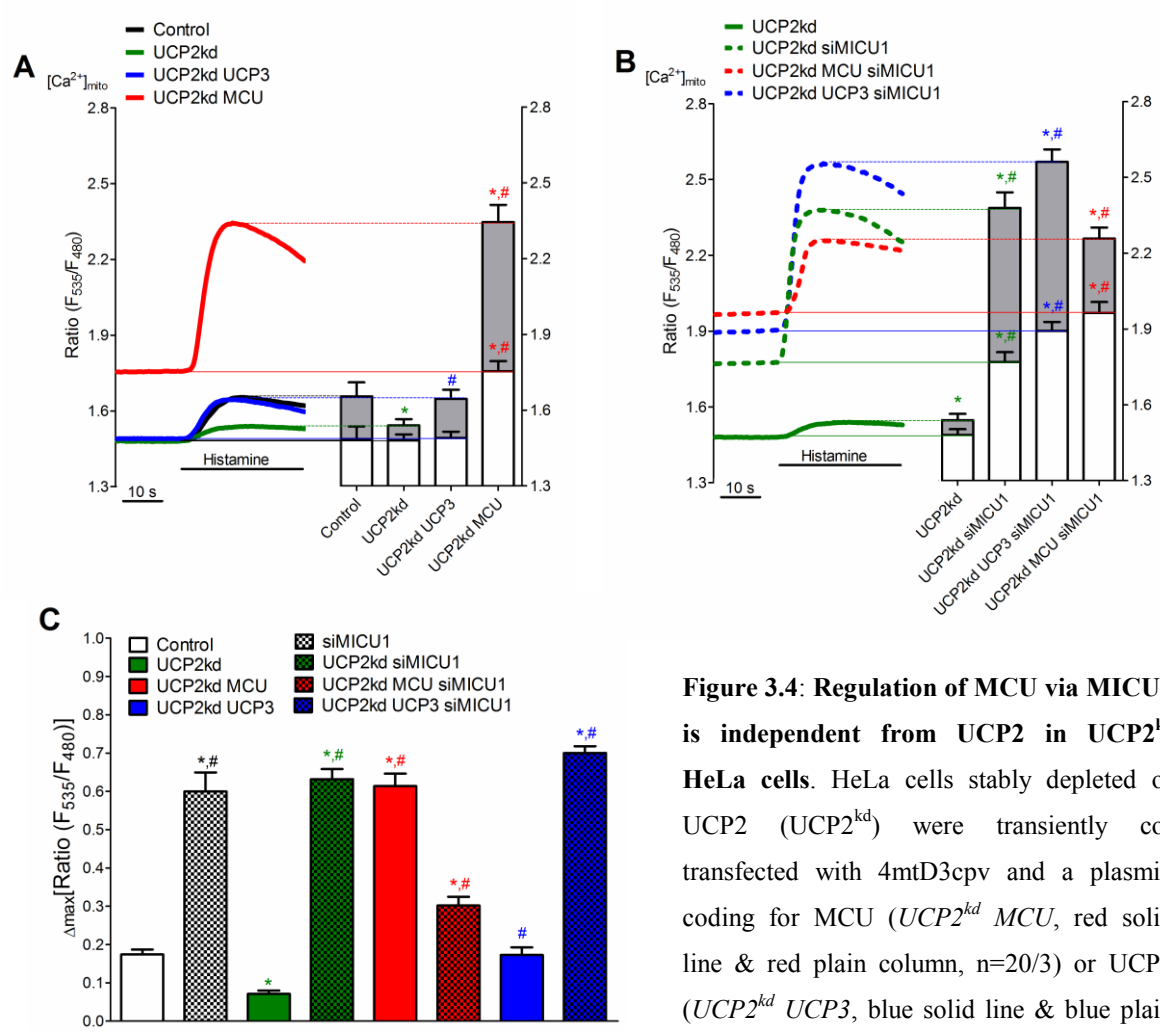

Figure 3.4: **Regulation of MCU via MICU1 is independent from UCP2 in UCP2^{kd} HeLa cells**. HeLa cells stably depleted of UCP2 (UCP2^{kd}) were transiently co-transfected with 4mtD3cpv and a plasmid coding for MCU (*UCP2^{kd} MCU*, red solid line & red plain column, n=20/3) or UCP3 (*UCP2^{kd} UCP3*, blue solid line & blue plain column, n=28/3) in a ratio 1:3 and either control siRNA (*UCP2^{kd}*, black solid line & blank plain column, n=31/3) or siRNA against MICU1 (*UCP2^{kd} siMICU1*, green dashed line & green cross column, n=30/3) or the combination of respective plasmids and siRNAs (*UCP2^{kd} MCU siMICU1*, red dashed line & red cross column, n=35/3; *UCP2^{kd} UCP3 siMICU1*, blue dashed line & blue cross column, n=25/3). After 48-72 hours transfection, $[Ca^{2+}]_{mito}$ in response to histamine 100 µM was measured in a Ca^{2+}-free buffer. **(A-B)** Avarage curves represent ratio of YFP/CFP over time. **(C)** The peak $[Ca^{2+}]_{mito}$ response of all conditions represented as Δ_{max} of ratio YFP/CFP. Bar charts indicate mean ± S.E.M. *; $p < 0.05$ versus *control*, #; $p < 0.05$ versus *UCP2^{kd}*.

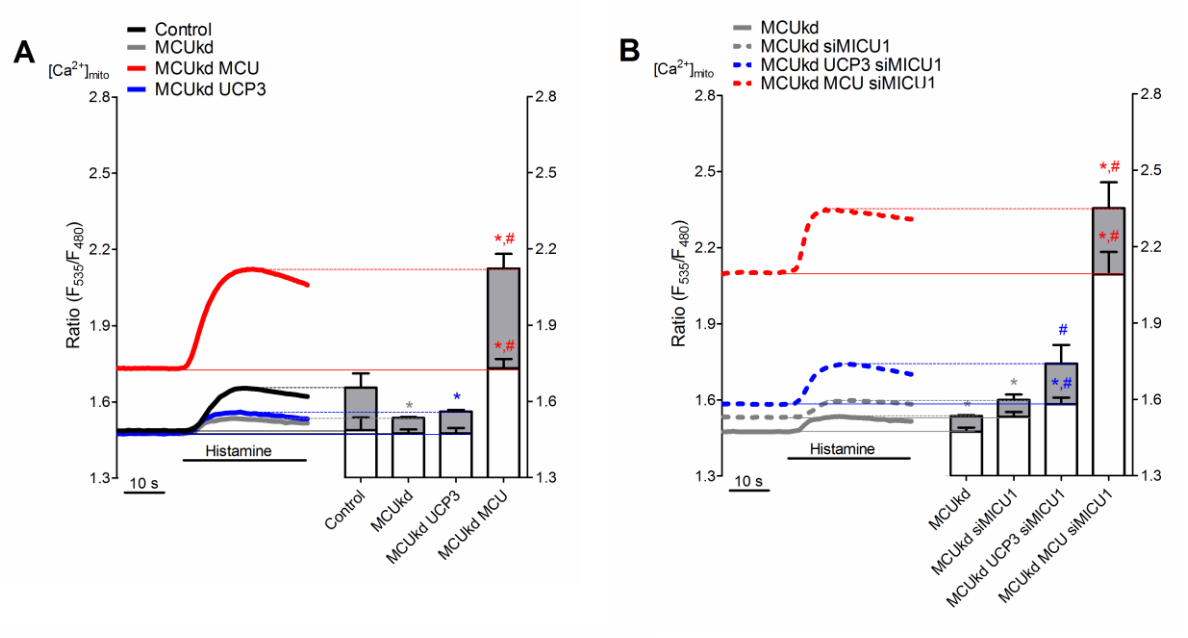

Figure 3.5: **In MCU^{kd} cells mitochondrial Ca^{2+} uptake is mainly mediated by UCP2/3 under the condition of UCP2/3 overexpression and silencing of MICU1.** The mitochondria targeted sensor, 4mtD3cpv, were transiently co-transfected MCU^{kd} HeLa cells with a plasmid coding for MCU (*MCU^{kd} MCU*, red solid line & red plain column, n=15/3) or UCP3 (*MCU^{kd} UCP3*, blue solid line & blue plain column, n=61/3) in a ratio 1:3 and either control siRNA (*MCU^{kd}*, grey solid line & grey plain column, n=86/3) or siRNA against MICU1 (*MCU^{kd} siMICU1*, grey dashed line & grey cross column, n=81/3) or the combination of respective plasmids and siRNAs (*MCU^{kd} MCU siMICU1*, red dashed line & red cross column, n=15/3; *MCU^{kd} UCP3 siMICU1*, blue dashed line & blue cross column, n=76/3, *MCU^{kd} UCP2 siMICU1*, light blue cross column, n=63/3). After exposure with 100 µM histamine, $[Ca^{2+}]_{mito}$ was quantified within 48-72 hours after transfection in a Ca^{2+}-free buffer. **(A-B)** Avarage curves represent ratio of YFP/CFP over time. **(C)** Average of maximum mitochondrial Ca^{2+} uptake of shControl and MCU^{kd} overexpressing MCU, UCP2 or UCP3 and each in comparison to silencing of MICU1 were reported as Δ_{max} of ratio YFP/CFP. Bar charts indicate mean ± S.E.M. *; $p < 0.05$ versus *control*, #; $p < 0.05$ versus *MCU^{kd}*.

3.1.6 A widely distributed and dominant rising of mitochondrial Ca^{2+} entry in MCU^{kd} cells depleted with MICU1 and overexpressing MCU or UCP2/3 highlights the exclusive contribution between these particular proteins

Considering about the average of maximum mitochondrial Ca^{2+} uptake (Δ_{max}) of $[Ca^{2+}]_{mito}$ after IP_3-mediated depletion of the ER Ca^{2+} stores by histamine, a rising of mitochondrial Ca^{2+} entry was highly distributed in MCU^{kd} cells overexpressing MCU or UCP2/3 together with diminution of MICU1 (**Figure 3.6A**). This unique phenomenon might be explained by the stoichiometric relationship of UCP2/3 and MICU1. By setting a threshold according to the Δ_{max} values of $[Ca^{2+}]_{mito}$ in shControl cells, the Δ_{max} within MCU^{kd} cells silencing MICU1 and overexpressing either MCU or UCP2/3 was categorized into three groups according to the responding levels; an *inoperative* MCU^{kd}-like (green), a *rescued* shControl-like (blue) and a *boosted* overexpressed MCU-like (red) (**Figure 3.6B**). Representative curves of mitochondrial Ca^{2+} mobilization from the three defined groups of the selected conditions were shown in **Figure 3.6C, 3.6D, and 3.6E**, respectively. Importantly, these particular groups of treated cells that represented distinguished augmentation of mitochondrial Ca^{2+} entry (a *boosted* pattern) emphasize the absolute engagement between MICU1 and UCP2/3 and draw our attention to further investigate whether and, if so, how these indicated proteins affect or cooperate with each other in the regulation of mitochondrial Ca^{2+} buffering in more detail.

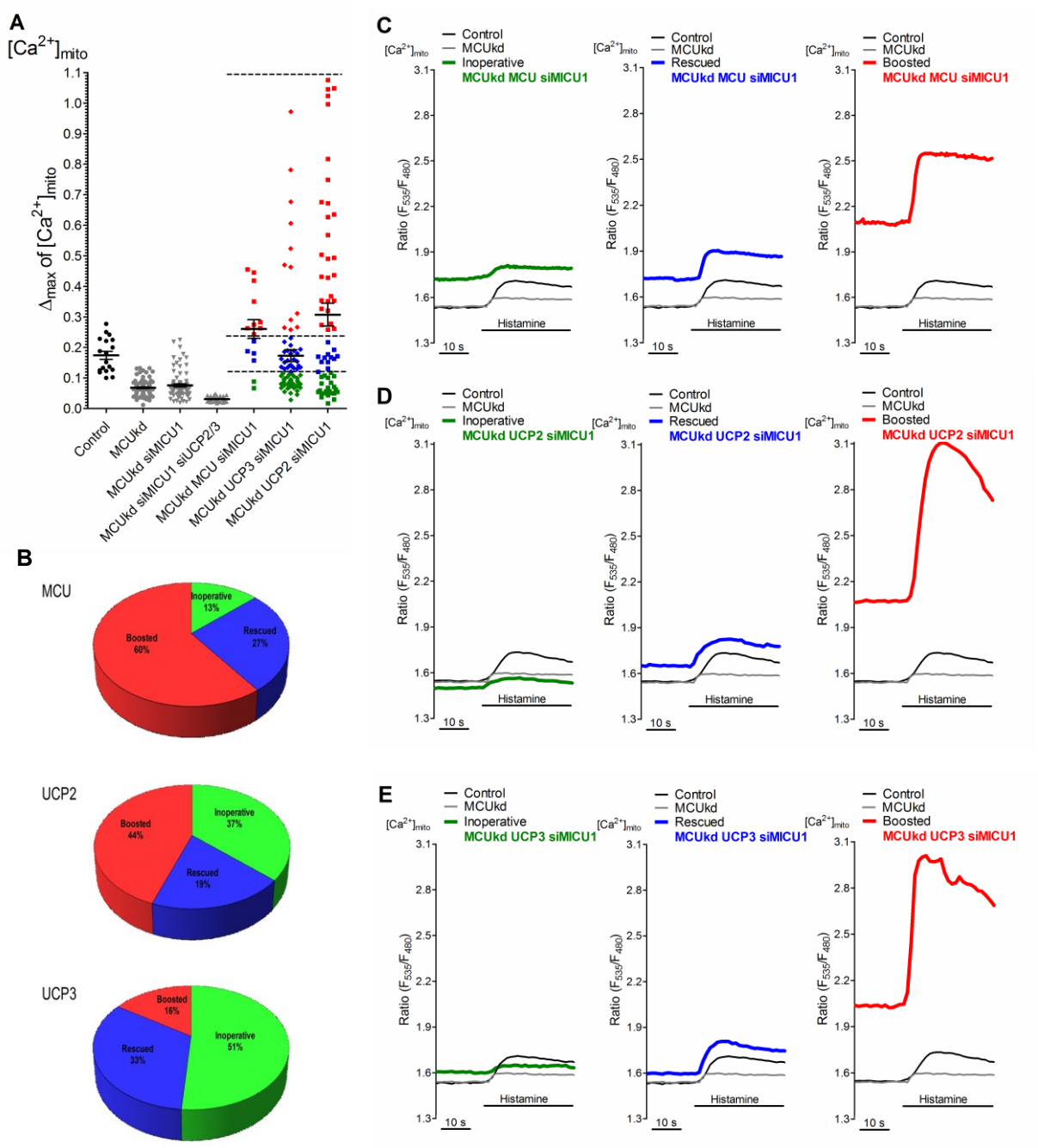

Figure 3.6: **Upon stimulation with histamine, the maximum of $[Ca^{2+}]_{mito}$ is largely distributed in MCU^{kd} cells treated with siRNA of MICU1 and plasmid overexpressed either MCU or UCP2/3, pointing to a stoichiometric relationship between MICU1 and UCP2/3. (A)** The scatter plot of maximum $[Ca^{2+}]_{mito}$ amplitude of all treated conditions was calculated from individual curves and represented as Δ_{max} of ratio YFP/CFP and mean ± S.E.M. **(B)** The pie diagrams show the Δ_{max} values of $[Ca^{2+}]_{mito}$ within MCU^{kd} cells silencing MICU1 and overexpressing either MCU, UCP2 or UCP3 which were classified into three groups of responders; an *inoperative* MCU^{kd}-like (green), a *rescued* shControl-like (blue) and a *boosted* overexpressed MCU-like (red). **(C-E)** Representative curves of mitochondrial Ca^{2+} uptake from the three defined groups of the selected conditions.

3.1.7 EMRE contributes to MCU and UCP2 in the regulation of mitochondrial Ca^{2+} entry

After the discovery of EMRE, an additional component of MCU complex, which have been reported to interact with MICU1 and MICU2 in the IMS and with MCU oligomers in the IMM and bridge the calcium-sensing role of MICU1 and MICU2 with the channel-conducting activity of MCU (Sancak et al., 2013). To explore the relationship between EMRE and UCP2 which remains unknown, siRNA against EMRE was used in this study. In shControl cells, both MCU and UCP2 depend on EMRE in the regulation of Ca^{2+} buffering processes. After histamine stimulation, diminution of EMRE resulted in considerable reduction of $[Ca^{2+}]_{mito}$ and its impact was more pronounced under the overexpression of MCU and UCP2 (**Figure 3.7A-3.7F**). For UCP2, the more potent effect was observed under the absence of MICU1 (**Figure 3.7C, 3.7F**). Moreover, MICU1 functions as a negative regulator of mitochondrial Ca^{2+} sequestration of both MCU and UCP2. Depletion of MICU1 led to substantial enhancement of $[Ca^{2+}]_{mito}$ uptake (**Figure 3.7C, 3.7F**). For this reason, we focused on the influence of EMRE in this study.

3.1.8 In MCU^{kd} cells overexpressed with UCP2 and depleted with MICU1, the boosted $[Ca^{2+}]_{mito}$ signals depend on MCU (rest of MCU) and EMRE, but not on MCUR1

In order to experimentally investigate the possible promising protein(s) that involved with the boosted $[Ca^{2+}]_{mito}$ signals in MCU^{kd} cells overexpressed with UCP2 and depleted with MICU1, the mitochondrial Ca^{2+} sequestration of MCU^{kd} cells were determined by silencing of MCUR1 or EMRE. The results clearly represent that this phenomenon is partially regulated by MCU (the rest of MCU in MCU^{kd} cells) and EMRE, but is not controlled by MCUR1 since diminution of MCU and EMRE significantly decreased mitochondrial Ca^{2+} entry, while depletion of MCUR1 had no effect (**Figure 3.8A, 3.8B**). Therefore, EMRE has an important impact on this phenomenon, whereas MCUR1 does not play a role.

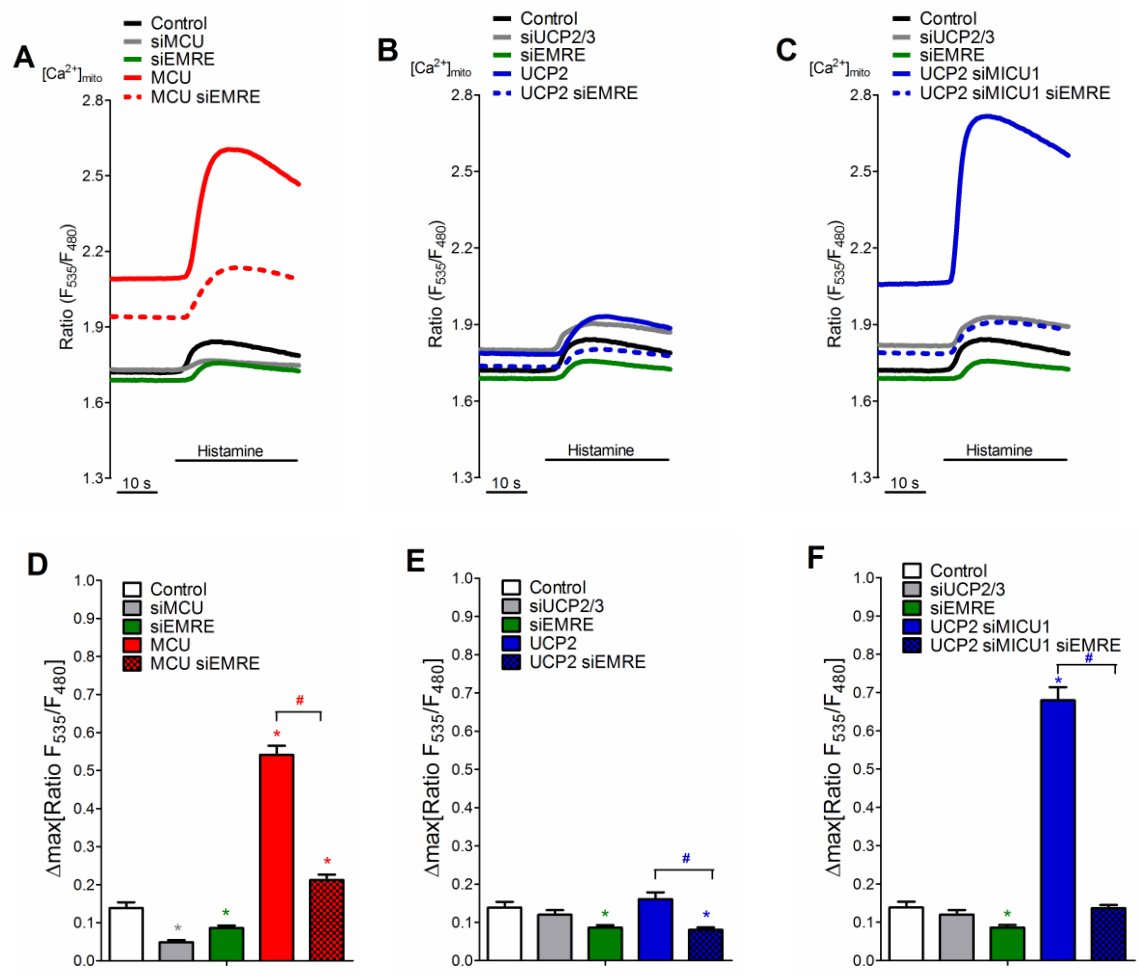

Figure 3.7: **In shControl cells, MCU and UCP2 depend on EMRE in the regulation of mitochondrial Ca^{2+} entry.** shControl HeLa cells were co-transfected with 4mtD3cpv and a plasmid coding for MCU (*MCU*, red solid line & red plain column, n=34/3) or UCP2 (*UCP2*, blue solid line & blue plain column, n=37/3) in a ratio 1:3 and either control siRNA (*Control*, black solid line & blank plain column, n=27/3), or siRNA against MCU, UCP2/3, EMRE (*siMCU*, grey solid line & grey plain column, n=19/3; *siUCP2/3*, grey solid line & grey plain column, n=26/3; *siEMRE*, green solid line & green plain column, n=36/3, respectively), and or combination of respective plasmids and siRNAs (*MCU siEMRE*, red dashed line & red cross column, n=32/3; *UCP2 siEMRE*, blue dashed line & blue cross column, n=34/3, *UCP2 siMICU1*, blue solid line & blue plain column, n=39/3, and *UCP2 siMICU1 siEMRE*, blue dashed line & blue cross column, n=33/3). After treatment with100 µM of histamine, $[Ca^{2+}]_{mito}$ was determined in a Ca^{2+}-free buffer. **(A)** Avarage curves represent ratio of YFP/CFP over time. **(B)** The peak $[Ca^{2+}]_{mito}$ of all conditions was shown as Δ_{max} of ratio YFP/CFP. Bar charts show mean ± S.E.M. *; $p < 0.05$ versus *control*, #; $p < 0.05$ versus respective control.

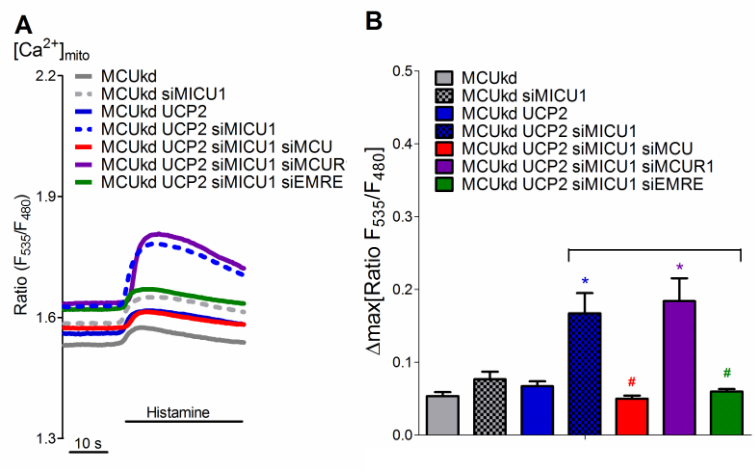

Figure 3.8: **The boosted [Ca $^{2+}$]$_{mito}$ signals of MCU^{kd} cells overexpressed with UCP2 and depleted with MICU1 are controlled by MCU and EMRE, but not on MCUR1.** MCU^{kd} HeLa cells were co-transfected with 4mtD3cpv and a plasmid coding for UCP2 (*MCU^{kd} UCP2*, blue solid line & blue plain column, n=48/3) in a ratio 1:3 and either control siRNA (*MCU^{kd}*, grey solid line & grey plain column, n=57/3), or siRNA against MICU1 (*MCU^{kd} siMICU1*, grey dashed line & grey cross column, n=58/3), or the combination of respective plasmids and siRNAs (*MCU^{kd} UCP2 siMICU1*, blue dashed line & blue cross column, n=48/3; *MCU^{kd} UCP2 siMICU1 siMCU*, red solid line & red plain column, n=56/3; *MCU^{kd} UCP2 siMICU1 siMCUR1*, violet solid line & violet plain column, n=39/3; and *MCU^{kd} UCP2 siMICU1 siEMRE*, green solid line & green plain column, n=58/3). After exposure with 100 µM histamine, [Ca^{2+}]$_{mito}$ was determined in a Ca^{2+}-free buffer. **(A)** Avarage curves represent ratio of YFP/CFP over time. **(B)** Δ_{max} of ratio YFP/CFP of all conditions. Bar charts indicate mean ± S.E.M. *; $p < 0.05$ versus *control*, #; $p < 0.05$ versus *MCU^{kd} UCP2 siMICU1*.

3.1.9 Mitochondrial Ca^{2+} sequestration from contact sites of the ER works exclusively via MCU and EMRE but not MCUR1

To verify whether or not EMRE and MCUR1 interact with MCU and contribute to the entry of Ca^{2+} into mitochondria in the same level, the expression of these proteins was simultaneously reduced by transient transfection of a mixture of all respective siRNAs. The mobilization of Ca^{2+} into mitochondria from contact sites of the ER works exclusively via MCU and EMRE but not MCUR1. In shControl cells, overexpression of MCU depends on EMRE and is not regulated by MCUR1. Upregulation of MCU and silencing of EMRE substantially diminished mitochondrial Ca^{2+} uptake via MCU. The result clearly showed that EMRE is more effective than MCUR1 in the regulation of MCU activity (**Figure 3.9A and 3.9B**).

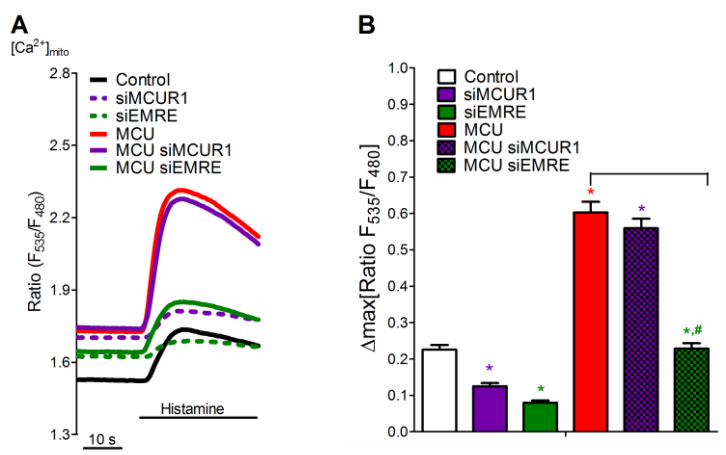

Figure 3.9: **At the contact sites of the ER, MCU and EMRE mainly modulated mitochondrial Ca^{2+} mobilization, while MCUR1 does not contribute.** In shControl HeLa cells were co-transfected with 4mtD3cpv and a plasmid coding for MCU (*MCU*, red solid line & red plain column, n32/3) in a ratio 1:3 and either control siRNA (*Control*, black solid line & blank plain column,n=33/3), or siRNA against MCUR1 or EMRE (*siMCUR1*, violet dashed line & violet plain column, n=33/3 or *siEMRE,* green dashed line & green plain column, n=36/3), or the combination of respective plasmids and siRNAs (*MCU siMCUR1*, violet solid line & violet cross column, n=46/3 or *MCU siEMRE*, green solid line & green cross column, n=31/3). After 48-72 hours transfection, mitochondrial Ca^{2+} entry in response to histamine 100 µM was evaluated. **(A)** Avarage curves represent ratio of YFP/CFP over time. **(B)** Δ_{max} of ratio YFP/CFP of all conditions. Bar charts indicate mean ± S.E.M. *; $p < 0.05$ versus *control*, #; $p < 0.05$ versus *MCU*.

3.1.10 UCP2/3 facilitates the function of MCU/EMRE in mitochondrial Ca^{2+} entry

MCU alone or together with UCP2 was overexpressed in $UCP2^{kd}$ cells treated with siRNAs against EMRE or MCUR1 to examine whether or not EMRE and MCUR1 is able to compensate the diminution of UCP2. Upon histamine stimulation, UCP2 facilitates the function of MCU without mimicking EMRE or MCUR1 under the presence of MICU1 in the model of $UCP2^{kd}$ cells (**Figure 3.10A**). Knockdown of either EMRE or MCUR1 caused no significantly change in a mitochondrial Ca^{2+} mobilization in $UCP2^{kd}$ cells overexpressed MCU or/and UCP2 (**Figure 3.10B**).

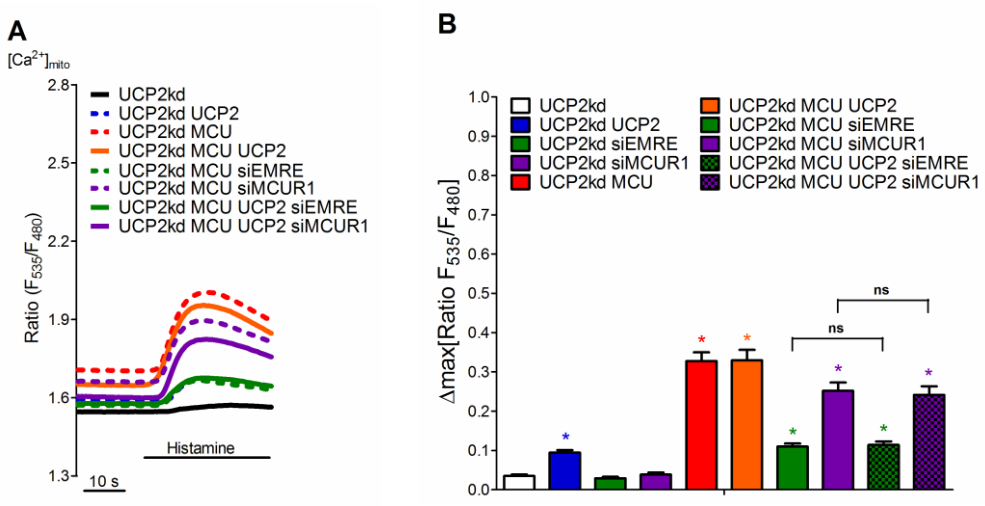

Figure 3.10: **UCP2/3 facilitates MCU/EMRE functions in mitochondrial Ca^{2+} buffering**. $UCP2^{kd}$ HeLa cells were co-transfected with 4mtD3cpv and a plasmid coding for MCU (*$UCP2^{kd}$ MCU*, red dashed line & red plain column, n65/3) or UCP2 (*$UCP2^{kd}$ UCP2*, blue dashed line & blue plain column, n56/3) in a ratio 1:3 and either control siRNA (*$UCP2^{kd}$*, black solid line & blank plain column, n=81/3) or siRNA against EMRE or MCUR1 (*$UCP2^{kd}$ siEMRE*, green plain column, n=51/3 or *$UCP2^{kd}$ siMCUR1*, violet plain column, n=46/3) or the combination of respective plasmids and siRNAs (*$UCP2^{kd}$ MCU UCP2*, yellow solid line & yellow plain column , n=52/3; *$UCP2^{kd}$ MCU siEMRE*, green dashed line & green plain column, n=64/3; *$UCP2^{kd}$ MCU siMCUR1*, violet dashed line & violet plain column, n=61/3; *$UCP2^{kd}$ MCU UCP2 siEMRE*, green solid line & green cross column, n=62/3; *$UCP2^{kd}$ MCU UCP2 siMCUR1*, violet solid line & violet cross column, n=67/3). $[Ca^{2+}]_{mito}$ in response to histamine 100 µM was measured. **(A)** Avarage curves represent ratio of YFP/CFP over time. **(B)** The peak $[Ca^{2+}]_{mito}$ response of all conditions was represented. Bar charts represent mean ± S.E.M. *; $p < 0.05$ versus *control*, #; $p < 0.05$ versus respective control.

PART II

3.2: Expression of MICU1 causes pronounced structural alteration pointing to the additional engagement of this protein in the structure and function of mitochondria

A morphological analysis of mitochondria was performed in order to investigate the impact of human MICU1 (hMICU1) on the structural change of mitochondria. The cells were evaluated into 3 different classes based on the morphology of mitochondria; normal tubular mitochondrial morphology (*Network*), network structure of shorter mitochondria or thick tubule (*Intermediate*), and fragmented mitochondrial structures (*Fragments* or *Dots*) (**Figure 3.11A**). The expression of hMICU1 showed a potent alteration in the morphology of mitochondria from highly interconnected and long tubular network to short tubular and less interconnected tubules. In comparison to mtDsRed-expressing group, the percentage of cells containing mitochondrial in the form of intermediate and fragments (dots) was significantly enhanced with an extensive reduction in cells having network structure in hMICU1-citrine group in both cell types (**Figure 3.11B**). Since expression of MICU1 yielded considerable structural changes, these interesting observations brought us to the point whether or not MICU1 contribute to an additional engagement in the ultrastructure and/or function of the mitochondria.

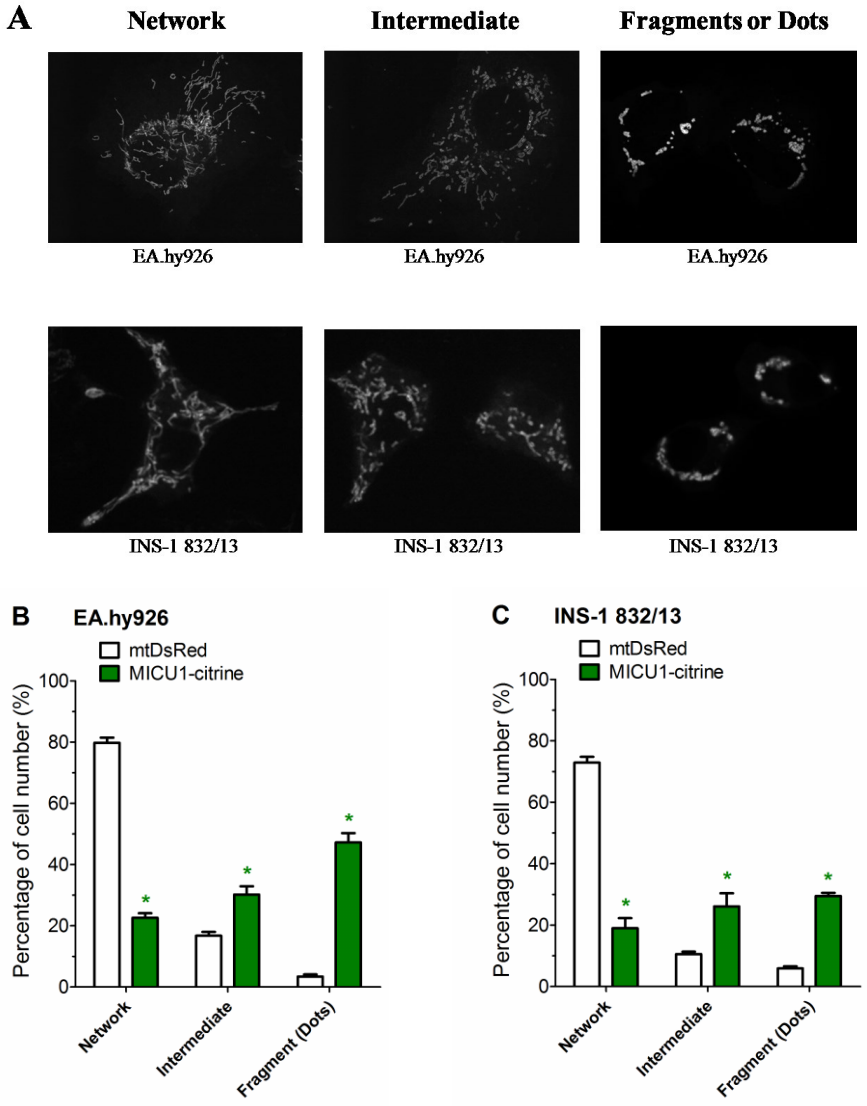

Figure 3.11: MICU1-citrine expressing cells show an alteration in the morphology of mitochondria in EA.hy926 and INS cells. Cells were transfected with mtDsRed (control) or hMICU1-citrine. After incubation for 24 hours, the cells were harvested and used for mitochondrial morphological analysis. **(A)** Live images were obtained by confocal microscopy. Cells were counted and divided into three groups based on the structure of mitochondria. The percentage of EA.hy926 cells **(B)** and INS-1 328/13 cells **(C)** in each indicated mitochondrial morphology was presented as mean ± S.E.M. A total of 758 and 890 EA.hy926 cells and 591 and 1,044 INS-1 328/13 cells were analyzed for mtDsRed and MICU1-citrine, respectively. Experiments were independently repeated 3 times in duplicate manner. *; $p < 0.05$ versus mtDsRed.

PART III

3.3: Rearrangement of MICU1 multimers for activation of MCU is solely controlled by cytosolic Ca^{2+}

Current chapter is based on the study of Markus Waldeck-Weiermair, Roland Malli*, Warisara Parichatikanond*, Benjamin Gottschalk, Corina T. Madreiter-Sokolowski, Christiane Klec, Rene Rost & Wolfgang F. Graier. Rearrangement of MICU1 multimers for activation of MCU is solely controlled by cytosolic Ca^{2+}. Sci. Rep. 5, 15602(2015) (Waldeck-Weiermair et al., 2015). (*; Equal contribution)*

3.3.1 Elevations of Ca^{2+} yield a rearrangement of MICU1 multimers in intact cells

3.3.1.1 Applying of a FRET-based live-cell imaging approach to monitor the reorganization of MICU1 oligomers

By measuring FRET between MICU1 proteins fused to either cyan or yellow fluorescent protein (MICU1-CFP or MICU1-YFP, respectively), the dynamic process of MICU1 rearrangement can be visualized and quantified. We used this approach to dynamically monitor whether and, if so, how an IP_3-generating agonist (histamine) induced intracellular Ca^{2+}-mobilization affects the arrangement of MICU1 in intact cells. Recently, Ca^{2+}-free MICU1 has been revealed to assemble in hexamers that binds and inhibits MCU and undergoes substantial conformational changes, resulting in the formation of multiple dimers to activate MCU upon Ca^{2+} binding, then regulates mitochondrial Ca^{2+} uptake (Wang et al., 2014). From this important finding, we assumed that under resting conditions the expressed MICU1-CFP and MICU1-YFP chimeras exist as hexamers, thus, facilitating FRET from CFPs to YFPs (**Figure 3.12**). On the other hand, the Ca^{2+} binding sites of MICU1 faced to the intermembrane space of mitochondria are occupied with Ca^{2+} in the presence of Ca^{2+}, consequently, leading to the dissociation of hexamers and declination of FRET.

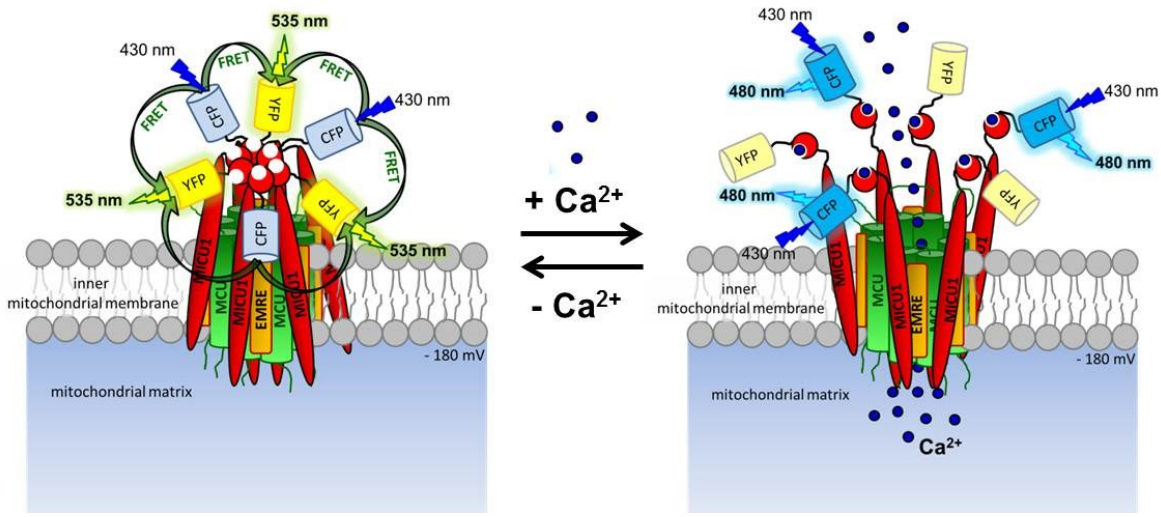

Figure 3.12: Ca^{2+}-induced rearrangement of MICU1 multimers by FRET approach. Schematic illustration of the putative Ca^{2+}-induced rearrangement of MICU1-CFP and MICU1-YFP hexamers that bind to the MCU/EMRE mitochondrial Ca^{2+} uptake machinery. It is hypothesized that Ca^{2+} binding to the MICU1 EF-hands reduces FRET between the respective MICU1-conjugated FPs.

3.3.1.2 Fast Ca^{2+} mobilization from the ER by IP3-generating agonist (histamine) caused disaggregation of MICU1 hexamers and strongly diminished the inter-MICU1 FRET signal

Since an elevation of cytosolic Ca^{2+} and its subsequent binding to MICU1 should yield disaggregation of MICU1 hexamers and reduce the inter-MICU1 FRET signal, an IP_3R agonist histamine was used to induce intracellular Ca^{2+} release from the ER and the inter-MICU1 FRET signal was observed. This results demonstrate that the inter-MICU1 FRET ratio was considerably decreased in the cells treated with the histamine (Waldeck-Weiermair et al., 2013) (**Figure 3.13A, 3.13B**), while expression of MICU1-YFP alone had no influence on the inter-MICU1 FRET signal (**Figure 3.14**). Upon removal of the histamine, the signal was restored (**Figure 3.13A, 3.13B**), indicating the reassembly of MICU1 to higher multimers upon the reduction of cytosolic Ca^{2+} levels.

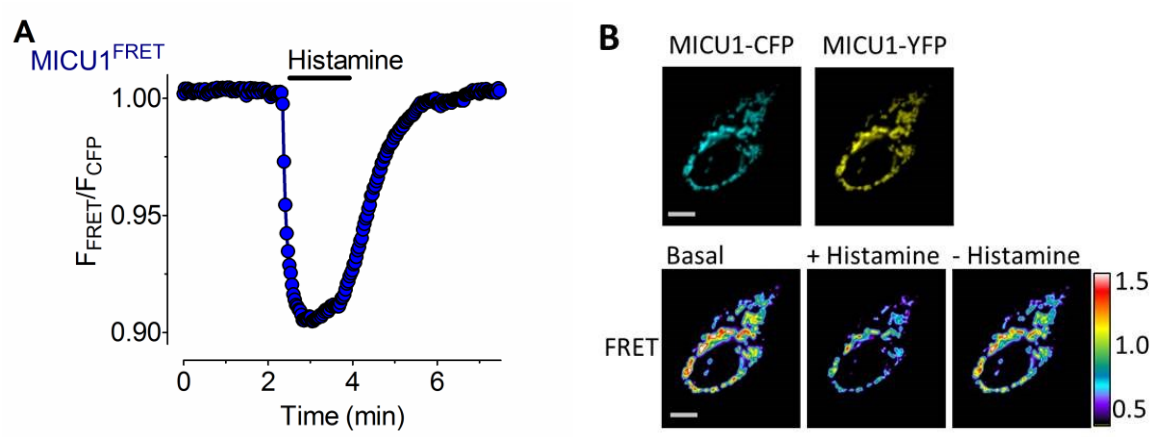

Figure 3.13: Ca^{2+} dynamically controls rearrangement of MICU1 multimers in intact cells. (A) Representative curve showing the inter-MICU1 FRET ratio signal of HeLa cells co-expressing MICU1-CFP and MICU1-YFP upon cell treatment with 100 µM histamine in the 2 mM Ca^{2+}-containing experimental buffer. **(B)** Representative images of a HeLa cell co-expressing MICU1-CFP and MICU1-YFP and respective FRET images (to panel A) under basal condition, upon stimulation with 100 µM histamine and 3 min. after stimulation (Scale bar, 10 µm).

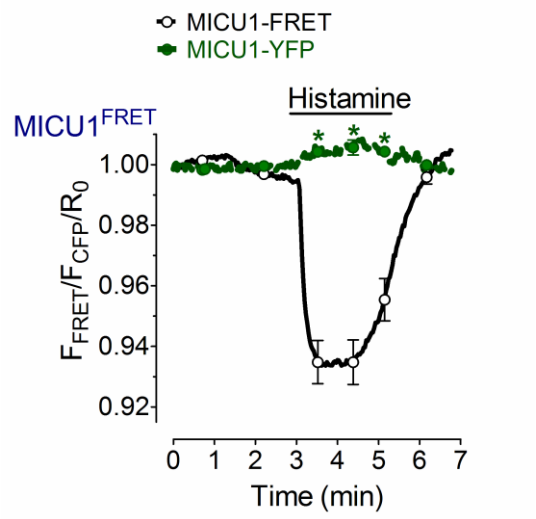

Figure 3.14: MICU1-YFP alone has no FRET signal after histamine stimulation. Average curves showing changes of the MICU1 FRET ratio of HeLa cells co-expressing either the combination of MICU1-CFP and MICU1-YFP (black curve, n=19) or MICU1-YFP alone (green dotted curve, n=13) after exposure with 100 µM histamine in calcium-free buffer. *; $p < 0.05$ versus MICU1-CFP and MICU1-YFP.

In addition, in the nominal absence of extracellular Ca^{2+}, the histamine-triggered decrease of inter-MICU1 FRET was more transient and slowly developed upon subsequent addition of extracellular Ca^{2+} (**Figure 3.15A**). In accordance with the inter-MICU1 FRET ratio, the cytosolic Ca^{2+} signals rose temporarily in response to Ca^{2+} release from the ER and delayed by additional Ca^{2+} entry, therefore, highlighting that inter-MICU1 FRET strictly follows cellular Ca^{2+} signals under these conditions (**Figure 3.15B**). Moreover, a rising of cytosolic Ca^{2+} signal and a reduction of inter-MICU1 FRET showed differences in the kinetics, since responses to the different concentrations and sources of Ca^{2+} by cytosolic Ca^{2+} ratio was faster than inter-MICU1 FRET signal by both IP_3-mediated intracellularly released and entering Ca^{2+} via SOCE.

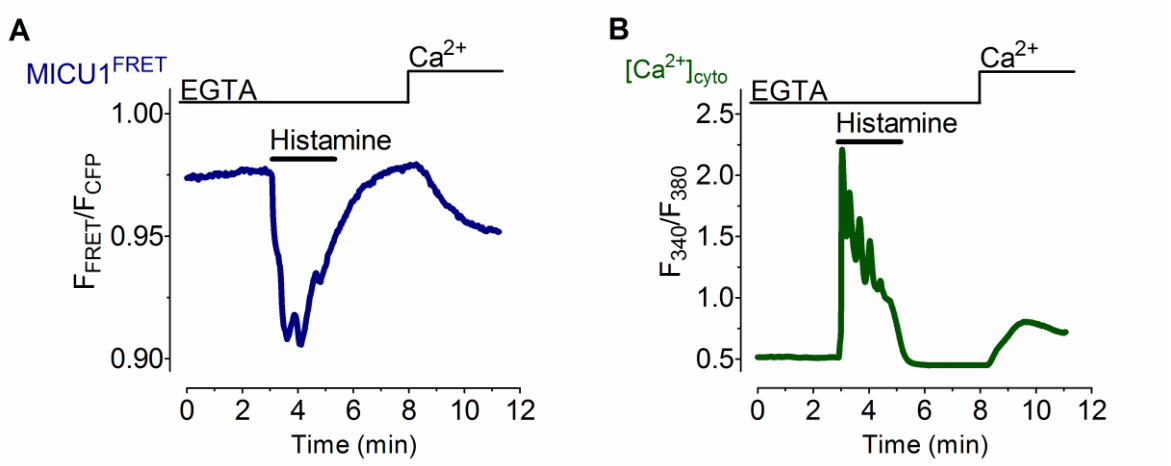

Figure 3.15: Rearrangement of MICU1 multimers in response to ER Ca^{2+} release and Ca^{2+} entry. (A) Representative changes of the MICU1 FRET ratio over time in HeLa cells co-expressing MICU1-CFP and MICU1-YFP. Cells were treated with 100 µM histamine in the nominal absence of Ca^{2+}. As indicated after removal of the IP_3-generated agonist 2 mM Ca^{2+} was added. **(B)** Cytosolic Ca^{2+} signals upon ER Ca^{2+} release and Ca^{2+} entry. Representative changes of $[Ca^{2+}]_{cyto}$ over time in HeLa cells that were loaded with fura-2/AM. Cells were treated with 100 µM histamine in the nominal absence of Ca^{2+}, and 2 mM of Ca^{2+} were added after removal of the IP_3-generated agonist.

3.3.1.3 Slow elevation of Ca^{2+} from the ER by the SERCA inhibitor slowly and weakly declined the inter-MICU1 FRET signal

In contrast to the fast intracellular Ca^{2+} entry in response to histamine, slow Ca^{2+} mobilization from the ER by the sarcoplasmic/endoplasmic reticulum Ca^{2+} ATPase (SERCA) inhibitor 2,5-di-tert-butylhydroquinone (BHQ) (Osibow et al., 2006) caused a decrease of the inter-MICU1 FRET signal in a delayed and weak manner (**Figure 3.16**). In line with these findings, mitochondrial Ca^{2+} mobilization in response to cell treatment with BHQ was moderate, but largely increased in cells treated with the siRNA-mediated knock down of MICU1 (**Figure 3.17**), despite an almost unaffected cytosolic Ca^{2+} elevation (**Figure 3.18**). These observations point out that the slow and weak ER depletion with BHQ yields only in insufficient MICU1-rearrangement, while the inhibitory function of MICU1 multimers on MCU remains under these conditions.

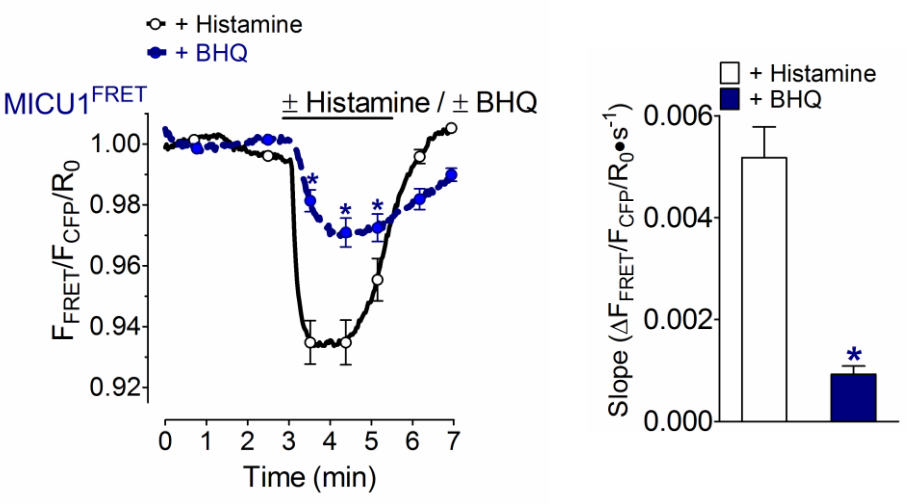

Figure 3.16: Moderate rearrangement of MICU1 multimers upon Ca^{2+} mobilization by SERCA inhibition. Average curves showing changes of the MICU1 FRET ratio upon cell treatment with 100 µM histamine (black curve, n=19) or 15 µM BHQ (blue dotted curve, n=21). Bars illustrating maximal slopes of the changes in the MICU1 FRET ratio signals (mean ± S.E.M) in response to 100 µM histamine (white column, n=19) or 15 µM BHQ (blue filled column, n=21). Cells were treated with histamine or BHQ in Ca^{2+}-free buffer. *; $p < 0.05$ versus histamine.

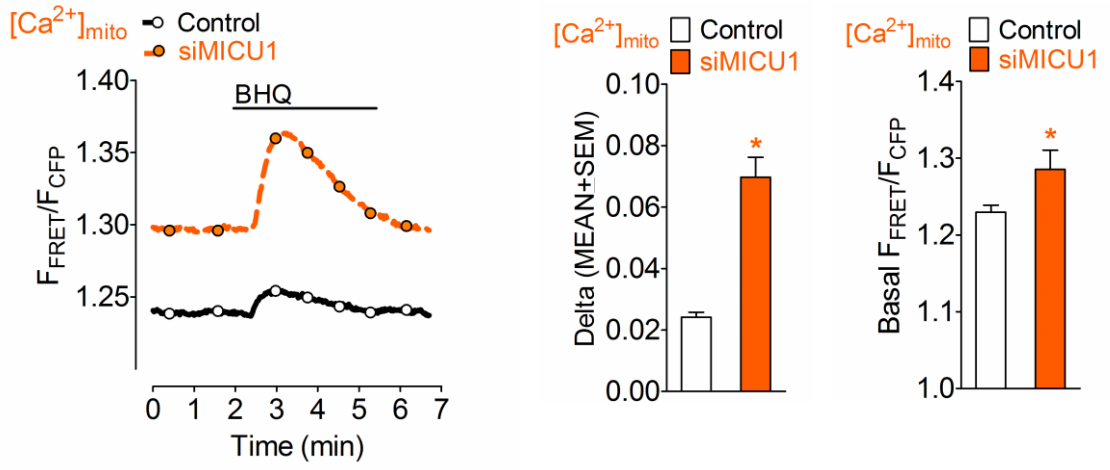

Figure 3.17: siRNA-mediated knock-down of MICU1 strongly increases mitochondrial Ca^{2+} sequestration upon Ca^{2+} mobilization by the SERCA inhibitor BHQ. Average data and statistics of mitochondrial Ca^{2+} uptake in response to SERCA inhibition by BHQ in control cells (black curve and white columns, n=33) and cells treated with siRNA against MICU1 (orange dotted curve and orange columns, n=24). HeLa cells expressing 4mtD3cpv were treated with 15 µM BHQ in the absence of extracellular Ca^{2+}. *; $p < 0.05$ versus control.

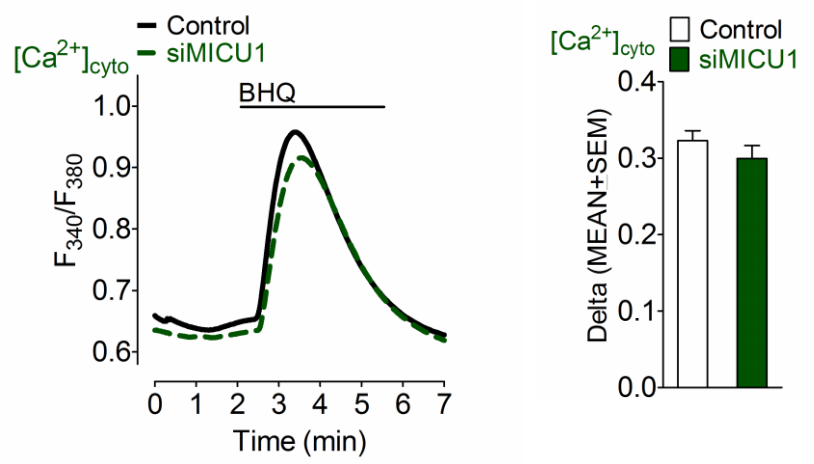

Figure 3.18: Silencing of MICU1 does not significantly affect cytosolic Ca^{2+} signals upon Ca^{2+} mobilization by the SERCA inhibitor BHQ. Average data and statistics of cytosolic Ca^{2+} signals. HeLa cells were stimulated with 15 µM BHQ in Ca^{2+}-free medium under control condition (black curve, white column, n=13) and in cells reduced of MICU1 (green dotted curve and green column, n=14).

3.3.1.4 Diminution of endogenous MICU1 could be rescued by simultaneous overexpression of wild-type MICU1-FP, whereas EF-hand mutated MICU1-FP expression in MICU1-silenced HeLa calls shows no recovery

To exclude the non-specific effects of the constructs of MICU1-FP tags (MICU1-CFP and MICU1-YFP), the rescue experiments of mitochondrial Ca^{2+} mobilization upon silencing of 3´UTR siRNA against MICU1 were performed. A mitochondrial targeted O-GECO (mtO-GECO) sensor was used to monitor changes of Ca^{2+} in mitochondria in order to avoid fluorescence contamination of the FP tagged MICU1 with mtD3cpV sensor, which is also based on CFP and YFP. Expression of one or both siRNA resistant FP tagged wild-type MICU1 (MICU1-FP) totally rescued mitochondrial Ca^{2+} entry in MICU1 depleted cells by treatment of BHG, and thus verified the functionality of MICU1-FP tags (**Figure 3.19**). On the other hand, using a MICU1 variant mutated in both canonical EF hands ($MICU1_{EFmut}$-FP) (Perocchi et al., 2010, Wang et al., 2014) was ineffective to rescue the siRNA mediated effect of MICU1 upon histamine induced Ca^{2+} release (**Figure 3.20**). In addition, co-expression of $MICU1_{EFmut}$-FP tags could not rearrange MICU1 multimers upon stimulation with histamine, while wild-type MICU1-FP tags does (**Figure 3.21**). For this reason, these results clearly confirmed that the tags are incapable of interfering with the function of intrinsic MICU1 and these constructs are functionally competent.

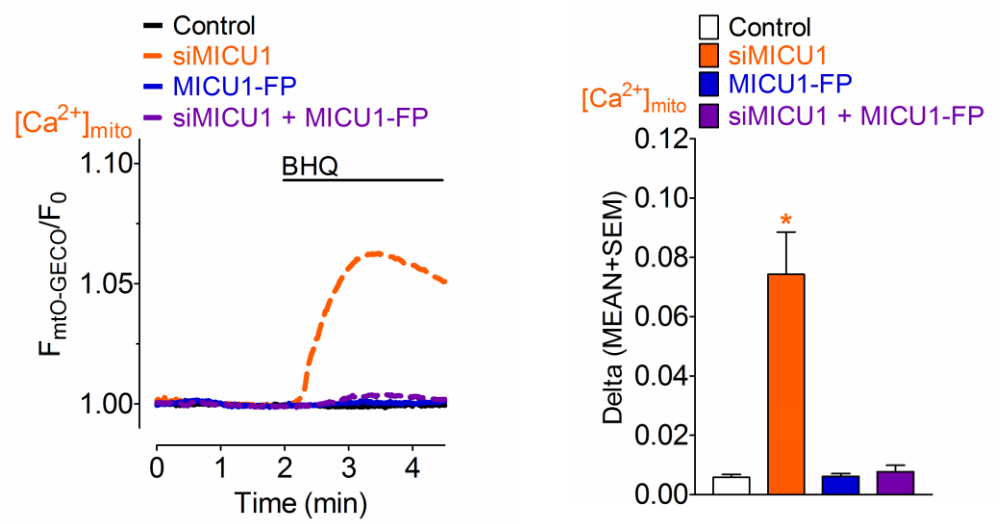

Figure 3.19: Expression of wild-type MICU1-FP tags (-CFP and -YFP) rescues siRNA-mediated depletion of MICU1. Average data and statistics of mitochondrial Ca^{2+} sequestration in response to BHQ in control cells (black curve and white column, n=27), cells treated with the 3´UTR-siRNA against MICU1 (orange dotted curve and orange column, n=35), overexpressing C-terminal FP-tagged MICU1 (blue curve and blue column, n=20) or transfected with a combination of siRNA against MICU1 and FP-tagged MICU1 (red dotted curve and red column, n=20). HeLa cells expressing mtO-GECO1 were treated with 15 µM BHQ in the absence of extracellular Ca^{2+}. *; $p < 0.05$ versus control.

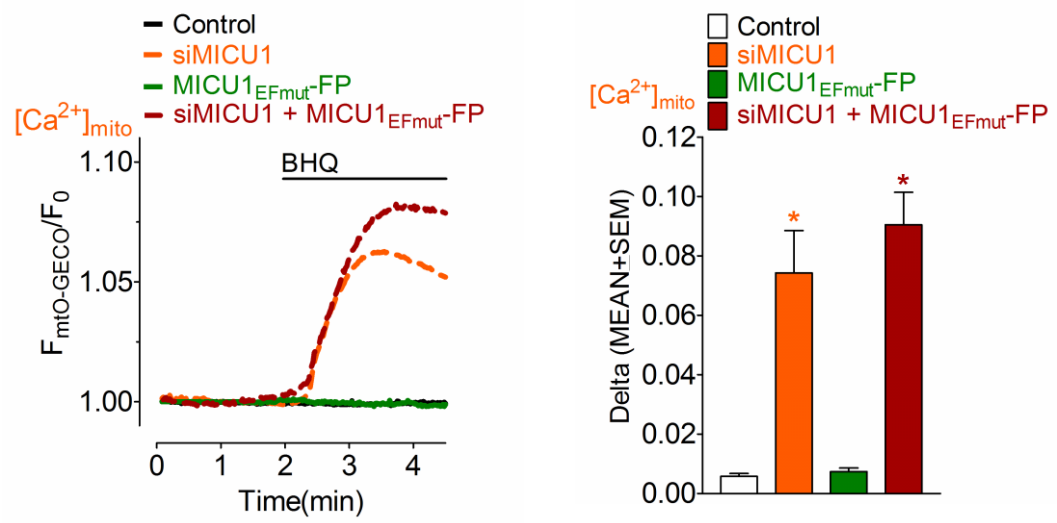

Figure 3.20: Expression of canonical EF hands mutated MICU1-CFP and -YFP ($MICU1_{EFmut}$-FP) is ineffective to rescue siRNA-mediated silencing of MICU1. Average data and statistics of mitochondrial Ca^{2+} mobilization measured by mtO-GECO1 in response to 15 µM BHQ in the absence of extracellular Ca^{2+} in control cells (black curve and white column, n=27), cells treated with siRNA against MICU1 (orange dotted curve and orange column, n=35), overexpression of EF hand mutated MICU1 C-terminally tagged with FP (green curve and green column, n=19) or transfected with a combination of siRNA against MICU1 and FP-tagged EF hand mutated MICU1 (red dotted curve and red column, n=18). *; $p < 0.05$ versus control.

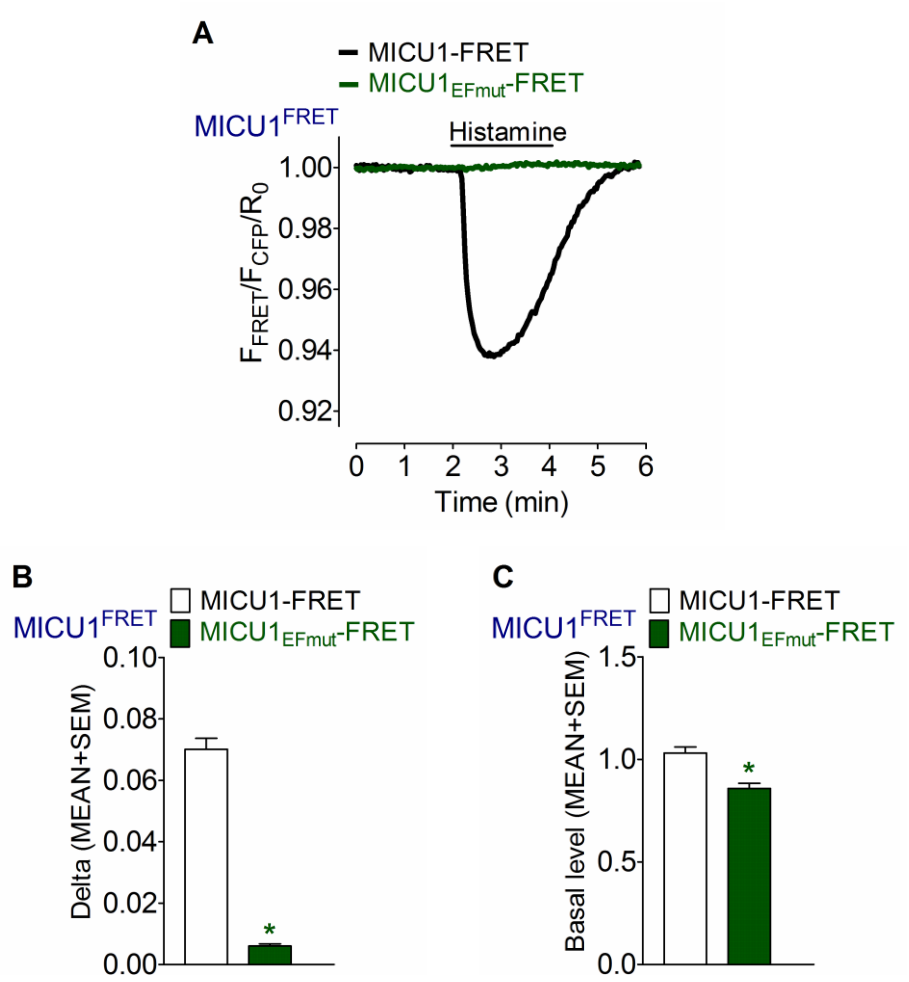

Figure 3.21: Co-expression of EF hand mutated MICU1-CFP and -YFP is incompetent to rearrange MICU1 multimers. Average data and statistics of MICU1 FRET in control cells (black curve and white columns, n=31) and in cells overexpressing of EF hand mutated MICU1 C-terminally tagged with CFP and YFP (green curve and green column, n=30). *; $p < 0.05$ versus control.

3.3.1.5 By stimulation with IP3-generating agonist, the rearrangement of MICU1 multimers occurs during the concentration range of Ca^{2+} found in hot spots between the ER and mitochondria

In order to determine the affinity of the MICU1 multimers for Ca^{2+} to generate their rearrangement *in situ*, the Ca^{2+} ionophore ionomycin was used to permeabilize cells, hence, clamp different cytosolic Ca^{2+} concentrations (**Figure 3.22A, 3.22B**). With the subsequent titration of extracellular Ca^{2+} ranging from 0 to 1000 µM we determined the dissociation constant of Ca^{2+} for MICU1 FRET rearrangement. To eliminate cell to cell variability we set the maximum value at 0 µM Ca^{2+} to 100 % and the minimum value at 1000 µM Ca^{2+} to 0 % of the actual MICU1 FRET ratios. For calculation of the K_d, we then used the percentage of decrease upon the application of the individual Ca^{2+} concentrations.

The results revealed a half maximal effective Ca^{2+} concentration (EC_{50}) to trigger rearrangement of the MICU1 multimers of 4.4 (3.7-5.2) µM in permeabilized HeLa cells (**Figure 3.22B**). Notably, the small effects during ionomycin incubation at the beginning (5 min) of the trace arise from ER Ca^{2+} release, which is beneficial for Ca^{2+} calibrating experiment since any side-effects during titration from that source are excluded and the main effects were shown from minute 5 to 15 of this representative curve are clearly reflecting a decrease of the inter-MICU1 FRET in a Ca^{2+} concentration-dependent manner (**Figure 3.22A**). Remarkably, these findings are in accordance with the studies reporting the existence of Ca^{2+} microdomains of up to 16 µM in hot spots between the ER and neighboring mitochondria in response to an IP_3-generating agonist (Giacomello et al., 2010). As a consequence, the huge Ca^{2+} hot spots as the indicated concentration created by intracellularly released Ca^{2+} would efficiently dissociate MICU1 multimers to multiple dimers and, hence, activate MCU. Our results provide a first demonstration that MICU1 rearrangement is reversibly regulated by high and low $[Ca^{2+}]_{cyto}$ in intact cells.

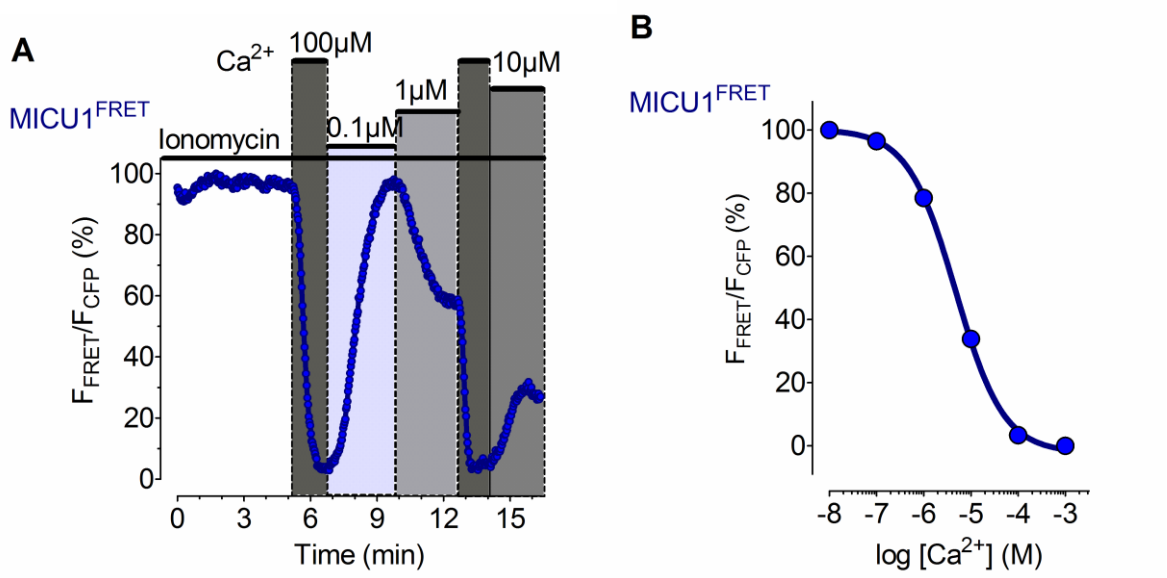

Figure 3.22: The affinity of the MICU1 multimers in permeabilized HeLa cells. (A) Representative MICU1 FRET ratio signals over time in HeLa cells upon addition and removal of different free Ca^{2+} concentrations in the presence of 3 µM ionomycin. The maximal Δ MICU1 FRET ratio signal (between 3 mM EGTA and 1000 µM Ca^{2+}) was defined as 100 %. **(B)** The *in situ* concentration response curve of the Ca^{2+}-induced reduction of the MICU1 FRET ratio signal in HeLa cells that were treated with 3 µM ionomycin and different Ca^{2+} concentrations as shown in panel (A); mean ± S.E.M. (n=7-9).

3.3.2 Ca^{2+}-triggered MICU1 de-multimerization occurs prior to mitochondrial Ca^{2+} sequestration

In order to compare the kinetics of cytosolic and mitochondrial Ca^{2+} signals, a simultaneous imaging of cytosolic and mitochondrial Ca^{2+} signals in individual single cells using a red-shifted mitochondria targeted cameleon (mtD1GO-Cam) in combination with the near ultra-violet excitable cytosolic Ca^{2+} sensor fura-2/AM was performed. This approach revealed a lag time (ΔT) of 1.50 ± 0.08 s between the cytosolic Ca^{2+} rise and its transition into the mitochondrial matrix upon intracellular Ca^{2+} mobilization by the IP_3-generating agonist histamine (**Figure 3.23A**). The molecular mechanism responsible for this temporal shift between rises of $[Ca^{2+}]_{cyto}$ and $[Ca^{2+}]_{mito}$ is so far unknown. The identical experiments were performed in cells transfected with siRNA against MICU1 to investigate whether or not the Ca^{2+}-dependent dissociation of MICU1 multimers might delay mitochondrial Ca^{2+} signals. The results clearly demonstrate that a known down of MICU1 in HeLa cells productively improved the coupling between cytosolic and mitochondrial Ca^{2+} signals and the mitochondrial Ca^{2+} signal followed almost immediately the cytosolic Ca^{2+} elevation upon histamine stimulation (ΔT = 0.93 ± 0.05 s) (**Figure 3.23B, 3.23C**).

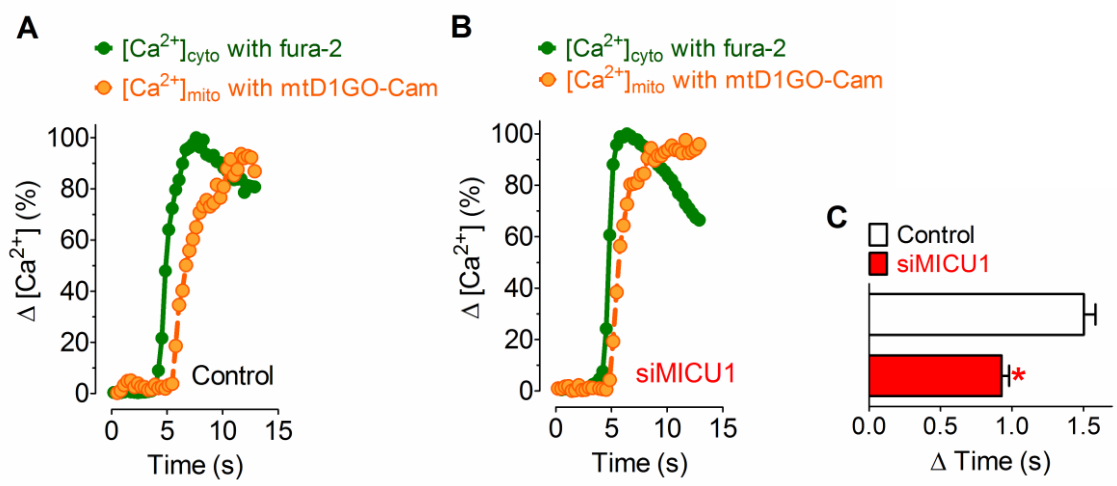

Figure 3.23: Rearrangement of MICU1 multimers occurs prior to mitochondrial Ca^{2+} uptake. Fura-2/AM loaded cells expressing 4mtD1GO-Cam were used to simultaneously record $[Ca^{2+}]_{cyto}$ (green traces) and $[Ca^{2+}]_{mito}$ (orange traces) in response to cell treatment with 100 µM histamine in the absence of extracellular Ca^{2+} in control HeLa cells **(A)** and cells reduced of MICU1 **(B)**. The respective Δ ratio values were defined as 100 %. **(C)** Bar graph showing Δ mean time values ± S.E.M. between the onset of cytosolic and mitochondrial Ca^{2+} signals in response to 100 µM histamine of individual control HeLa cells (white column, n=7) and cells diminished of MICU1 (red column, n=9). *; $p < 0.05$ versus control.

In order to investigate how the temporal pattern of MICU1 dissociation is related to cytosolic Ca^{2+} signals, dynamic changes of MICU1 FRET simultaneously with cytosolic Ca^{2+} in response to histamine were observed (**Figure 3.24A**). Simultaneous measurement of $[Ca^{2+}]_{cyto}$ and inter-MICU FRET signal was performed in HeLa cells by using O-GECO and a combination of MICU1-CFP/MICU1-YFP, respectively. The recordings showed that upon stimulation by histamine MICU1 rearrangement was slightly delayed from the increase of cytosolic Ca^{2+} signals and, then, continued with mitochondrial Ca^{2+} entry (**Figure 3.24B**). Notably, approximately 90 % of the maximal histamine-induced augmentation of $[Ca^{2+}]_{cyto}$ trigger ≥ 50 % of MICU1 de-oligomerization that appears essential to initiate considerable uptake of Ca^{2+} by mitochondria (**Figure 3.24A, 3.24B**). These data dissect the transfer of cytosolic Ca^{2+} into mitochondria into (at least) four sequential steps: *first* cytosolic Ca^{2+} elevation and transfer into the intermembrane space, *second* binding of Ca^{2+} to MICU1 multimers, *thrid* MICU1 de-oligomerization, and *forth* activation of the MCU.

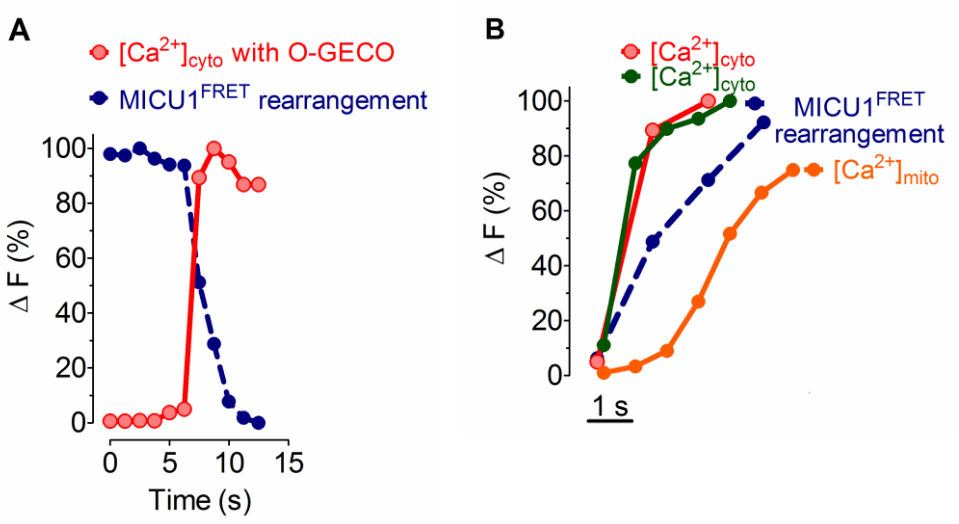

Figure 3.24: Simultaneously dynamic changes of MICU1 FRET in response to histamine. (A) Representative simultaneous recording of $[Ca^{2+}]_{cyto}$ and MICU1 FRET in response to 100 µM histamine in Ca^{2+}-free conditions using HeLa cells co-expressing O-GECO, MICU1-CFP and MICU1-YFP. **(B)** Temporal correlation of $[Ca^{2+}]_{cyto}$, $[Ca^{2+}]_{mito}$ and MICU1 FRET in response to cell treatment with 100 µM histamine in the absence of extracellular Ca^{2+}. The MICU1 FRET signal (blue dotted trace) was reversed.

3.3.3 Rearrangement of MICU1 multimers is independent on the mitochondrial membrane potential (Ψ_{mito}) and matrix Ca^{2+} elevation

In order to check whether or not the Ψ_{mito} has an impact on the rearrangement of MICU1 multimers, cells were treated with oligomycin and the uncoupling agent carbonyl cyanide-4-(trifluoromethoxy) phenylhydrazone (FCCP) to efficiently depolarize

mitochondria, hence, only very small mitochondrial Ca^{2+} signals in response to histamine were observed approving the loss of Ψ_{mito} under these conditions (**Figure 3.25A**). However, depolarization of mitochondria did neither affect basal MICU1 FRET nor the histamine-triggered reduction of the inter-MICU1 FRET signal (**Figure 3.25B**). These data indicate that the rearrangement of MICU1 multimers upon intracellular Ca^{2+} mobilization with an IP_3-generating agonist occurs independently of Ψ_{mito} and the mitochondrial matrix Ca^{2+} elevation.

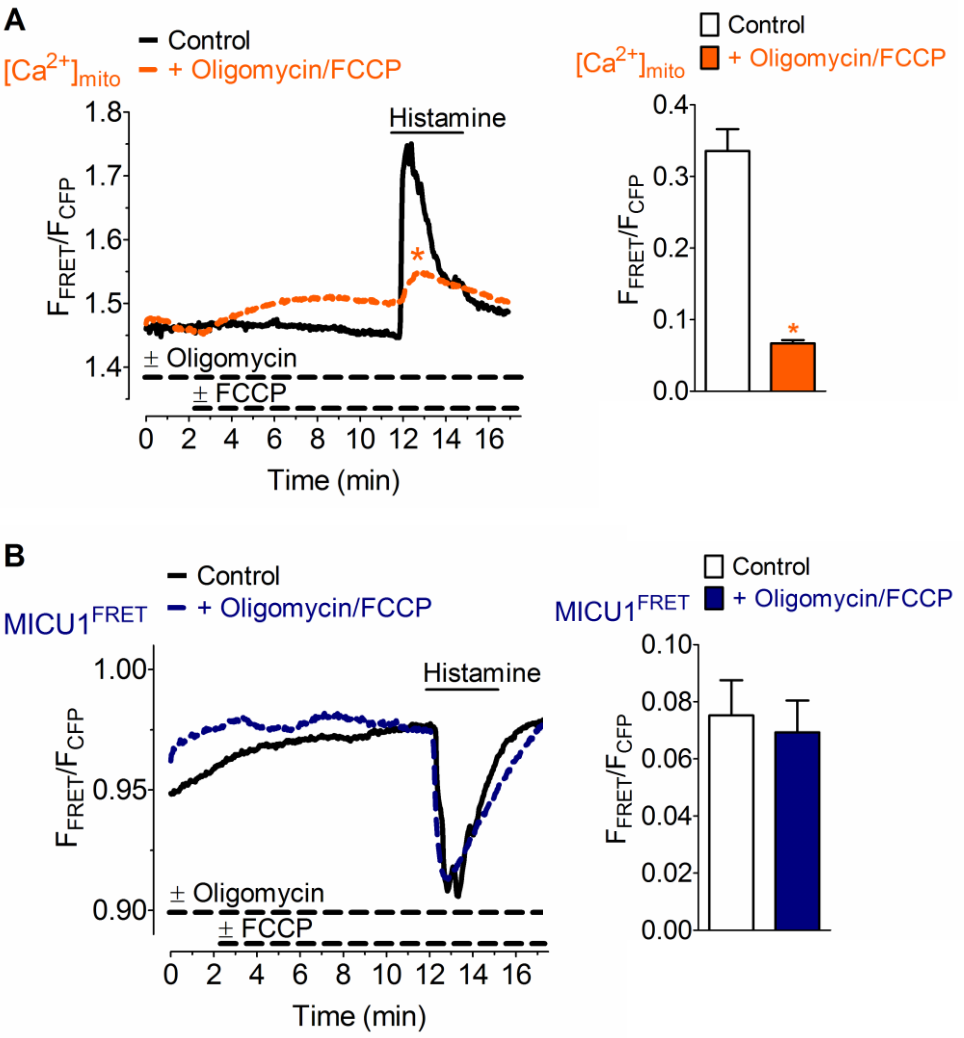

Figure 3.25: The Ca^{2+}-induced rearrangement of MICU1 multimers is independent of Ψ_{mito}. (A) Average curves reflecting mitochondrial Ca^{2+} signals over time of HeLa cells expressing 4mtD3cpv upon cell treatment with 100 µM histamine in the absence of extracellular Ca^{2+} under control conditions (black curve, n=10) and in the presence of 2 µM oligomycin and 4 µM FCCP (orange curve, n=14). Bar graph shows respective maximal Δ ratio signals; mean ± S.E.M. *; $p < 0.05$ versus control. **(B)** Average MICU1 FRET ratio signals of HeLa cells co-expressing MICU1-CFP and MICU1-YFP in response to 100 µM histamine in Ca^{2+}-free conditions in the absence of oligomycin and FCCP (control, black curve, n=3) and the presence of 2 µM oligomycin and 4 µM FCCP (blue curve, n=6). Bar graph shows respective maximal Δ MICU1 FRET ratio signals; mean ± S.E.M.

3.3.4 MICU1 multimers rearrange irrespective of the expression level of MCU and EMRE

MICU1 is known to interact with EMRE (Sancak et al., 2013) that represents the second pore forming protein of the mitochondrial Ca^{2+} complex beside MCU (Foskett and Philipson, 2015, De Stefani and Rizzuto, 2014, Kamer et al., 2014), which is regulated by MICU1 (Patron et al., 2014, Hoffman et al., 2013, Kevin Foskett and Madesh, 2014). To examine the contribution of EMRE and MCU for the Ca^{2+}-triggered rearrangement of MICU1 multimers, expression of either EMRE or MCU were effectively diminished by respective verified siRNAs and validated by qPCR (**Figure 3.26C**). Silencing of the expression of either MCU or EMRE potently decreased mitochondrial Ca^{2+} uptake (**Figure 3.26A**), while no influence on cytosolic Ca^{2+} signaling was observed (**Figure 3.26B**). However, the rearrangement of the MICU1 multimers upon stimulation with histamine was neither affected by knockdown of MCU (**Figure 3.27A, 3.27B**) nor EMRE (**Figure 3.27A, 3.27C**). In line with these findings, the EC_{50} of Ca^{2+} to decrease the inter-MICU1 FRET signal remained unaltered in cells depleted with either MCU or EMRE (**Figure 3.28**).

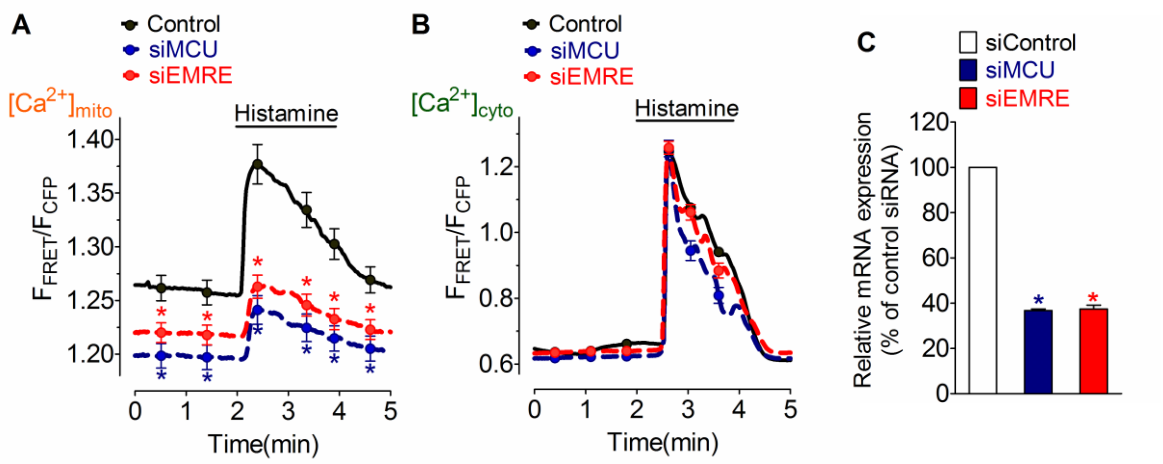

Figure 3.26: Knock-down of either MCU or EMRE extensively suppresses mitochondrial Ca^{2+} mobilization and has no effect on cytosolic Ca^{2+} level. (A) Average curves showing mitochondrial Ca^{2+} signals over time in control cells (black curve, n= 21), cells treated with siRNA against MCU (blue dotted curve, n=15), and cells treated with siRNA against EMRE (red curve, n=18). **(B)** Average cytosolic Ca^{2+} level in control cells (black curve, filled circles, n= 13), cells treated with siMCU (blue dotted curve, blue filled circles, n=10), and cells treated with siEMRE (red curve, red filled circles, n=15). Cells transfected with 4mtD3cpv were loaded with fura-2/AM and stimulated with 100 µM histamine in Ca^{2+}-free experimental buffer. **(C)** MCU and EMRE gene expression after siRNA-mediated knock-down. Bars illustrate relative mRNA expression levels of control cells (white bar, 100 %, n=4), cells treated with siRNA against MCU (blue column, n=4) and cells treated with siRNA against EMRE (red column, n=4). Mean ± S.E.M. *; $p < 0.05$ versus control.

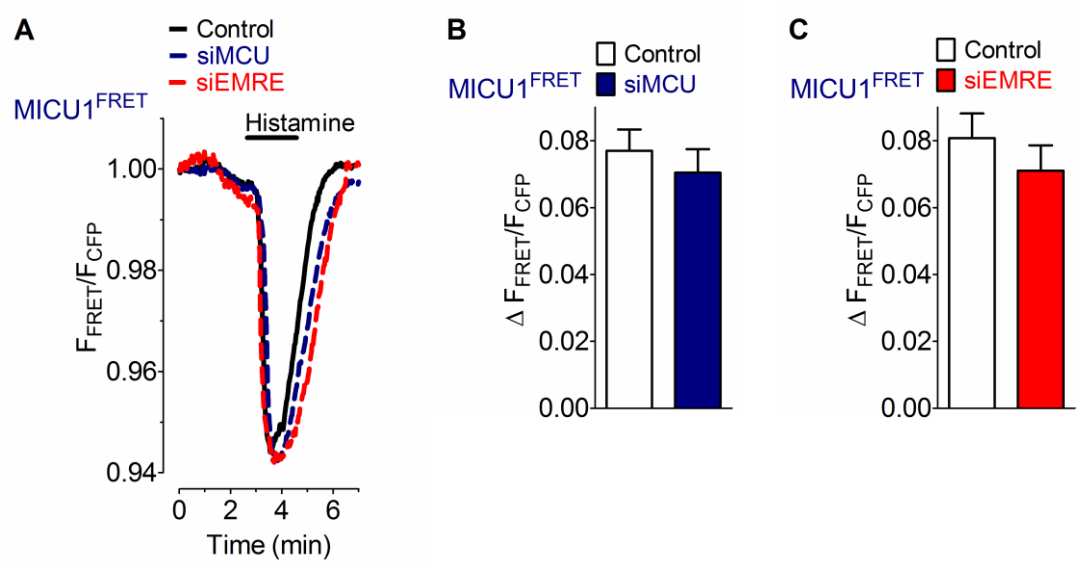

Figure 3.27: The Ca^{2+}-induced rearrangement of MICU1 multimers is independent of the expression level of MCU and EMRE. (A) Average curves of MICU1 FRET ratio signals over time in response to 100 µM histamine in Ca^{2+}-free solution of control HeLa cells (black curve, n=23) and cells treated with siRNA against MCU (blue curve, n=22). **(B)** Bars represent maximal Δ MICU1 FRET ratio values (mean ± S.E.M) extracted from curves shown in panel A. **(C)** Bars represent maximal Δ MICU1 FRET ratio values upon cell treatment with 100 µM histamine in Ca^{2+}-free solution of control HeLa cells (white column, n=19) and cells treated with siRNA against EMRE (red column, n=12).

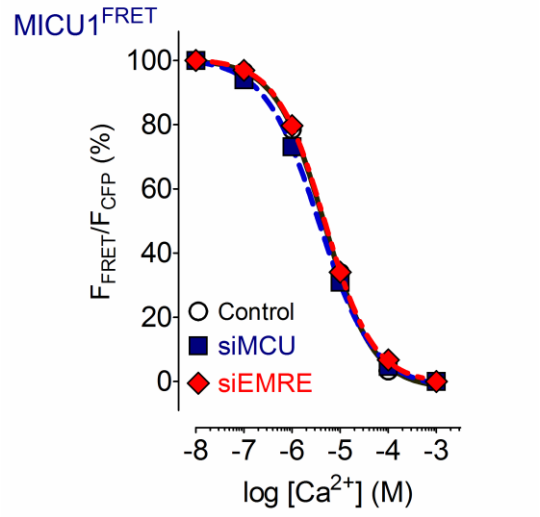

Figure 3.28: Concentration response curves showing the impact of different Ca^{2+} concentrations on the MICU1 FRET ratio in ionomycin (3 µM) treated control HeLa cells. Average curves of control cells (black curve, white circles, n=7-9), cells depleted of MCU (blue dotted curve, blue filled squares, n=8-10), and cells reduced of EMRE (red dotted curve, red filled rhombs, n=10).

CHAPTER IV
DISCUSSION

PART I

4.1: MICU1 is a negative regulator of the MCU that is under the control of UCP2/3 in mitochondrial Ca^{2+} uptake

Mitochondrial Ca^{2+} uptake plays a crucial role in numerous cellular functions. After extensive studies for a decade, the molecular components and critical regulators of the MCU complex have been recently revealed, including MICU1, UCP2/3, EMRE, and MCUR1. In addition, their structural and functional characterizations have been characterized and reported. However, the mechanism by which these protein molecules interact and coordinate with each other to regulate the mobilization of Ca^{2+} through mitochondrial membranes remains elusive. Comprehensive understanding of these regulatory processes is the aims of our study that leads us to the development of an investigation and a molecular intervention of mitochondrial dysfunction related diseases in the future.

In this study, the entry of Ca^{2+} into mitochondrial matrix was greatly diminished by a stable knockdown of one of the two proteins located in the IMM, which has been shown to be involved in mitochondrial Ca^{2+} entry (Waldeck-Weiermair et al., 2013), including MCU or UCP2 in MCU^{kd} or $UCP2^{kd}$ HeLa cells, respectively (Baughman et al., 2011, De Stefani et al., 2011, Trenker et al., 2007). MCU is the pore-forming subunit of a mitochondrial Ca^{2+} channel and contributes to mitochondrial Ca^{2+} entry which is independent of the mode of Ca^{2+} mobilization and Ca^{2+} source (Baughman et al., 2011, De Stefani et al., 2011). On the other side, UCP2 has been reported to be involved with mitochondrial Ca^{2+} uptake mainly the Ca^{2+} from areas of high Ca^{2+} concentration (known as Ca^{2+} microdomains) which are structured by ER Ca^{2+} depletion (Waldeck-Weiermair et al., 2013). In line with previous observations, our data represent that both UCP2 and MCU are essential to achieve mitochondrial Ca^{2+} entry in HeLa cells after exposure with IP_3R agonist, pointing to a possible functional connection of these proteins, which is still need further investigation. In addition, these findings were further confirmed by the exploration of three distinct mitochondrial Ca^{2+} channel currents identified at the IMM of HeLa cells by using patch clamp technique. The most frequently occurring one (the intermediate conductance mitochondrial Ca^{2+} current; i-MCC) depends on the presence of MCU

(Bondarenko et al., 2014). Moreover, our data support the previous reports that demonstrate that the depletion of MCU or UCP2 has a selective influence on the specific modes of mitochondrial Ca^{2+} uptake, either intracellularly Ca^{2+} released from the ER or extracellularly Ca^{2+} entering via SOCE (Waldeck-Weiermair et al., 2011, Waldeck-Weiermair et al., 2010a, Deak et al., 2014). Hence, MCU^{kd} and $UCP2^{kd}$ HeLa cells serve as suitable models to investigate the role of mitochondrial Ca^{2+} uptake from both sources of Ca^{2+}. For this reason, these cell types were employed for studying the role of particular proteins on mitochondrial Ca^{2+} entry specifically via the IP_3-induced Ca^{2+} release throughout our study.

Although a significant contribution of MCU and UCP2/3 to mitochondrial Ca^{2+} buffering has been extensively unveiled, the impact of the recently discovered protein located in the IMM, MICU1 (Perocchi et al., 2010) on the function of UCP2/3 remains elusive, while the MCU was shown to be tightly regulated by MICU1 (Baughman et al., 2011, De Stefani et al., 2011, Mallilankaraman et al., 2012b, Csordas et al., 2013, Hoffman et al., 2013, Kamer and Mootha, 2014, Patron et al., 2014). Co-IP experiments indicated that MICU1 and MCU physically interact with each other (Baughman et al., 2011, Mallilankaraman et al., 2012b, Hoffman et al., 2013, Wang et al., 2014). Originally, MICU1 was reported to be an essential component of the uniporter complex and facilitates MCU-dependent mitochondrial Ca^{2+} via the cooperative of EF-hands in HeLa cells (Perocchi et al., 2010) and clonal pancreatic beta-cells (Alam et al., 2012) but not endothelial cells (Waldeck-Weiermair et al., 2011). Nevertheless, a recent study revealed the contradictory role of MICU1 in HeLa and endothelial cells that functions as a gatekeeper and limit MCU-induced Ca^{2+} influx, hence, preventing MCU-mediated mitochondrial Ca^{2+} overloads (Mallilankaraman et al., 2012b). Our findings are in agreement with this report since diminution of MICU1 resulted in an increase of basal $[Ca^{2+}]_{mito}$ level under the resting condition and mitochondrial Ca^{2+} entry upon IP_3-mediated depletion of ER Ca^{2+} store by histamine. The role of MICU1 as MCU gatekeeper was confirmed later, MICU1 regulates MCU-mediated Ca^{2+} uptake in a dose-dependent manner based on cytosolic Ca^{2+} (Csordas et al., 2013). Under a low $[Ca^{2+}]_{cyto}$, MICU1 does not bind Ca^{2+}, then, Ca^{2+}-free MICU1 inhibits Ca^{2+} uptake into mitochondria and sets a threshold for MCU, whereas MICU1 binds Ca^{2+} and further activates mitochondrial Ca^{2+} uptake under a high $[Ca^{2+}]_{cyto}$. Nevertheless, the various experimental conditions were discussed to be one of the reasons for the varied results from different research groups. For instance, it is mandatory to use the fluorescent dyes with the similar Ca^{2+} concentration

range for Ca^{2+} measurements in order to avoid contrasting interpretations (Wang et al., 2014). They also mentioned that the affinity of MICU1 for Ca^{2+} is around 15-20 μM, consequently, MICU1 shows less tendency to bind Ca^{2+} in a resting cells, which is in line with the previous proposed model (Csordas et al., 2013).

Despite the evidence that supported UCP2/3 as being part of the MCU is increasing (Trenker et al., 2007, Wu et al., 2009, Graier et al., 2008, Waldeck-Weiermair et al., 2010b, Dejean et al., 2004), the supposed engagement of UCP2/3 to mitochondrial Ca^{2+} uptake is still controversial (Graier et al., 2007, Carafoli, 2010, Contreras et al., 2010, Santo-Domingo and Demaurex, 2010). Additionally, the specific mode of mitochondrial Ca^{2+} uptake has been recently demonstrated to be modulated by the function of either one or more than one different proteins (Michels et al., 2009, Waldeck-Weiermair et al., 2010b, Jiang et al., 2009, Naghdi et al., 2010), thus, challenging the concept of one protein/phenomenon to be responsible for mitochondrial Ca^{2+} sequestration. Previous assumptions suggest that it is unlikely that UCP proteins transport Ca^{2+} directly into mitochondria (Pendin et al., 2014). Our data is in consistent with the previous study that found that the diminution of UCP2/3 by specific siRNA considerable diminished mitochondrial Ca^{2+} uptake, whereas overexpression of these respective proteins enhanced the efficacy of mitochondrial Ca^{2+} accumulation (Trenker et al., 2007). Nevertheless, another study reports neither of the two proteins, when expressed in budding yeast conferred to their mitochondria the capacity of accumulating Ca^{2+} in the matrix, leading the authors to suggest that UCP2/3 are modulators of MCU and not MCU itself (Trenker et al., 2007). As a consequence, we hypothesize that UCP2/3 might indirectly regulate MCU via the contribution of other candidate proteins located in the IMM, hence, our study aim to explore the mechanistic interaction of UCP2/3-dependent mitochondrial Ca^{2+} uptake machinery by focusing on the contribution of the promising recently discovered IMM protein, especially the MICU1, which remains unknown so far. Our data exhibit that diminution of MICU1 boosts the effect of UCP2/3 on MCU activity in MCU^{kd} cells overexpressed with UCP2/3, while this phenomenon was not observed in these indicated condition but without overexpression of UCP2/3, pointing to UCP2/3 might interact and involve with the MICU1 in mitochondrial Ca^{2+} sequestration process. Therefore, our results indicate that UCP2/3 facilitates mitochondrial Ca^{2+} uptake by MCU complex and thereby counteracts the inhibitory function of MICU1 on the MCU complex.

Considering about the patterns of the response from MCU^{kd} cells with silencing of MICU1 and overexpression of MCU or UCP2/3 found in our study, an overexpression of

MCU or UCP2/3 in MICU1-depleted MCU^{kd} cells could restore or even boost mitochondrial Ca^{2+} entry, which were categorized as a *rescued* (shControl-like) and a *boosted* (overexpressed MCU-like), respectively. An extensively distributed pattern of mitochondrial Ca^{2+} entry in MCU^{kd} cells depleted with MICU1 and overexpressing MCU or UCP2/3 gives us a clue that these particular proteins might exclusively interact with each other in the unique manner that affects their regulatory roles of Ca^{2+} transportation into mitochondria. The possible explanation of this phenomenon could be the variable expression pattern of MICU1 and MCU or UCP2/3 which might cause the difference of stoichiometric interaction of MICU1 with MCU or UCP2/3. This varied interaction might be responsible for different patterns of responses in such indicated condition. Another reason might be explained by the existence of more than one isoforms of MICU1 and MCU since they might interact differently, thereby, brings another possibility about the various regulatory pattern of MICU1. However, further studies are still in demand to clarify the exact contribution of these particular candidates in the process of mitochondrial Ca^{2+} sequestration.

Recently, other associated proteins located in the IMM have been discovered to be essential for mitochondrial Ca^{2+} entry, including EMRE (Sancak et al., 2013) and MCUR1 (Mallilankaraman et al., 2012a), pointing to these particular proteins might assist us to explain the intricate regulation of the MCU or UCP2/3 activity by MICU1. EMRE was reported to be essential for Ca^{2+} channel activity and keep the MICU1/MICU2 dimer interacted to MCU complex since downregulation or knockout of EMRE abolished the interaction between MICU1/MICU2 and MCU (Sancak et al., 2013) which was supported by our data that exhibit transient silencing of EMRE diminished mitochondrial Ca^{2+} sequestration after histamine stimulation in HeLa cells. Likewise, our findings clearly represent that EMRE contributes to MCU and UCP2 in the regulation of mitochondrial Ca^{2+} entry upon an overexpression of MCU or UCP2/3. Additionally, EMRE was presented to interact with MICU1 and MICU2 in the IMS (Promerova et al.) and with MCU oligomers in the IMM, consequently, bridging the calcium-sensing role of MICU1 and MICU2 with the channel-conducting activity of MCU (Sancak et al., 2013).

MCUR1 is a critical associated protein discovered to bind MCU (but not MICU1) and regulate MCU-dependent Ca^{2+} uptake (Mallilankaraman et al., 2012a). Although, it was shown that silencing MCUR1 is extensively inhibited both agonist-induced mitochondrial Ca^{2+} uptake and basal mitochondrial matrix [Ca^{2+}], we observed only a reduction of mitochondrial Ca^{2+} entry but not basal level in our experiment. Furthermore, our study found that mitochondrial Ca^{2+} sequestration from contact sites of the ER works

exclusively via MCU and EMRE but not MCUR1. Moreover, the boosted $[Ca^{2+}]_{mito}$ signals that we observed in MCU^{kd} cells overexpressed with UCP2 and depleted with MICU1 depend on MCU (rest MCU) and EMRE, but not on MCUR1. However, the direct involvement of MCUR1 in the modulation of the MCU complex was contradict with the recent study, since the silencing of MCUR1 causes a drop of Ψ_{mito} that correlates with a decrease of complex IV assembly and activity (Paupe et al., 2015). As Ψ_{mito} is the main driving force guiding the entrance of all cations inside organelle matrix, this might explain the decrease of $[Ca^{2+}]_{mito}$ and most of the data described in the previous report (Mallilankaraman et al., 2012a), in which differences in Ψ_{mito} were measured but not detected. In summary, our results indicate that UCP2/3 facilitates mitochondrial Ca^{2+} uptake by MCU/EMRE complex and thereby counteracts the inhibitory function of MICU1 on the MCU/EMRE complex, whereas the contribution of MCUR1 to the regulation of the MCU complex still needs further investigation.

To sum up, the present findings represent that mitochondrial Ca^{2+} mobilization from contact sites of the ER upon IP_3-mediated depletion of the Ca^{2+} stores works exclusively via MCU and EMRE but not via MCUR1. MICU1 functions as a negative regulator of the MCU/EMRE complex. Moreover, UCP2/3 promotes the functions of the MCU/EMRE complex and counteracts MICU1, while diminution of MICU1 boosts the effect of UCP2/3 on MCU activity in MCU^{kd} cells overexpressed with UCP2/3. Therefore, our results indicate that UCP2/3 facilitates mitochondrial Ca^{2+} uptake by MCU/EMRE complex and thereby counteracts the inhibitory function of MICU1 on the MCU/EMRE complex. Nevertheless, further studies are necessary for investigation of the specific role of each individual proteins and their interaction between each other especially in response to different routes and sources of mitochondrial Ca^{2+} mobilization. This work strongly emphasizes that mitochondrial Ca^{2+} uptake is not a simple process but extensively requires complex contributions of several mitochondrial membrane proteins; hence, many approaches are still in greatly demand to verify these complicated interactions.

PART II

4.2: Expression of MICU1 causes pronounced structural alteration pointing out to the additional engagement of this protein in the structure and function of mitochondria

Mitochondria are highly dynamic organelles and have drastically variable shapes and sizes depending on the cell type and even in the one single cell; the morphology of mitochondria can be completely different, from small spheres or short rods to long tubules (Chan, 2006, Okamoto and Shaw, 2005). These organelles constantly fuse and divide to adjust their internal structure in response to their physiological state, and are actively transported to specific subcellular locations (Detmer and Chan, 2007b). At steady state, the overall morphology of the mitochondria is maintained by the balance of fusion and fission processes (Nunnari et al., 1997). Previous studies reported that high populations of fragmented mitochondria have been found in yeast and mammal cells which have a low fusion-to-fission ratio (Bleazard et al., 1999, Chen et al., 2003, Sesaki and Jensen, 1999, Smirnova et al., 2001). Remarkably, in our study, we observed that overexpression of MICU1 caused considerable changes in the structure of mitochondria, which might give us a hint about an additional engagement of this protein in the ultrastructure and/or function of the mitochondria. From our assumption, the MICU1 might directly involve with mitochondrial dynamics or indirectly affect either the associated proteins of MCU or other mediators of fusion and fission, for instance, mitofusins (MFN1, MFN2) and optic atrophy 1 protein (OPA1), proteins which have already known to be essential for controlling the fusion process in mammalian cells and reported by several studies that mitochondria undergoes fragmentation in the absence of these protein (Chen et al., 2003, Detmer and Chan, 2007a, Chen et al., 2005, Koshiba et al., 2004, Cipolat et al., 2004, Legros et al., 2002). Nevertheless, there is a conflicting report that found overexpression of RyR1 induced mitochondrial fragmentation in cardiac H9C2 myoblast cells, while overexpression of MICU1, MCU, Letm1, or RyR2 has no effect on the structure of mitochondria (J et al., 2013). They also explained this phenomenon occurs through the fission process but not by $[Ca^{2+}]_{cyto}$ elevation, mitochondrial ROS elevation, and Ψ_{mito} depolarization. As a consequence, searching of the approaches to study the involvement of MICU1 is mandatory to further investigate the molecular mechanisms of MICU1 that influence mitochondrial dynamics and functions, and whether or not they demand an interaction with the associated proteins located in the IMM that we focus on in our study.

PART III

4.3: Rearrangement of MICU1 multimers for activation of MCU is solely controlled by cytosolic Ca^{2+}

Current chapter is based on the study of Markus Waldeck-Weiermair, Roland Malli*, Warisara Parichatikanond*, Benjamin Gottschalk, Corina T. Madreiter-Sokolowski, Christiane Klec, Rene Rost & Wolfgang F. Graier. Rearrangement of MICU1 multimers for activation of MCU is solely controlled by cytosolic Ca^{2+}. Sci. Rep. 5, 15602 (2015) (Waldeck-Weiermair et al., 2015). (*; Equal contribution)*

In this study, the correlation between the rearrangement of MICU1 oligomers and elevations of cytosolic Ca^{2+} in live cells has been explored. Using the FRET technology, we could explain the dynamic association of the Ca^{2+} induced reorganization of MICU1 multimers with the activation of MCU. Additionally, the contribution of mitochondrial Ca^{2+}, Ψ_{mito} and the expression levels of MCU and EMRE to MICU1 (re-)organization were investigated. Our data have revealed that an elevation of free Ca^{2+} in cytosol rearranges MICU1 multimers to smaller complexes in intact cells. These findings are in line with a recent report showing that Ca^{2+}-free MICU1 assembled in hexamers that binds and inhibits MCU and undergoes substantial conformational changes, resulting in the rearrangement to multiple dimers to activate MCU in the presence of Ca^{2+}, then regulates mitochondrial Ca^{2+} uptake (Wang et al., 2015, Wang et al., 2014). Therefore, our results that demonstrate the existence of large MICU1 complexes that suppresses mitochondrial Ca^{2+} sequestration at low cytosolic Ca^{2+} levels are consistent with our previous reports about the inactivity of MCU under resting conditions (Mallilankaraman et al., 2012a, Csordas et al., 2013).

In the present study, we established a live-cell FRET approach and used as a tool to monitor an alteration of the inter-MICU1 FRET signals that assists us to observe the correlation of the kinetics of MICU1 (re-)organization with cellular Ca^{2+} dynamics. Our data revealed that the disassembly of MICU1 multimers by cytosolic Ca^{2+} strictly associates with the Ca^{2+} concentration in the cytosol and is rapidly reversible. Certainly, cytosolic Ca^{2+} elevation upon histamine treatment leads to a transient cytosolic Ca^{2+} signal even in the presence of extracellular Ca^{2+} in this HeLa cell type. Consequently, if there is no washout of histamine, the inter-MICU1 FRET would also lead to higher order oligomers but slower according to the actual level of cytosolic Ca^{2+} concentration. Moreover, these cells occasionally show oscillatory cytosolic Ca^{2+} signals which are also reflected in the MICU1 FRET signal. In permeabilized cells, the *in situ* calibration reveals that the rearrangement of MICU1 senses Ca^{2+} alterations in the range between the low

basal Ca^{2+} levels of 100 nM up to 100 µM. With an EC_{50} of ~4.4 µM that we determined from our study, the Ca^{2+} sensitivity of MICU1 rearrangement lays exactly in the range of high Ca^{2+} concentration hot spots during a histamine induced intracellular Ca^{2+} release (between 3.78 and 16.42 µM) that have been measured over the OMM between the junction of mitochondria and the ER (Giacomello et al., 2010) which are known as "MAMs" (Patergnani et al., 2011, Bononi et al., 2012, van Vliet et al., 2014, Vance, 1990). In line with this report, the IP_3-mediated intracellular Ca^{2+} mobilization almost instantly yielded MICU1 re-organization, whereas Ca^{2+} entry via the SOCE pathway (Putney, 1986, Parekh, 2003) triggered only a delay and moderate rearrangement of MICU1 multimers. These differences between the kinetics of MICU1 rearrangement upon intracellular Ca^{2+} release and entering Ca^{2+} are consistent with previous reports that described a slow kinetics of entering Ca^{2+} at the mitochondrial surface without the formation of Ca^{2+} hot spots and slow mitochondrial Ca^{2+} accumulation via activation of SOCE (Waldeck-Weiermair et al., 2010b, Giacomello et al., 2010, Waldeck-Weiermair et al., 2010a).

Practically, we observed a stable reduction of the inter-MICU1 FRET between 5 and 15 % upon IP_3 mediated Ca^{2+} release from the ER. As mentioned above, this reduction highly depends on $[Ca^{2+}]_{cyto}$, but even more it depends on the expression levels of the donor and acceptor FRET pairs. In our experiments, the inter-MICU1 FRET signal was only visible if both FP-tagged MICU1 proteins were highly expressed and the fluorescence of the FPs exceeded a distinct level. In addition, the EC_{50} of MICU1 FRET at ~4.4 µM Ca^{2+} we detected in our experiment seems rather high when considered about global cytosolic Ca^{2+} which is around 1 µM after histamine stimulation. However, the rearrangements of MICU1 FRET would mainly occur within these high Ca^{2+} concentration hot spots or MAMs and consequently just a small part of MICU1 hexamers would be converted to dimers. Furthermore, additional FRET may also exist between neighboring hexamers. In this study, we observed the donor consistently showed 3-5 fold lower signals than the acceptor suggesting a model where MICU1-CFP is transferring its energy to more than just one MICU1-YFP, which is supported by the study that had been already described the amount of energy transfer observed in constructs having multiple acceptors is significantly greater than the FRET efficiency predicted from the sum of the individual donor to acceptor transfer rates (Koushik et al., 2009). This means that the dissociation of MICU1 may theoretically result in more than 50 % reduction of FRET.

According to entering Ca^{2+}, the rearrangement of MICU1 multimers was slow and moderate in response to intracellular Ca^{2+} release by SERCA inhibition, hence, explains

the marginal effect of SERCA inhibition on mitochondrial Ca^{2+} uptake. Since the inhibition of SERCA by BHQ caused considerably enhancement of mitochondrial Ca^{2+} mobilization by the diminution of MICU1 expression, the prominent role of MICU1 as a negative regulator of MCU is clearly proved. This hypothesis is further supported by our experiments in which cytosolic and mitochondrial free Ca^{2+} were simultaneously measured in cells after histamine stimulation. The silencing of MICU1 practically yielded the dissipation of the lag time of ~1.5 second between cytosolic Ca^{2+} elevation and the mitochondrial Ca^{2+} uptake. Therefore, the correlation between cytosolic Ca^{2+} elevation, the rearrangement of MICU1 multimers and mitochondrial Ca^{2+} signals, revealed that MICU1 reorganization temporally develops in-between the rising of Ca^{2+} within the two compartments that are the cytosolic and the mitochondria. Remarkably, significant mitochondrial Ca^{2+} uptake appears to occur at ~50% rearrangement of MICU1 multimers. We could anticipate from these observations that for activation of the MCU/EMRE complex to achieve mitochondrial Ca^{2+} influx, ~50% of the MICU1 multimers have to be rearranged. Although these findings might be due to the overexpression of MICU1 in our model, the MICU1-dependent lack of mitochondrial Ca^{2+} uptake in response to SERCA inhibition likely supports this assumption.

It was long known that the Ca^{2+} uptake into mitochondria is mainly mediated by a MCU driven by a highly negative Ψ_{mito} (-150 to -180 mV) (Kirichok et al., 2004). In addition, silencing of MICU1 did neither disrupt mitochondrial respiration nor membrane potential, but it attenuated metabolic coupling between cytosolic Ca^{2+} transients and activation of matrix dehydrogenases (Rottenberg and Scarpa, 1974). Nevertheless, the impact of Ψ_{mito} on MICU1 reorganization has not been investigated so far. By using the protocol with completely depolarized mitochondria (oligomycin/FCCP), our results apparently represented Ψ_{mito} unaffected dynamics of MICU1 as unchanged the inter-MICU1 FRET signals despite an extensively reduced mitochondrial Ca^{2+} uptake. These data obviously demonstrate that neither Ψ_{mito} nor matrix Ca^{2+} have an influence on the rearrangement of MICU1 complexes and supports cytosolic Ca^{2+} as possible the sole regulator of MICU1 (re-)organization (Wang et al., 2014). Notably, the basal mitochondrial Ca^{2+} was slightly increased upon FCCP incubation which might be due to the reason that FCCP affects partial Ca^{2+} release from internal stores which had been already described by others in various cell types (Williamson et al., 1983, Luo et al., 1997, Hacker and Medler, 2008). Furthermore, the high Ca^{2+} concentration gradient between IMS and cytosol during a histamine induced intracellular Ca^{2+} release is supposed to be

sufficient to create the driving force and pull Ca^{2+} inside the IMS by passive diffusion through the OMM, although the active transport of Ca^{2+} through the IMM is largely inhibited upon FCCP induced dissipation of the Ψ_{mito}. As a consequence, Ca^{2+} could reach the binding sites at MICU1 faced to IMS to undergo dissociation and a reduction of the inter-MICU1 FRET signal could be detected under the absence of Ψ_{mito}.

Studies of mitochondrial Ca^{2+} machinery have recently resulted in great progress, and the components of the sophisticated MCU complex and several regulators that are either required for its channel activity or regulate it under various conditions have been identified and characterized. EMRE was found to be an important regulator that required to interact with MICU1/2 in the IMS and with MCU oligomers in the IMM (Wang et al., 2015, Sancak et al., 2013, Csordas et al., 2013, Patron et al., 2014, Wang et al., 2014, Kevin Foskett and Madesh, 2014, De Stefani and Rizzuto, 2014). Considering the interaction of MICU1 with EMRE and MCU, the importance of these two pore-forming proteins for the structural reorganization of MICU1 was evaluated in our study. Even though the siRNA-mediated depletion of either of these proteins resulted in strongly reduced mitochondrial Ca^{2+} uptake, the Ca^{2+}-induced rearrangement of MICU1 multimers, their arrangement upon the reduction of cytosolic Ca^{2+} to basal levels, and the sensitivity to cytosolic Ca^{2+} remained unaffected by the diminution of MCU or EMRE. These findings demonstrate that the structural (re-)organization of MICU1 upon elevation of cytosolic free Ca^{2+} does not involve MCU or EMRE indicating that the Ca^{2+}-induced rearrangement of MICU1 multimers is a robust process that is feasible to independent develop without require any other interaction partners, including MCU and EMRE, which are rather downstream of the uptake mechanism.

Even though, studying of the topology of MICU1 can aid in understanding the mechanism underlying its operation. Nevertheless, the results of its topology are still under debate (Csordas et al., 2013, Hoffman et al., 2013, Kamer and Mootha, 2014, Kevin Foskett and Madesh, 2014), our data have shown , *first*, MICU1 FRET rearrangement closely follows cytosolic but not matrix mitochondrial Ca^{2+}, *second*, MICU1 knockdown results in a faster mitochondrial Ca^{2+} uptake, *third*, rearrangement of MICU1 FRET allows mitochondrial Ca^{2+} uptake, *forth*, MICU1 FRET is independent from Ψ_{mito}, and *fifth*, neither knockdown of MCU nor of EMRE influences MICU1 FRET rearrangement. From the findings mentioned above, we hypothesize that MICU1 anchors with its N-terminus in the IMM while the core protein is oriented towards IMS and not to the matrix which is consistent with the function by which it senses cytosolic Ca^{2+} changes and regulates MCU-

mediated Ca^{2+} entry (Wang et al., 2014, Csordas et al., 2013, Patron et al., 2014, Kamer and Mootha, 2014).

Although, our assumption supports the published reports from other groups, there are still conflicting reports about the localization of MICU1 from *Hoffman et al* (Hoffman et al., 2013) that described MICU1 is mobile and supposed to be submitochondrial. We could argue by make point-to-point explanations from our findings that are consistent with reports from other groups as followed. Our data are closely in line with the model of *Csordas et al* (Csordas et al., 2013) who defined that the major part (almost 90%) of MICU1 faces the IMS controlling the mitochondrial Ca^{2+} entry as a gatekeeper via its EF hands. Otherwise MICU1 FRET would not rearrange before mitochondrial Ca^{2+} elevation occurs and MCU or EMRE knockdown would affect the MICU1 FRET rearrangement. We further support the data of *Wang et al* (Wang et al., 2014, Wang et al., 2015) who elaborated the oligomerization of MICU1 via its C-terminal tail under resting conditions. Ca^{2+} elevation leads to large conformational changes and dissociation of MICU1 multimers, a process that largely depends on the binding of Ca^{2+} to the EF hands of MICU1. Thus, using a MICU1 variant mutated in both canonical EF hands did neither rescue intrinsic MICU1 ablation nor rearrange a MICU1 FRET.

In summary, our results provide new mechanistic insights in the regulation of mitochondrial Ca^{2+} uptake. For the first time, the kinetics and adjustments of one of the most important molecular gatekeeper of mitochondrial Ca^{2+} uptake was visualized in intact cells. Our data revealed cytosolic Ca^{2+} as the most prominent regulator of the structural organization of MICU1, which in the form of a homo-multimere potently inhibits the MCU/EMRE mitochondrial Ca^{2+} channel complex. Moreover, neither Ψ_{mito} nor matrix Ca^{2+}, nor MCU or EMRE were found to affect the Ca^{2+}-controlled (dis)assembly of MICU1 multimers. Finally, our data provide important details for a better understanding of the molecular regulation of intricate mitochondrial Ca^{2+} uptake machinery.

BIBLIOGRAPHY

Abramov, A. Y. & Duchen, M. R. 2003. Actions of ionomycin, 4-BrA23187 and a novel electrogenic Ca^{2+} ionophore on mitochondria in intact cells. *Cell Calcium,* 33**,** 101-12.

Ahuja, M. & Muallem, S. 2014. The gatekeepers of mitochondrial calcium influx: MICU1 and MICU2. *EMBO Rep,* 15**,** 205-6.

Alam, M. R., Groschner, L. N., Parichatikanond, W., Kuo, L., Bondarenko, A. I., Rost, R., Waldeck-Weiermair, M., Malli, R. & Graier, W. F. 2012. Mitochondrial Ca^{2+} uptake 1 (MICU1) and mitochondrial Ca^{2+} uniporter (MCU) contribute to metabolism-secretion coupling in clonal pancreatic beta-cells. *J Biol Chem,* 287**,** 34445-54.

Allen, D. G. & Blinks, J. R. 1978. Calcium transients in aequorin-injected frog cardiac muscle. *Nature,* 273**,** 509-13.

Altschafl, B. A., Beutner, G., Sharma, V. K., Sheu, S. S. & Valdivia, H. H. 2007. The mitochondrial ryanodine receptor in rat heart: a pharmaco-kinetic profile. *Biochim Biophys Acta,* 1768**,** 1784-95.

Arnaudeau, S., Kelley, W. L., Walsh, J. V., Jr. & Demaurex, N. 2001. Mitochondria recycle Ca^{2+} to the endoplasmic reticulum and prevent the depletion of neighboring endoplasmic reticulum regions. *J Biol Chem,* 276**,** 29430-9.

Babcock, D. F., Herrington, J., Goodwin, P. C., Park, Y. B. & Hille, B. 1997. Mitochondrial participation in the intracellular Ca^{2+} network. *J Cell Biol,* 136**,** 833-44.

Baughman, J. M., Perocchi, F., Girgis, H. S., Plovanich, M., Belcher-Timme, C. A., Sancak, Y., Bao, X. R., Strittmatter, L., Goldberger, O., Bogorad, R. L., Koteliansky, V. & Mootha, V. K. 2011. Integrative genomics identifies MCU as an essential component of the mitochondrial calcium uniporter. *Nature,* 476**,** 341-5.

Beech, D. J., Bahnasi, Y. M., Dedman, A. M. & Al-Shawaf, E. 2009. TRPC channel lipid specificity and mechanisms of lipid regulation. *Cell Calcium,* 45**,** 583-8.

Berardi, M. J., Shih, W. M., Harrison, S. C. & Chou, J. J. 2011. Mitochondrial uncoupling protein 2 structure determined by NMR molecular fragment searching. *Nature,* 476**,** 109-13.

Bernardi, P. 1999. Mitochondrial transport of cations: channels, exchangers, and permeability transition. *Physiol Rev,* 79**,** 1127-55.

Bernardi, P., Krauskopf, A., Basso, E., Petronilli, V., Blachly-Dyson, E., Di Lisa, F. & Forte, M. A. 2006. The mitochondrial permeability transition from *in vitro* artifact to disease target. *FEBS J,* 273**,** 2077-99.

Berridge, M. J. 2001. The versatility and complexity of calcium signalling. *Novartis Found Symp,* 239**,** 52-64; discussion 64-7, 150-9.

Beutner, G., Sharma, V. K., Giovannucci, D. R., Yule, D. I. & Sheu, S. S. 2001. Identification of a ryanodine receptor in rat heart mitochondria. *J Biol Chem,* 276**,** 21482-8.

Beutner, G., Sharma, V. K., Lin, L., Ryu, S. Y., Dirksen, R. T. & Sheu, S. S. 2005. Type 1 ryanodine receptor in cardiac mitochondria: transducer of excitation-metabolism coupling. *Biochim Biophys Acta,* 1717**,** 1-10.

Bezprozvanny, I., Watras, J. & Ehrlich, B. E. 1991. Bell-shaped calcium-response curves of Ins(1,4,5)P_3- and calcium-gated channels from endoplasmic reticulum of cerebellum. *Nature,* 351**,** 751-4.

Bick, A. G., Calvo, S. E. & Mootha, V. K. 2012. Evolutionary diversity of the mitochondrial calcium uniporter. *Science,* 336**,** 886.

Bleazard, W., Mccaffery, J. M., King, E. J., Bale, S., Mozdy, A., Tieu, Q., Nunnari, J. & Shaw, J. M. 1999. The dynamin-related GTPase Dnm1 regulates mitochondrial fission in yeast. *Nat Cell Biol,* 1**,** 298-304.

Bogeski, I., Gulaboski, R., Kappl, R., Mirceski, V., Stefova, M., Petreska, J. & Hoth, M. 2011. Calcium binding and transport by coenzyme Q. *J Am Chem Soc,* 133**,** 9293-303.

Bondarenko, A. I., Jean-Quartier, C., Parichatikanond, W., Alam, M. R., Waldeck-Weiermair, M., Malli, R. & Graier, W. F. 2014. Mitochondrial Ca^{2+} uniporter (MCU)-dependent and MCU-independent Ca^{2+} channels coexist in the inner mitochondrial membrane. *Pflugers Arch,* 466**,** 1411-20.

Bononi, A., Missiroli, S., Poletti, F., Suski, J. M., Agnoletto, C., Bonora, M., De Marchi, E., Giorgi, C., Marchi, S., Patergnani, S., Rimessi, A., Wieckowski, M. R. & Pinton, P. 2012. Mitochondria-associated membranes (MAMs) as hotspot Ca^{2+} signaling units. *Adv Exp Med Biol,* 740**,** 411-37.

Boyman, L., Williams, G. S., Khananshvili, D., Sekler, I. & Lederer, W. J. 2013. NCLX: the mitochondrial sodium calcium exchanger. *J Mol Cell Cardiol,* 59**,** 205-13.

Brand, M. D., Chen, C. H. & Lehninger, A. L. 1976. Stoichiometry of H^+ ejection during respiration-dependent accumulation of Ca^{2+} by rat liver mitochondria. *J Biol Chem,* 251**,** 968-74.

Brauner, P. & Fridlender, B. 1981. Use of chelating agents as terminators of alkaline phosphatase activity in enzyme-linked immunosorbent assay (ELISA) tests. *J Immunol Methods,* 42**,** 375-9.

Buntinas, L., Gunter, K. K., Sparagna, G. C. & Gunter, T. E. 2001. The rapid mode of calcium uptake into heart mitochondria (RaM): comparison to RaM in liver mitochondria. *Biochim Biophys Acta,* 1504**,** 248-61.

Calcraft, P. J., Ruas, M., Pan, Z., Cheng, X., Arredouani, A., Hao, X., Tang, J., Rietdorf, K., Teboul, L., Chuang, K. T., Lin, P., Xiao, R., Wang, C., Zhu, Y., Lin, Y., Wyatt, C. N., Parrington, J., Ma, J., Evans, A. M., Galione, A. & Zhu, M. X. 2009. NAADP mobilizes calcium from acidic organelles through two-pore channels. *Nature,* 459**,** 596-600.

Carafoli, E. 2010. The fateful encounter of mitochondria with calcium: how did it happen? *Biochim Biophys Acta,* 1797**,** 595-606.

Carafoli, E. 2012. The interplay of mitochondria with calcium: an historical appraisal. *Cell Calcium,* 52**,** 1-8.

Carafoli, E., Tiozzo, R., Lugli, G., Crovetti, F. & Kratzing, C. 1974. The release of calcium from heart mitochondria by sodium. *J Mol Cell Cardiol,* 6**,** 361-71.

Carlson, H. J. & Campbell, R. E. 2009. Genetically encoded FRET-based biosensors for multiparameter fluorescence imaging. *Curr Opin Biotechnol,* 20**,** 19-27.

Chacon, E. & Acosta, D. 1991. Mitochondrial regulation of superoxide by Ca^{2+}: an alternate mechanism for the cardiotoxicity of doxorubicin. *Toxicol Appl Pharmacol,* 107**,** 117-28.

Chan, D. C. 2006. Mitochondrial fusion and fission in mammals. *Annu Rev Cell Dev Biol,* 22**,** 79-99.

Chandel, N. S. 2014. Mitochondria as signaling organelles. *BMC Biol,* 12**,** 34.

Chen, H., Chomyn, A. & Chan, D. C. 2005. Disruption of fusion results in mitochondrial heterogeneity and dysfunction. *J Biol Chem,* 280**,** 26185-92.

Chen, H., Detmer, S. A., Ewald, A. J., Griffin, E. E., Fraser, S. E. & Chan, D. C. 2003. Mitofusins Mfn1 and Mfn2 coordinately regulate mitochondrial fusion and are essential for embryonic development. *J Cell Biol,* 160**,** 189-200.

Cipolat, S., Martins De Brito, O., Dal Zilio, B. & Scorrano, L. 2004. OPA1 requires mitofusin 1 to promote mitochondrial fusion. *Proc Natl Acad Sci U S A,* 101**,** 15927-32.

Clapham, D. E. 2007. Calcium signaling. *Cell,* 131**,** 1047-58.

Collins, S. & Meyer, T. 2010. Cell biology: A sensor for calcium uptake. *Nature,* 467**,** 283.

Contreras, L., Drago, I., Zampese, E. & Pozzan, T. 2010. Mitochondria: the calcium connection. *Biochim Biophys Acta,* 1797**,** 607-18.

Cooper, G. & Hausman, R. 2007. *The Cell: A Molecular Approach,* Washington, D.C., ASM Press.

Cox, D. A., Conforti, L., Sperelakis, N. & Matlib, M. A. 1993. Selectivity of inhibition of Na^+-Ca^{2+} exchange of heart mitochondria by benzothiazepine CGP-37157. *J Cardiovasc Pharmacol,* 21**,** 595-9.

Crompton, M. 1999. The mitochondrial permeability transition pore and its role in cell death. *Biochem J,* 341**,** 233-49.

Csordas, G., Golenar, T., Seifert, E. L., Kamer, K. J., Sancak, Y., Perocchi, F., Moffat, C., Weaver, D., De La Fuente Perez, S., Bogorad, R., Koteliansky, V., Adijanto, J., Mootha, V. K. & Hajnoczky, G. 2013. MICU1 controls both the threshold and cooperative activation of the mitochondrial Ca^{2+} uniporter. *Cell Metab,* 17**,** 976-87.

Csordas, G., Renken, C., Varnai, P., Walter, L., Weaver, D., Buttle, K. F., Balla, T., Mannella, C. A. & Hajnoczky, G. 2006. Structural and functional features and significance of the physical linkage between ER and mitochondria. *J Cell Biol,* 174**,** 915-21.

Csordas, G., Varnai, P., Golenar, T., Roy, S., Purkins, G., Schneider, T. G., Balla, T. & Hajnoczky, G. 2010. Imaging interorganelle contacts and local calcium dynamics at the ER-mitochondrial interface. *Mol Cell,* 39**,** 121-32.

De Giorgi, F., Ahmed, Z., Bastianutto, C., Brini, M., Jouaville, L. S., Marsault, R., Murgia, M., Pinton, P., Pozzan, T. & Rizzuto, R. 1999. Targeting GFP to organelles. *Methods Cell Biol,* 58**,** 75-85.

De Stefani, D., Patron, M. & Rizzuto, R. 2015. Structure and function of the mitochondrial calcium uniporter complex. *Biochim Biophys Acta,* 1853, 2006-11.

De Stefani, D., Raffaello, A., Teardo, E., Szabo, I. & Rizzuto, R. 2011. A forty-kilodalton protein of the inner membrane is the mitochondrial calcium uniporter. *Nature,* 476**,** 336-40.

De Stefani, D. & Rizzuto, R. 2014. Molecular control of mitochondrial calcium uptake. *Biochem Biophys Res Commun,* 449**,** 373-6.

Deak, A. T., Blass, S., Khan, M. J., Groschner, L. N., Waldeck-Weiermair, M., Hallstrom, S., Graier, W. F. & Malli, R. 2014. IP_3-mediated STIM1 oligomerization requires intact mitochondrial Ca^{2+} uptake. *J Cell Sci,* 127**,** 2944-55.

Dedkova, E. N. & Blatter, L. A. 2009. Characteristics and function of cardiac mitochondrial nitric oxide synthase. *J Physiol,* 587**,** 851-72.

Dedkova, E. N. & Blatter, L. A. 2013. Calcium signaling in cardiac mitochondria. *J Mol Cell Cardiol,* 58**,** 125-33.

Dejean, L., Camara, Y., Sibille, B., Solanes, G. & Villarroya, F. 2004. Uncoupling protein-3 sensitizes cells to mitochondrial-dependent stimulus of apoptosis. *J Cell Physiol,* 201**,** 294-304.

Deluca, H. F. & Engstrom, G. W. 1961. Calcium uptake by rat kidney mitochondria. *Proc Natl Acad Sci U S A,* 47**,** 1744-50.

Detmer, S. A. & Chan, D. C. 2007a. Complementation between mouse Mfn1 and Mfn2 protects mitochondrial fusion defects caused by CMT2A disease mutations. *J Cell Biol,* 176**,** 405-14.

Detmer, S. A. & Chan, D. C. 2007b. Functions and dysfunctions of mitochondrial dynamics. *Nat Rev Mol Cell Biol,* 8**,** 870-9.

Dimmer, K. S., Navoni, F., Casarin, A., Trevisson, E., Endele, S., Winterpacht, A., Salviati, L. & Scorrano, L. 2008. LETM1, deleted in Wolf-Hirschhorn syndrome is required for normal mitochondrial morphology and cellular viability. *Hum Mol Genet,* 17**,** 201-14.

Doonan, P. J., Chandramoorthy, H. C., Hoffman, N. E., Zhang, X., Cardenas, C., Shanmughapriya, S., Rajan, S., Vallem, S., Chen, X., Foskett, J. K., Cheung, J. Y., Houser, S. R. & Madesh, M. 2014. LETM1-dependent mitochondrial Ca^{2+} flux modulates cellular bioenergetics and proliferation. *FASEB J,* 28**,** 4936-49.

Drago, I., De Stefani, D., Rizzuto, R. & Pozzan, T. 2012. Mitochondrial Ca^{2+} uptake contributes to buffering cytoplasmic Ca^{2+} peaks in cardiomyocytes. *Proc Natl Acad Sci U S A,* 109**,** 12986-91.

Drago, I., Pizzo, P. & Pozzan, T. 2011. After half a century mitochondrial calcium in- and efflux machineries reveal themselves. *EMBO J,* 30**,** 4119-25.

Feng, S., Li, H., Tai, Y., Huang, J., Su, Y., Abramowitz, J., Zhu, M. X., Birnbaumer, L. & Wang, Y. 2013. Canonical transient receptor potential 3 channels regulate mitochondrial calcium uptake. *Proc Natl Acad Sci U S A,* 110**,** 11011-6.

Feske, S., Skolnik, E. Y. & Prakriya, M. 2012. Ion channels and transporters in lymphocyte function and immunity. *Nat Rev Immunol,* 12**,** 532-47.

Filippin, L., Abad, M. C., Gastaldello, S., Magalhaes, P. J., Sandona, D. & Pozzan, T. 2005. Improved strategies for the delivery of GFP-based Ca^{2+} sensors into the mitochondrial matrix. *Cell Calcium,* 37**,** 129-36.

Finkel, T., Menazza, S., Holmstrom, K. M., Parks, R. J., Liu, J., Sun, J., Pan, X. & Murphy, E. 2015. The ins and outs of mitochondrial calcium. *Circ Res,* 116**,** 1810-1819.

Foskett, J. K. & Philipson, B. 2015. The mitochondrial Ca^{2+} uniporter complex. *J Mol Cell Cardiol,* 78**,** 3-8.

Friedman, J. R., Lackner, L. L., West, M., Dibenedetto, J. R., Nunnari, J. & Voeltz, G. K. 2011. ER tubules mark sites of mitochondrial division. *Science,* 334**,** 358-62.

Froschauer, E., Nowikovsky, K. & Schweyen, R. J. 2005. Electroneutral K^+/H^+ exchange in mitochondrial membrane vesicles involves Yol027/Letm1 proteins. *Biochim Biophys Acta,* 1711**,** 41-8.

Fu, L. W., Pan, H. L. & Longhurst, J. C. 1997. Endogenous histamine stimulates ischemically sensitive abdominal visceral afferents through H_1 receptors. *Am J Physiol,* 273**,** H2726-37.

Gandhi, S., Wood-Kaczmar, A., Yao, Z., Plun-Favreau, H., Deas, E., Klupsch, K., Downward, J., Latchman, D. S., Tabrizi, S. J., Wood, N. W., Duchen, M. R. & Abramov, A. Y. 2009. PINK1-associated Parkinson's disease is caused by neuronal vulnerability to calcium-induced cell death. *Mol Cell,* 33**,** 627-38.

Giacomello, M., Drago, I., Bortolozzi, M., Scorzeto, M., Gianelle, A., Pizzo, P. & Pozzan, T. 2010. Ca^{2+} hot spots on the mitochondrial surface are generated by Ca^{2+} mobilization from stores, but not by activation of store-operated Ca^{2+} channels. *Mol Cell,* 38**,** 280-90.

Graier, W. F., Frieden, M. & Malli, R. 2007. Mitochondria and Ca^{2+} signaling: old guests, new functions. *Pflugers Arch,* 455**,** 375-96.

Graier, W. F., Trenker, M. & Malli, R. 2008. Mitochondrial Ca^{2+}, the secret behind the function of uncoupling proteins 2 and 3? *Cell Calcium,* 44**,** 36-50.

Griffiths, E. J. 1999. Reversal of mitochondrial Na/Ca exchange during metabolic inhibition in rat cardiomyocytes. *FEBS Lett,* 453**,** 400-4.

Grynkiewicz, G., Poenie, M. & Tsien, R. Y. 1985. A new generation of Ca^{2+} indicators with greatly improved fluorescence properties. *J Biol Chem,* 260**,** 3440-50.

Gunter, T. E., Buntinas, L., Sparagna, G., Eliseev, R. & Gunter, K. 2000. Mitochondrial calcium transport: mechanisms and functions. *Cell Calcium,* 28**,** 285-96.

Hacker, K. & Medler, K. F. 2008. Mitochondrial calcium buffering contributes to the maintenance of basal calcium levels in mouse taste cells. *J Neurophysiol,* 100**,** 2177-91.

Hajnoczky, G. & Csordas, G. 2010. Calcium signalling: fishing out molecules of mitochondrial calcium transport. *Curr Biol,* 20**,** R888-91.

Hajnoczky, G., Davies, E. & Madesh, M. 2003. Calcium signaling and apoptosis. *Biochem Biophys Res Commun,* 304**,** 445-54.

Hashimi, H., Mcdonald, L., Stribrna, E. & Lukes, J. 2013. Trypanosome Letm1 protein is essential for mitochondrial potassium homeostasis. *J Biol Chem,* 288**,** 26914-25.

Hassessian, H., Vaca, L. & Kunze, D. L. 1994. Blockade of the inward rectifier potassium current by the Ca^{2+}-ATPase inhibitor 2',5'-di(tert-butyl)-1,4-benzohydroquinone (BHQ). *Br J Pharmacol,* 112**,** 1118-22.

Herrington, J., Park, Y. B., Babcock, D. F. & Hille, B. 1996. Dominant role of mitochondria in clearance of large Ca^{2+} loads from rat adrenal chromaffin cells. *Neuron,* 16**,** 219-28.

Hoffman, N. E., Chandramoorthy, H. C., Shamugapriya, S., Zhang, X., Rajan, S., Mallilankaraman, K., Gandhirajan, R. K., Vagnozzi, R. J., Ferrer, L. M., Sreekrishnanilayam, K., Natarajaseenivasan, K., Vallem, S., Force, T., Choi, E. T., Cheung, J. Y. & Madesh, M. 2013. MICU1 motifs define mitochondrial calcium uniporter binding and activity. *Cell Rep,* 5**,** 1576-88.

Hung, V., Zou, P., Rhee, H. W., Udeshi, N. D., Cracan, V., Svinkina, T., Carr, S. A., Mootha, V. K. & Ting, A. Y. 2014. Proteomic mapping of the human mitochondrial intermembrane space in live cells via ratiometric APEX tagging. *Mol Cell,* 55**,** 332-41.

J, O. U., Jhun, B. S., Hurst, S., Bisetto, S., Gross, P., Chen, M., Kettlewell, S., Park, J., Oyamada, H., Smith, G. L., Murayama, T. & Sheu, S. S. 2013. Overexpression of ryanodine receptor type 1 enhances mitochondrial fragmentation and Ca^{2+}-induced

ATP production in cardiac H9c2 myoblasts. *Am J Physiol Heart Circ Physiol,* 305**,** H1736-51.

Jakob, R., Beutner, G., Sharma, V. K., Duan, Y., Gross, R. A., Hurst, S., Jhun, B. S., J, O. U. & Sheu, S. S. 2014. Molecular and functional identification of a mitochondrial ryanodine receptor in neurons. *Neurosci Lett,* 575**,** 7-12.

Jiang, D., Zhao, L. & Clapham, D. E. 2009. Genome-wide RNAi screen identifies Letm1 as a mitochondrial Ca^{2+}/H^{+} antiporter. *Science,* 326**,** 144-7.

Joiner, M. L., Koval, O. M., Li, J., He, B. J., Allamargot, C., Gao, Z., Luczak, E. D., Hall, D. D., Fink, B. D., Chen, B., Yang, J., Moore, S. A., Scholz, T. D., Strack, S., Mohler, P. J., Sivitz, W. I., Song, L. S. & Anderson, M. E. 2012. CaMKII determines mitochondrial stress responses in heart. *Nature,* 491**,** 269-73.

Jouaville, L. S., Ichas, F., Holmuhamedov, E. L., Camacho, P. & Lechleiter, J. D. 1995. Synchronization of calcium waves by mitochondrial substrates in *Xenopus laevis* oocytes. *Nature,* 377**,** 438-41.

Kamer, K. J. & Mootha, V. K. 2014. MICU1 and MICU2 play nonredundant roles in the regulation of the mitochondrial calcium uniporter. *EMBO Rep,* 15**,** 299-307.

Kamer, K. J. & Mootha, V. K. 2015. The molecular era of the mitochondrial calcium uniporter. *Nat Rev Mol Cell Biol,* 16**,** 545-53.

Kamer, K. J., Sancak, Y. & Mootha, V. K. 2014. The uniporter: from newly identified parts to function. *Biochem Biophys Res Commun,* 449**,** 370-2.

Kevin Foskett, J. & Madesh, M. 2014. Regulation of the mitochondrial Ca^{2+} uniporter by MICU1 and MICU2. *Biochem Biophys Res Commun,* 449**,** 377-83.

Kirichok, Y., Krapivinsky, G. & Clapham, D. E. 2004. The mitochondrial calcium uniporter is a highly selective ion channel. *Nature,* 427**,** 360-4.

Koshiba, T., Detmer, S. A., Kaiser, J. T., Chen, H., Mccaffery, J. M. & Chan, D. C. 2004. Structural basis of mitochondrial tethering by mitofusin complexes. *Science,* 305**,** 858-62.

Koushik, S. V., Blank, P. S. & Vogel, S. S. 2009. Anomalous surplus energy transfer observed with multiple FRET acceptors. *PLoS One,* 4**,** e8031.

Kovacs-Bogdan, E., Sancak, Y., Kamer, K. J., Plovanich, M., Jambhekar, A., Huber, R. J., Myre, M. A., Blower, M. D. & Mootha, V. K. 2014. Reconstitution of the mitochondrial calcium uniporter in yeast. *Proc Natl Acad Sci U S A,* 111**,** 8985-90.

Kroemer, G., Galluzzi, L. & Brenner, C. 2007. Mitochondrial membrane permeabilization in cell death. *Physiol Rev,* 87**,** 99-163.

Lam, S. S., Martell, J. D., Kamer, K. J., Deerinck, T. J., Ellisman, M. H., Mootha, V. K. & Ting, A. Y. 2015. Directed evolution of APEX2 for electron microscopy and proximity labeling. *Nat Methods,* 12**,** 51-4.

Lawrie, A. M., Rizzuto, R., Pozzan, T. & Simpson, A. W. 1996. A role for calcium influx in the regulation of mitochondrial calcium in endothelial cells. *J Biol Chem,* 271**,** 10753-9.

Legros, F., Lombes, A., Frachon, P. & Rojo, M. 2002. Mitochondrial fusion in human cells is efficient, requires the inner membrane potential, and is mediated by mitofusins. *Mol Biol Cell,* 13**,** 4343-54.

Lemasters, J. J., Theruvath, T. P., Zhong, Z. & Nieminen, A. L. 2009. Mitochondrial calcium and the permeability transition in cell death. *Biochim Biophys Acta,* 1787**,** 1395-401.

Liao, Y., Erxleben, C., Yildirim, E., Abramowitz, J., Armstrong, D. L. & Birnbaumer, L. 2007. Orai proteins interact with TRPC channels and confer responsiveness to store depletion. *Proc Natl Acad Sci U S A,* 104**,** 4682-7.

Luo, Y., Bond, J. D. & Ingram, V. M. 1997. Compromised mitochondrial function leads to increased cytosolic calcium and to activation of MAP kinases. *Proc Natl Acad Sci U S A,* 94**,** 9705-10.

Lytton, J. 2007. Na^+/Ca^{2+} exchangers: three mammalian gene families control Ca^{2+} transport. *Biochem J,* 406**,** 365-82.

Malli, R., Frieden, M., Trenker, M. & Graier, W. F. 2005. The role of mitochondria for Ca^{2+} refilling of the endoplasmic reticulum. *J Biol Chem,* 280**,** 12114-22.

Mallilankaraman, K., Cardenas, C., Doonan, P. J., Chandramoorthy, H. C., Irrinki, K. M., Golenar, T., Csordas, G., Madireddi, P., Yang, J., Muller, M., Miller, R., Kolesar, J. E., Molgo, J., Kaufman, B., Hajnoczky, G., Foskett, J. K. & Madesh, M. 2012a. MCUR1 is an essential component of mitochondrial Ca^{2+} uptake that regulates cellular metabolism. *Nat Cell Biol,* 14**,** 1336-43.

Mallilankaraman, K., Doonan, P., Cardenas, C., Chandramoorthy, H. C., Muller, M., Miller, R., Hoffman, N. E., Gandhirajan, R. K., Molgo, J., Birnbaum, M. J., Rothberg, B. S., Mak, D. O., Foskett, J. K. & Madesh, M. 2012b. MICU1 is an essential gatekeeper for MCU-mediated mitochondrial Ca^{2+} uptake that regulates cell survival. *Cell,* 151**,** 630-44.

Marchi, S. & Pinton, P. 2014. The mitochondrial calcium uniporter complex: molecular components, structure and physiopathological implications. *J Physiol,* 592**,** 829-39.

Martell, J. D., Deerinck, T. J., Sancak, Y., Poulos, T. L., Mootha, V. K., Sosinsky, G. E., Ellisman, M. H. & Ting, A. Y. 2012. Engineered ascorbate peroxidase as a genetically encoded reporter for electron microscopy. *Nat Biotechnol,* 30**,** 1143-8.

Matlib, M. A., Zhou, Z., Knight, S., Ahmed, S., Choi, K. M., Krause-Bauer, J., Phillips, R., Altschuld, R., Katsube, Y., Sperelakis, N. & Bers, D. M. 1998. Oxygen-bridged dinuclear ruthenium amine complex specifically inhibits Ca^{2+} uptake into mitochondria *in vitro* and *in situ* in single cardiac myocytes. *J Biol Chem,* 273**,** 10223-31.

Mccormack, J. G., Halestrap, A. P. & Denton, R. M. 1990. Role of calcium ions in regulation of mammalian intramitochondrial metabolism. *Physiol Rev,* 70**,** 391-425.

Michels, G., Khan, I. F., Endres-Becker, J., Rottlaender, D., Herzig, S., Ruhparwar, A., Wahlers, T. & Hoppe, U. C. 2009. Regulation of the human cardiac mitochondrial Ca^{2+} uptake by 2 different voltage-gated Ca^{2+} channels. *Circulation,* 119**,** 2435-43.

Miyawaki, A., Llopis, J., Heim, R., Mccaffery, J. M., Adams, J. A., Ikura, M. & Tsien, R. Y. 1997. Fluorescent indicators for Ca^{2+} based on green fluorescent proteins and calmodulin. *Nature,* 388**,** 882-7.

Moore, C. L. 1971. Specific inhibition of mitochondrial Ca^{2+} transport by ruthenium red. *Biochem Biophys Res Commun,* 42**,** 298-305.

Nagai, T., Sawano, A., Park, E. S. & Miyawaki, A. 2001. Circularly permuted green fluorescent proteins engineered to sense Ca^{2+}. *Proc Natl Acad Sci U S A,* 98**,** 3197-202.

Nagamune, H., Fukushima, Y., Takada, J., Yoshida, K., Unami, A., Shimooka, T. & Terada, H. 1993. The lipophilic weak base (Z)-5-methyl-2-[2-(1-naphthyl)ethenyl]-4-piperidinopyridine (AU-1421) is a potent protonophore type cationic uncoupler of oxidative phosphorylation in mitochondria. *Biochim Biophys Acta,* 1141**,** 231-7.

Naghdi, S., Waldeck-Weiermair, M., Fertschai, I., Poteser, M., Graier, W. F. & Malli, R. 2010. Mitochondrial Ca^{2+} uptake and not mitochondrial motility is required for STIM1-Orai1-dependent store-operated Ca^{2+} entry. *J Cell Sci,* 123**,** 2553-64.

Nakai, J., Ohkura, M. & Imoto, K. 2001. A high signal-to-noise Ca^{2+} probe composed of a single green fluorescent protein. *Nat Biotechnol,* 19**,** 137-41.

Nicholls, D. G. & Crompton, M. 1980. Mitochondrial calcium transport. *FEBS Lett,* 111**,** 261-8.

Nicholls, D. G. & Rial, E. 1999. A history of the first uncoupling protein, UCP1. *J Bioenerg Biomembr,* 31**,** 399-406.

Nowikovsky, K. & Bernardi, P. 2014. LETM1 in mitochondrial cation transport. *Front Physiol,* 5**,** 83.

Nowikovsky, K., Froschauer, E. M., Zsurka, G., Samaj, J., Reipert, S., Kolisek, M., Wiesenberger, G. & Schweyen, R. J. 2004. The LETM1/YOL027 gene family encodes a factor of the mitochondrial K^+ homeostasis with a potential role in the Wolf-Hirschhorn syndrome. *J Biol Chem,* 279**,** 30307-15.

Nunnari, J., Marshall, W. F., Straight, A., Murray, A., Sedat, J. W. & Walter, P. 1997. Mitochondrial transmission during mating in *Saccharomyces cerevisiae* is determined by mitochondrial fusion and fission and the intramitochondrial segregation of mitochondrial DNA. *Mol Biol Cell,* 8**,** 1233-42.

Okamoto, K. & Shaw, J. M. 2005. Mitochondrial morphology and dynamics in yeast and multicellular eukaryotes. *Annu Rev Genet,* 39**,** 503-36.

Ong, H. L., Cheng, K. T., Liu, X., Bandyopadhyay, B. C., Paria, B. C., Soboloff, J., Pani, B., Gwack, Y., Srikanth, S., Singh, B. B., Gill, D. L. & Ambudkar, I. S. 2007. Dynamic assembly of TRPC1-STIM1-Orai1 ternary complex is involved in store-operated calcium influx. Evidence for similarities in store-operated and calcium release-activated calcium channel components. *J Biol Chem,* 282**,** 9105-16.

Orrenius, S., Zhivotovsky, B. & Nicotera, P. 2003. Regulation of cell death: the calcium-apoptosis link. *Nat Rev Mol Cell Biol,* 4**,** 552-65.

Osibow, K., Malli, R., Kostner, G. M. & Graier, W. F. 2006. A new type of non-Ca^{2+}-buffering Apo(a)-based fluorescent indicator for intraluminal Ca^{2+} in the endoplasmic reticulum. *J Biol Chem,* 281**,** 5017-25.

Pagliarini, D. J., Calvo, S. E., Chang, B., Sheth, S. A., Vafai, S. B., Ong, S. E., Walford, G. A., Sugiana, C., Boneh, A., Chen, W. K., Hill, D. E., Vidal, M., Evans, J. G., Thorburn, D. R., Carr, S. A. & Mootha, V. K. 2008. A mitochondrial protein compendium elucidates complex I disease biology. *Cell,* 134**,** 112-23.

Pagliarini, D. J. & Rutter, J. 2013. Hallmarks of a new era in mitochondrial biochemistry. *Genes Dev,* 27**,** 2615-27.

Palmer, A. E., Giacomello, M., Kortemme, T., Hires, S. A., Lev-Ram, V., Baker, D. & Tsien, R. Y. 2006. Ca^{2+} indicators based on computationally redesigned calmodulin-peptide pairs. *Chem Biol,* 13**,** 521-30.

Palmer, A. E. & Tsien, R. Y. 2006. Measuring calcium signaling using genetically targetable fluorescent indicators. *Nat Protoc,* 1**,** 1057-65.

Palty, R., Silverman, W. F., Hershfinkel, M., Caporale, T., Sensi, S. L., Parnis, J., Nolte, C., Fishman, D., Shoshan-Barmatz, V., Herrmann, S., Khananshvili, D. & Sekler, I. 2010. NCLX is an essential component of mitochondrial Na^+/Ca^{2+} exchange. *Proc Natl Acad Sci U S A,* 107**,** 436-41.

Pan, X., Liu, J., Nguyen, T., Liu, C., Sun, J., Teng, Y., Fergusson, M. M., Rovira, Ii, Allen, M., Springer, D. A., Aponte, A. M., Gucek, M., Balaban, R. S., Murphy, E. & Finkel, T. 2013. The physiological role of mitochondrial calcium revealed by mice lacking the mitochondrial calcium uniporter. *Nat Cell Biol,* 15**,** 1464-72.

Parekh, A. B. 2003. Store-operated Ca^{2+} entry: dynamic interplay between endoplasmic reticulum, mitochondria and plasma membrane. *J Physiol,* 547**,** 333-48.

Park, M. K., Ashby, M. C., Erdemli, G., Petersen, O. H. & Tepikin, A. V. 2001. Perinuclear, perigranular and sub-plasmalemmal mitochondria have distinct functions in the regulation of cellular calcium transport. *EMBO J,* 20**,** 1863-74.

Patergnani, S., Suski, J. M., Agnoletto, C., Bononi, A., Bonora, M., De Marchi, E., Giorgi, C., Marchi, S., Missiroli, S., Poletti, F., Rimessi, A., Duszynski, J., Wieckowski, M. R. & Pinton, P. 2011. Calcium signaling around mitochondria associated membranes (MAMs). *Cell Commun Signal,* 9**,** 19.

Patron, M., Checchetto, V., Raffaello, A., Teardo, E., Vecellio Reane, D., Mantoan, M., Granatiero, V., Szabo, I., De Stefani, D. & Rizzuto, R. 2014. MICU1 and MICU2 finely tune the mitochondrial Ca^{2+} uniporter by exerting opposite effects on MCU activity. *Mol Cell,* 53**,** 726-37.

Paupe, V., Prudent, J., Dassa, E. P., Rendon, O. Z. & Shoubridge, E. A. 2015. CCDC90A (MCUR1) is a cytochrome c oxidase assembly factor and not a regulator of the mitochondrial calcium uniporter. *Cell Metab,* 21**,** 109-16.

Pendin, D., Greotti, E. & Pozzan, T. 2014. The elusive importance of being a mitochondrial Ca^{2+} uniporter. *Cell Calcium,* 55**,** 139-45.

Perocchi, F., Gohil, V. M., Girgis, H. S., Bao, X. R., Mccombs, J. E., Palmer, A. E. & Mootha, V. K. 2010. MICU1 encodes a mitochondrial EF hand protein required for Ca^{2+} uptake. *Nature,* 467**,** 291-6.

Pinton, P., Pozzan, T. & Rizzuto, R. 1998. The Golgi apparatus is an inositol 1,4,5-trisphosphate-sensitive Ca^{2+} store, with functional properties distinct from those of the endoplasmic reticulum. *EMBO J,* 17**,** 5298-308.

Plovanich, M., Bogorad, R. L., Sancak, Y., Kamer, K. J., Strittmatter, L., Li, A. A., Girgis, H. S., Kuchimanchi, S., De Groot, J., Speciner, L., Taneja, N., Oshea, J.,

Koteliansky, V. & Mootha, V. K. 2013. MICU2, a paralog of MICU1, resides within the mitochondrial uniporter complex to regulate calcium handling. *PLoS One,* 8**,** e55785.

Poburko, D., Liao, C. H., Van Breemen, C. & Demaurex, N. 2009. Mitochondrial regulation of sarcoplasmic reticulum Ca^{2+} content in vascular smooth muscle cells. *Circ Res,* 104**,** 104-12.

Pozzan, T., Rizzuto, R., Volpe, P. & Meldolesi, J. 1994. Molecular and cellular physiology of intracellular calcium stores. *Physiol Rev,* 74**,** 595-636.

Promerova, M., Andersson, L. S., Juras, R., Penedo, M. C., Reissmann, M., Tozaki, T., Bellone, R., Dunner, S., Horin, P., Imsland, F., Imsland, P., Mikko, S., Modry, D., Roed, K. H., Schwochow, D., Vega-Pla, J. L., Mehrabani-Yeganeh, H., Yousefi-Mashouf, N., E, G. C., Lindgren, G. & Andersson, L. 2014. Worldwide frequency distribution of the 'Gait keeper' mutation in the DMRT3 gene. *Anim Genet,* 45**,** 274-82.

Putney, J. W., Jr. 1986. A model for receptor-regulated calcium entry. *Cell Calcium,* 7**,** 1-12.

Qiu, J., Tan, Y. W., Hagenston, A. M., Martel, M. A., Kneisel, N., Skehel, P. A., Wyllie, D. J., Bading, H. & Hardingham, G. E. 2013. Mitochondrial calcium uniporter Mcu controls excitotoxicity and is transcriptionally repressed by neuroprotective nuclear calcium signals. *Nat Commun,* 4**,** 2034.

Raffaello, A., De Stefani, D., Sabbadin, D., Teardo, E., Merli, G., Picard, A., Checchetto, V., Moro, S., Szabo, I. & Rizzuto, R. 2013. The mitochondrial calcium uniporter is a multimer that can include a dominant-negative pore-forming subunit. *EMBO J,* 32**,** 2362-76.

Reed, K. C. & Bygrave, F. L. 1974. The inhibition of mitochondrial calcium transport by lanthanides and ruthenium red. *Biochem J,* 140**,** 143-55.

Rey, B., Roussel, D., Romestaing, C., Belouze, M., Rouanet, J. L., Desplanches, D., Sibille, B., Servais, S. & Duchamp, C. 2010. Up-regulation of avian uncoupling protein in cold-acclimated and hyperthyroid ducklings prevents reactive oxygen species production by skeletal muscle mitochondria. *BMC Physiol,* 10**,** 5.

Ricquier, D. & Bouillaud, F. 2000. The uncoupling protein homologues: UCP1, UCP2, UCP3, StUCP and AtUCP. *Biochem J,* 345 Pt 2**,** 161-79.

Rizzuto, R., De Stefani, D., Raffaello, A. & Mammucari, C. 2012. Mitochondria as sensors and regulators of calcium signalling. *Nat Rev Mol Cell Biol,* 13**,** 566-78.

Rizzuto, R., Pinton, P., Carrington, W., Fay, F. S., Fogarty, K. E., Lifshitz, L. M., Tuft, R. A. & Pozzan, T. 1998. Close contacts with the endoplasmic reticulum as determinants of mitochondrial Ca^{2+} responses. *Science,* 280**,** 1763-6.

Rizzuto, R. & Pozzan, T. 2006. Microdomains of intracellular Ca^{2+}: molecular determinants and functional consequences. *Physiol Rev,* 86**,** 369-408.

Rottenberg, H. & Scarpa, A. 1974. Calcium uptake and membrane potential in mitochondria. *Biochemistry,* 13**,** 4811-7.

Rowland, A. A. & Voeltz, G. K. 2012. Endoplasmic reticulum-mitochondria contacts: function of the junction. *Nat Rev Mol Cell Biol,* 13**,** 607-25.

Ryu, S. Y., Beutner, G., Dirksen, R. T., Kinnally, K. W. & Sheu, S. S. 2010. Mitochondrial ryanodine receptors and other mitochondrial Ca^{2+} permeable channels. *FEBS Lett,* 584**,** 1948-55.

Ryu, S. Y., Beutner, G., Kinnally, K. W., Dirksen, R. T. & Sheu, S. S. 2011. Single channel characterization of the mitochondrial ryanodine receptor in heart mitoplasts. *J Biol Chem,* 286**,** 21324-9.

Sancak, Y., Markhard, A. L., Kitami, T., Kovacs-Bogdan, E., Kamer, K. J., Udeshi, N. D., Carr, S. A., Chaudhuri, D., Clapham, D. E., Li, A. A., Calvo, S. E., Goldberger, O. & Mootha, V. K. 2013. EMRE is an essential component of the mitochondrial calcium uniporter complex. *Science,* 342**,** 1379-82.

Santo-Domingo, J. & Demaurex, N. 2010. Calcium uptake mechanisms of mitochondria. *Biochim Biophys Acta,* 1797**,** 907-12.

Satrustegui, J., Pardo, B. & Del Arco, A. 2007. Mitochondrial transporters as novel targets for intracellular calcium signaling. *Physiol Rev,* 87**,** 29-67.

Sesaki, H. & Jensen, R. E. 1999. Division versus fusion: Dnm1p and Fzo1p antagonistically regulate mitochondrial shape. *J Cell Biol,* 147**,** 699-706.

Sharma, V. K., Ramesh, V., Franzini-Armstrong, C. & Sheu, S. S. 2000. Transport of Ca^{2+} from sarcoplasmic reticulum to mitochondria in rat ventricular myocytes. *J Bioenerg Biomembr,* 32**,** 97-104.

Smirnova, E., Griparic, L., Shurland, D. L. & Van Der Bliek, A. M. 2001. Dynamin-related protein Drp1 is required for mitochondrial division in mammalian cells. *Mol Biol Cell,* 12**,** 2245-56.

Sparagna, G. C., Gunter, K. K., Sheu, S. S. & Gunter, T. E. 1995. Mitochondrial calcium uptake from physiological-type pulses of calcium. A description of the rapid uptake mode. *J Biol Chem,* 270**,** 27510-5.

Streb, H., Irvine, R. F., Berridge, M. J. & Schulz, I. 1983. Release of Ca^{2+} from a nonmitochondrial intracellular store in pancreatic acinar cells by inositol-1,4,5-trisphosphate. *Nature,* 306**,** 67-9.

Stuart, J. A., Cadenas, S., Jekabsons, M. B., Roussel, D. & Brand, M. D. 2001. Mitochondrial proton leak and the uncoupling protein 1 homologues. *Biochim Biophys Acta,* 1504**,** 144-58.

Szabadkai, G., Bianchi, K., Varnai, P., De Stefani, D., Wieckowski, M. R., Cavagna, D., Nagy, A. I., Balla, T. & Rizzuto, R. 2006. Chaperone-mediated coupling of endoplasmic reticulum and mitochondrial Ca^{2+} channels. *J Cell Biol,* 175**,** 901-11.

Takeuchi, A., Kim, B. & Matsuoka, S. 2015. The destiny of Ca^{2+} released by mitochondria. *J Physiol Sci,* 65**,** 11-24.

Tarasov, A. I., Semplici, F., Ravier, M. A., Bellomo, E. A., Pullen, T. J., Gilon, P., Sekler, I., Rizzuto, R. & Rutter, G. A. 2012. The mitochondrial Ca^{2+} uniporter MCU is essential for glucose-induced ATP increases in pancreatic beta-cells. *PLoS One,* 7**,** e39722.

Trenker, M., Malli, R., Fertschai, I., Levak-Frank, S. & Graier, W. F. 2007. Uncoupling proteins 2 and 3 are fundamental for mitochondrial Ca^{2+} uniport. *Nat Cell Biol,* 9**,** 445-52.

Tsai, M. F., Jiang, D., Zhao, L., Clapham, D. & Miller, C. 2014. Functional reconstitution of the mitochondrial Ca^{2+}/H^{+} antiporter Letm1. *J Gen Physiol,* 143**,** 67-73.

Van Vliet, A. R., Verfaillie, T. & Agostinis, P. 2014. New functions of mitochondria associated membranes in cellular signaling. *Biochim Biophys Acta,* 1843**,** 2253-62.

Vance, J. E. 1990. Phospholipid synthesis in a membrane fraction associated with mitochondria. *J Biol Chem,* 265**,** 7248-56.

Vasington, F. D. & Murphy, J. V. 1962. Ca ion uptake by rat kidney mitochondria and its dependence on respiration and phosphorylation. *J Biol Chem,* 237**,** 2670-7.

Waldeck-Weiermair, M., Alam, M. R., Khan, M. J., Deak, A. T., Vishnu, N., Karsten, F., Imamura, H., Graier, W. F. & Malli, R. 2012. Spatiotemporal correlations between cytosolic and mitochondrial Ca^{2+} signals using a novel red-shifted mitochondrial targeted cameleon. *PLoS One,* 7**,** e45917.

Waldeck-Weiermair, M., Deak, A. T., Groschner, L. N., Alam, M. R., Jean-Quartier, C., Malli, R. & Graier, W. F. 2013. Molecularly distinct routes of mitochondrial Ca^{2+} uptake are activated depending on the activity of the sarco/endoplasmic reticulum Ca^{2+} ATPase (SERCA). *J Biol Chem,* 288**,** 15367-79.

Waldeck-Weiermair, M., Duan, X., Naghdi, S., Khan, M. J., Trenker, M., Malli, R. & Graier, W. F. 2010a. Uncoupling protein 3 adjusts mitochondrial Ca^{2+} uptake to high and low Ca^{2+} signals. *Cell Calcium,* 48**,** 288-301.

Waldeck-Weiermair, M., Jean-Quartier, C., Rost, R., Khan, M. J., Vishnu, N., Bondarenko, A. I., Imamura, H., Malli, R. & Graier, W. F. 2011. Leucine zipper EF hand-containing transmembrane protein 1 (Letm1) and uncoupling proteins 2 and 3 (UCP2/3) contribute to two distinct mitochondrial Ca^{2+} uptake pathways. *J Biol Chem,* 286**,** 28444-55.

Waldeck-Weiermair, M., Malli, R., Naghdi, S., Trenker, M., Kahn, M. J. & Graier, W. F. 2010b. The contribution of UCP2 and UCP3 to mitochondrial Ca^{2+} uptake is differentially determined by the source of supplied Ca^{2+}. *Cell Calcium,* 47**,** 433-40.

Waldeck-Weiermair, M., Malli, R., Parichatikanond, W., Gottschalk, B., Madreiter-Sokolowski, C. T., Klec, C., Rost, R. & Graier, W. F. 2015. Rearrangement of MICU1 multimers for activation of MCU is solely controlled by cytosolic Ca^{2+}. *Sci Rep,* 5**,** 15602.

Wang, L., Yang, X., Li, S., Wang, Z., Liu, Y., Feng, J., Zhu, Y. & Shen, Y. 2014. Structural and mechanistic insights into MICU1 regulation of mitochondrial calcium uptake. *EMBO J,* 33**,** 594-604.

Wang, L., Yang, X. & Shen, Y. 2015. Molecular mechanism of mitochondrial calcium uptake. *Cell Mol Life Sci,* 72**,** 1489-98.

Wang, X. 2001. The expanding role of mitochondria in apoptosis. *Genes Dev,* 15**,** 2922-33.

Williams, G. S., Boyman, L. & Lederer, W. J. 2015. Mitochondrial calcium and the regulation of metabolism in the heart. *J Mol Cell Cardiol,* 78**,** 35-45.

Williamson, J. R., Williams, R. J., Coll, K. E. & Thomas, A. P. 1983. Cytosolic free Ca^{2+} concentration and intracellular calcium distribution of Ca^{2+}-tolerant isolated heart cells. *J Biol Chem,* 258**,** 13411-4.

Wu, Z., Zhang, J. & Zhao, B. 2009. Superoxide anion regulates the mitochondrial free Ca^{2+} through uncoupling proteins. *Antioxid Redox Signal,* 11**,** 1805-18.

Zhao, Y., Araki, S., Wu, J., Teramoto, T., Chang, Y. F., Nakano, M., Abdelfattah, A. S., Fujiwara, M., Ishihara, T., Nagai, T. & Campbell, R. E. 2011. An expanded palette of genetically encoded Ca^{2+} indicators. *Science,* 333**,** 1888-91.

PUBLICATIONS

The following original studies have been published in international SCI-listed journals. Current dissertation is based on the results of the publications No. 1.

1. Waldeck-Weiermair, M.[*], Malli, R.[*], **Parichatikanond, W.[*]**, Gottschalk, B., Madreiter-Sokolowski, C.T., Klec, C., Rost, R. & Graier, W.F. 2015. Rearrangement of MICU1 multimers for activation of MCU is solely controlled by cytosolic Ca^{2+}. *Sci Rep*, 22(5), 15602. **([*]; authors equally contributed)**

2. Bondarenko, A.I., **Parichatikanond, W.**, Madreiter, C.T., Rost, R., Waldeck-Weiermair, M., Malli, R. & Graier, W.F. 2015. UCP2 modulates single-channel properties of a MCU-dependent Ca^{2+} inward current in mitochondria. *Pflugers Arch*, 467(12), 2509-18.

3. Bondarenko, A.I., Jean-Quartier, C., **Parichatikanond, W.**, Alam, M.R., Waldeck-Weiermair, M., Malli, R. & Graier, W.F. 2014. Mitochondrial Ca^{2+} uniporter (MCU)-dependent and MCU-independent Ca^{2+} channels coexist in the inner mitochondrial membrane. *Pflugers Arch*, 466(7), 1411-20.

4. Alam, M.R., Groschner, L.N., **Parichatikanond, W.**, Kuo, L., Bondarenko, A.I., Rost, R., Waldeck-Weiermair, M., Malli, R. & Graier, W.F. 2012. Mitochondrial Ca^{2+} uptake 1 (MICU1) and mitochondrial Ca^{2+} uniporter (MCU) contribute to metabolism-secretion coupling in clonal pancreatic β-cells. *J Biol Chem*, 5, 287(41), 34445-54.